

Charles University
Faculty of Science

Dissertation

2021

Jin Zhang

Charles University

Faculty of Science

Study program: Physical chemistry



Mgr. Jin Zhang

Design of sustainable catalysts by post-synthesis modification of germanosilicate zeolites

Doctoral thesis

Supervisor: Dr. Mariya Shamzhy

Advisor: Dr. Jan Přečh

Prague, 2021

Univerzita Karlova

Přírodovědecká fakulta

Studijní program: Fyzikální chemie



Mgr. Jin Zhang

Návrh udržitelných katalyzátorů postsyntetickou modifikací germanosilikátových zeolitů

Disertační práce

Školitel: Dr. Mariya Shamzhy

Konzultant: Dr. Jan Přečh

Praha, 2021

Prohlášení:

Disertační práce byla vypracována v oddělení Syntézy a katalýzy Ústavu fyzikální chemie J. Heyrovského AV ČR v období 15. 09. 2017 – 31. 12. 2018 a na Přírodovědecké fakultě Univerzity Karlovy od 01. 01. 2019.

Prohlašuji, že jsem závěrečnou práci zpracovala samostatně a že jsem uvedla všechny použité informační zdroje a literaturu. Tato práce ani její podstatná část nebyla předložena k získání jiného nebo stejného akademického titulu.

V Praze, 31.05.2021

Podpis _____

Contents

Acknowledgements.....	1
List of publications	2
Abstract.....	3
Abstrakt.....	5
1. Aims of the study	9
2. Introduction.....	10
2.1. Zeolites.....	10
2.1.1. Structure, classification, acidity	10
2.1.2. Hydrothermal synthesis, mechanism of crystallization	14
2.1.3. Organic structure-directing agents, structure-directing propensity of germanium	15
2.2. Post-synthesis modification of germanosilicate zeolites	20
2.2.1. Tailoring textural properties.....	21
2.2.2. Structure modification <i>via</i> ADOR strategy.....	22
2.2.3. Alteration of chemical composition <i>via</i> isomorphous substitution.....	26
2.3. Zeolites as solid acid catalysts	29
2.3.1. Brønsted acid catalysis.....	30
2.3.2. Lewis acid catalysis	32
3. Experimental part.....	37
3.1. Chemicals and materials	37
3.2. Synthesis of organic structure directing agents	39
3.3. Synthesis of zeolites.....	40
3.3.1. Zeolite ITH	40
3.3.2. Zeolite IWW	41
3.3.3. Zeolite UTL	41

3.3.4. Zeolite *CTH.....	42
3.4. Post-synthesis modification	42
3.4.1. Germanium leaching	42
3.4.2. Ge recovery/recycling	43
3.4.3. ADOR transformation	43
3.4.3.1. Water-methanol medium	43
3.4.3.2. Al-containing water-methanol medium	44
3.4.4. Post-synthesis stabilization of germanosilicate zeolites	44
3.4.5. Lewis acid zeolites by post-synthesis treatment of germanosilicates	44
3.4.6. Post-synthesis dealumination-metalation of commercial *BEA zeolite.....	46
3.5. Characterization techniques	46
3.6. Catalytic tests	48
4. Results and discussion	51
4.1. Structure-activity relationships for germanosilicate zeolite catalysts.....	51
4.1.1. Structural and acidic properties of IWW and UTL germanosilicates.....	51
4.1.2. Catalytic performance of IWW and UTL zeolites in ketalization of polyols	56
4.2. Zeolite catalysts by degermanation-metalation coupled with Ge recycling	62
4.2.1. Degermanation and germanium recovery	62
4.2.2. Germanium recycling.....	67
4.2.3. Metalation: synthesis of Ti-, Sn-, Zr-substituted zeolite catalysts	73
4.2.3.1. Structural and textural characteristics	73
4.2.3.2. Acidic properties	78
4.2.3.3. Catalytic performance	83
4.3. Controlling disassembly step within the ADOR process for the synthesis of zeolites	
.....	89

4.3.1. “Slow deintercalation/slow rearrangement” of UTL in water-methanol systems	89
4.3.2. “Slow deintercalation/fast rearrangement” of UTL in Al-containing water-methanol systems	91
5. Conclusions.....	99
6. References.....	102
7. Enclosures	125

Acknowledgements

Upon the completion of my doctoral dissertation, I am grateful to those who have offered me invaluable encouragement and support during my four-year PhD study.

First of all, special gratitude is given to my supervisor, Dr. Mariya Shamzhy, for her constructive suggestions and patient instructions. She has maintained efficient communication with me to ensure that I can complete my experimental and writing work smoothly. Her kind help and encouragement have inspired me a lot over the last four years.

Then, I would like to extend my hearty thanks to the leader of “Heterogeneous Catalysis and Advanced Materials” group Prof. Jiří Čejka for giving me the chance to become a PhD student at the Charles University, I am deeply grateful for his scientific guidance and advice during my PhD study.

Besides, I have benefited a lot from Dr. Maksym Opanasenko and Dr. Jan Přečh, their patient instructions in various courses, precious suggestions and comments for my study.

Further, I would like to extend my sincere gratitude to my colleagues: Dr. Martin Kubů and Ondrej Vesely for gas physisorption, Qiudi Yue for SEM and chemical analysis, Dr. Michal Mazur and Ang Li for TEM, Dr. Zdeněk Tošner for NMR spectroscopy.

I would like to thank other members of our group, i.e., Dr. Roman Barakov, Dr. Yong Zhou, Yuyan Zhang, Sarra Abdi, Milan Eliáš, for their kind support and encouragement.

Finally, I am very grateful to my parents and sister. It is their selfless support, encouragement and love that turned into the power of my struggle. It is my greatest fortune to become their family in my life.

List of publications

The dissertation was completed based on the following publications:

1. **Zhang J.**, Yue Q., Mazur M., Opanasenko M., Shamzhy M., Čejka J. Selective Recovery and Recycling of Germanium for the Design of Sustainable Zeolite Catalysts. *ACS Sustainable Chemistry & Engineering*, 2020, 8, 8235-8246. (**Q1, IF = 7.63**)
2. **Zhang J.**, Veselý O., Tošner Z., Mazur M., Opanasenko M., Čejka J., Shamzhy M. Towards Controlling Disassembly Step within the ADOR Process for the Synthesis of Zeolites. *Chemistry of Materials*, 2021, 33, 1228-1237. (**D1, IF = 9.57**)
3. Podolean I., **Zhang J.**, Shamzhy M., Pârvulescu V. I., Čejka J. Solvent-Free Ketalization of Polyols over Germanosilicate Zeolites: The Role of the Nature and Strength of Acid Sites. *Catalysis Science & Technology*, 2020, 10, 8254-8264. (**Q2, IF = 5.73**)
4. Shamzhy M., Přečh J., **Zhang J.**, Ruaux V., El-Siblani H., Mintova S. Quantification of Lewis Acid Sites in 3D and 2D TS-1 Zeolites: FTIR Spectroscopic Study. *Catalysis Today*, 2020, 345, 80-87. (**Q1, IF = 5.83**)

Further publications

1. **Zhang J.**, Veselý O., Shamzhy M., Opanasenko M., Čejka J. High Activity of Ga-Containing Nanosponge MTW Zeolites in Acylation of P-xylene. *Catalysis Today*, 2020, 345, 110-115. (**Q1, IF = 5.83**)
2. Yue Q., **Zhang J.**, Shamzhy M., Opanasenko M. Seeded Growth of Isomorphously Substituted Chabazites in Proton-Form. *Microporous and Mesoporous Materials*, 2019, 280, 331-336. (**Q1, IF = 4.28**)

Abstract

Due to the presence of small structural units (e.g., D4R, D3R), the frameworks of germanosilicate zeolites are generally characterized by high pore volumes and multidimensional/extra-large pore systems, making them especially suitable in processing bulky molecules (in particular, involved in biomass-derived compounds valorization). However, weak acidity, low hydrothermal stability and high cost of Ge significantly limit the practical use of Ge-containing zeolites.

This thesis is aimed at design of sustainable germanosilicate zeolite-based catalysts of modifiable chemical composition and tunable porosity for relevant acid-catalyzed reactions, such as ketalization of polyols, epoxidation of olefins, Baeyer-Villiger oxidation of cyclic ketones and Meerwein-Ponndorf-Verley reduction of aldehydes.

Germanosilicate zeolites of different structures, including medium-pore **ITH**, large pore **IWW**, extra-large pore **UTL** and ***CTH**, were thoroughly characterized using a combination of techniques (i.e., XRD, physisorption, electron microscopy, chemical analysis, among others) and subjected to different post-synthesis modifications to address synthesis-structure-activity relationships in the designed germanosilicate-zeolite based catalysts.

In ketalization of glycerol to solketal, weak acid centers of **IWW** and **UTL** germanosilicates were found as active sites capable to selective catalyze the targeted reaction. Noticeably, large pore **IWW** catalyst was shown featuring both Lewis and Brønsted acidity, while extra-large pore **UTL** zeolite was found to possess exclusively Ge-associated Lewis acid centers. Water-induced formation of Brønsted acid sites in **IWW** germanosilicate was verified using FTIR-monitored dose-by-dose water adsorption, followed by probing acid sites with pyridine.

To tailor germanosilicate zeolite-based catalysts with different nature of acid sites, post-synthesis isomorphous substitution of Ge with different tetravalent elements (e.g., Ti, Sn, Zr) coupled with Ge recovery and recycling was elaborated. Up to 94 % of Ge was recovered from

germanosilicate zeolites of different structures (**ITH**, **IWW** and **UTL**) under optimized leaching conditions (i.e., pH, T, duration of the treatment). The method of Ge-containing leaching solution separation from parent zeolite (i.e., *filtration* or *microfiltration*) was shown as a useful tool to direct the phase selectivity of zeolite formation upon Ge recycling. In particular, *microfiltration* yielded GeO₂ as a versatile Ge source for the synthesis of different zeolites (exemplified for **ITH**, **IWW** and **UTL**). In turn, *filtration* produced GeO₂ containing trace amounts of initial zeolite, thus favoring seed-assisted crystallization of parent zeolite, albeit possessing larger crystals, independently on the re-synthesis conditions applied.

Subsequent metalation of degermanated large pore (**IWW**) and extra-large pore (**UTL**, ***CTH**) zeolites gave rise to Lewis acid solids of variable nature, proven as active and selective catalysts in model reactions, such as epoxidation of 1-octene for Ti-substituted zeolites, Baeyer-Villiger oxidation of cyclohexanone for Sn-containing materials and Meerwein-Ponndorf-Verley reduction of furfural for Sn- and Zr-substituted zeolites.

Water-induced disassembly of **UTL** germanosilicate in combination with Ge-for-Al isomorphous substitution was developed, optimized and proved as an efficient method for controllable alternation of both structural and acidic properties of zeolite catalysts. In particular, de-intercalation and rearrangement processes competing upon **UTL** disassembly, were efficiently regulated by adjusting water-to-zeolite ratio and concentration of framework-building Al ions in water-methanol medium. Unprecedentedly, Al-assisted rearrangement under slow deintercalation conditions allowed to achieve the cycled structural transformation of **UTL** (D4R interlayer units) → Al-**OKO** (S4R) → Al-**UTL** (D4R).

The synthetic methods designed in this thesis are envisaged to pave the way towards new nanoporous materials expanding the scope of highly active and selective heterogeneous catalysts engineered for specific application.

Abstrakt

Vzhledem k přítomnosti malých strukturních jednotek (např. D4R, D3R), germanosilikátové zeolity jsou obecně charakterizovány vysokým objemem pórů a multidimenzionálními/extra-velkými pórovými systémy, takže jsou zvláště vhodné při zpracování objemných molekul (zejména podílejících se na valorizaci sloučenin získaných z biomasy). Nízká kyselost, nízká hydrotermální stabilita a vysoká cena Ge však výrazně omezují praktické používání zeolitů obsahujících Ge.

Cílem této práce bylo navrhnout nové katalyzátory modifikovatelného chemického složení na bázi germanosilikátového zeolitu a s laditelnou pórovitostí pro relevantní kyselé katalyzované reakce, jako je ketalizace polyalkoholů, epoxidace olefinů, Baeyer-Villigerova oxidace cyklických ketonů a Meerwein-Ponndorf-Verleyho redukce aldehydů.

Germanosilikátové zeolity různých struktur, včetně středněporézního **ITH**, širokoporézního **IWW**, nebo extraporézních **UTL** a ***CTH**, byly důkladně charakterizovány kombinací technik (tj. XRD, fyziosorpce, elektronová mikroskopie, chemická analýza, mimo jiné) a podrobeny různým postsyntetizačním modifikacím, s cílem pochopit vztahy syntéza-struktura-aktivita v navržených katalyzátorech na bázi germanosilikát-zeolit.

V ketalizaci glycerolu na solketal byla nalezena slabá kyselá centra **IWW** a **UTL** germanosilikátů jako aktivní místa schopná selektivně katalyzovat cílenou reakci. Pozoruhodné je, že širokoporézní katalyzátor **IWW** vykazoval Lewisovu i Brønstedovu kyselost, zatímco u extraporézního zeolitu **UTL** bylo zjištěno, že má výhradně Lewisova kyselá centra spojená s Ge. Vodou indukovaná tvorba kyselých Brønstedových center v **IWW** germanosilikátu byla ověřena pomocí FTIR monitorováním postupné adsorpce vody, následované sondováním míst kyseliny pyridinem.

Pro přizpůsobení germanosilikátových katalyzátorů na bázi zeolitu s různou povahou kyselých míst byla provedena postsyntézní izomorfní substituce Ge různými tetravalentními prvky (např. Si, Sn, Zr) ve spojení s recyklací Ge. Až 94 % Ge bylo získáno z

germanosilikátových zeolitů různých struktur (**ITH**, **IWW** a **UTL**) za optimalizovaných podmínek vyluhování (tj. pH, T, trvání léčby). Metoda oddělení roztoku obsahujícího Ge od mateřského zeolitu (tj. filtrace nebo mikrofiltrace) byla prokázána jako užitečný nástroj pro řízení fázové selektivity tvorby zeolitu při recyklaci Ge. Mikrofiltrací bylo získáno GeO₂ jako univerzální zdroj Ge pro syntézu různých strukturních typů zeolitů (příkladem pro **ITH**, **IWW** a **UTL**). Naopak, GeO₂ získané filtrací, obsahovalo jistá množství původního zeolitu, čímž upřednostňovalo krystalizaci mateřského zeolitu nezávisle na použitých podmínkách syntézy.

Následná metalizace degermanovaného širokoporézního (**IWW**) a extraporézního (**UTL**, ***CTH**) zeolitu vedly ke vzniku Lewisových center proměnlivé povahy, které vykazovaly katalytickou aktivitu v modelových reakcích, jako je epoxidace 1-oktenu pro Ti-substituované zeolity, Baeyer-Villigerova oxidace cyklohexanonu pro materiály obsahující Sn a Meerwein-Ponndorf-Verleyho redukce furfuralu pro zeolity substituované Sn- a Zr.

Vodou indukovaná rozpad **UTL** germanosilikátu v kombinaci s izomorfní substitucí Ge za Al byl optimalizován a posloužil jako účinná metoda pro regulovatelné řízení strukturních i kyselých vlastností zeolitových katalyzátorů. Zejména de-interkalační a transformační procesy, které konkurují rozkladu **UTL**, byly účinně regulovány úpravou poměru vody k zeolitu a koncentrací Al-iontů v systému voda-methanol. Transformace za přítomnosti Al za pomalých podmínek deinterkalace umožnila dosáhnout cyklické strukturální transformace **UTL** (D4R mezivrstvy) → Al-**OKO** (S4R) → Al-**UTL** (D4R).

Předpokládá se, že syntetické metody navržené v této diplomové práci otevírají cestu k novým nanoporézním materiálům rozšiřujícím rozsah vysoce aktivních a selektivních heterogenních katalyzátorů navržených pro specifické použití.

List of abbreviations

1D	one-dimensional
2D	two-dimensional
3D	three-dimensional
ADOR	Assembly-Disassembly-Organization-Reassembly
BAS	Brønsted acid sites
BET	surface area according to Brunauer, Emmett and Teller theory
BVO	Baeyer-Villiger oxidation
CBUs	composite building units
C_B	concentration of Brønsted acid sites
C_L	concentration of Lewis acid sites
D4R/D3R	double four ring/double three ring
DMAD	(6R,10S)-6,10-dimethyl-5-azoniaspiro[4.5]decane hydroxide
DMBI	1,2-dimethyl-3-(3-methylbenzyl)imidazolium hydroxide
DR UV-vis	diffuse reflectance ultraviolet-visible spectroscopy
EDS	energy-dispersive X-ray spectroscopy
ESI-MS	electrospray ionization mass spectrometry
FCC	fluid catalytic cracking
FTIR	Fourier transmission infrared spectroscopy
FWHM	full width at half the maximum intensity
GC-MS	gas chromatography-mass spectrometry
HRTEM	high resolution transmission electron microscopy
HM	hexamethonium
ICP-OES	inductively coupled plasma optical emission spectroscopy
IZA	International Zeolite Association
LAS	Lewis acid sites
LUMO	the lowest unoccupied molecular orbital
MAS NMR	magic angle spinning nuclear magnetic resonance

MPP(OH) ₂	1,5-bis-(methylpyrrolidinium)pentane dihydroxide
MPV	Meerwein-Ponndorf-Verley
MPVO	Meerwein-Ponndorf-Verley-Oppenauer
PSD	pore size distribution
PBUs	primary building units
Py	pyridine
S4R	single four ring
SBUs	secondary building units
SDA	structure directing agent
SEM	scanning electron microscopy
SSIE	solid-state ion-exchange
Si/Al	molar ratio of silicon to aluminum
Si/Ge	molar ratio of silicon to germanium
Si/Sn	molar ratio of silicon to tin
Si/Ti	molar ratio of silicon to titanium
Si/Zr	molar ratio of silicon to zirconium
TAAOH	tetraalkylammonium hydroxide
TBHP	tert-butyl hydroperoxide
TEAOH	tetraethylammonium hydroxide
TEOS	tetraethyl orthosilicate
TMAOH	tetramethylammonium hydroxide
TMHDA	N,N,N',N'-tetramethyl-1,6-hexanediamine
TPAOH	tetrapropylammonium hydroxide
V _{micro}	micropore volume
XRD	X-ray diffraction

1. Aims of the study

This thesis focuses on post-synthesis modifications of the structure and chemical composition of germanosilicate zeolites coupled with Ge recycling to design sustainable catalysts with tailored acidic characteristics.

The main objectives are as follows:

- To elaborate a cost-efficient post-synthesis degermanation/metalation approach, coupled with Ge recovery and recycling to prepare Lewis acid zeolite catalysts with targeted chemical composition.
- To incorporate post-synthetically Ti, Sn, and Zr into large and extra-large pore germanosilicate zeolites of different structures (e.g., **IWW**, **UTL**, ***CTH**).
- To assess the nature of active sites in germanosilicate zeolite catalysts.
- To address the structure-acidity-activity relationship for prepared zeolites in model acid-catalyzed reactions, such as the Baeyer-Villiger oxidation of cyclic ketones, epoxidation of alkenes, the Meerwein-Ponndorf-Verley reduction of furfural.
- To determine the role of Al on the structural and chemical properties of **UTL**-derived zeolites formed *via* Assembly-Disassembly-Organization-Reassembly route.

2. Introduction

2.1. Zeolites

2.1.1. Structure, classification, acidity

Zeolites per definition are traditionally considered as crystalline microporous aluminosilicates with three-dimensional frameworks built from corner-sharing $[\text{SiO}_4]$ and $[\text{AlO}_4]$ tetrahedra^{1,2}. Al^{3+} with similar ionic radii³, T-O bond lengths^{4,5} and T-O-T bond angles⁵ as Si^{4+} , is an ideal element for isomorphous substitution of Si^{4+} in zeolite frameworks. Moreover, the possibility of altering the “fine structure” of zeolite framework (e.g., bond lengths and angles) can compensate structural strains caused by the isomorphous substitution. This allows the introduction of elements other than Al into the framework, such as phosphorus⁶, titanium⁷ or germanium⁸. Up to now, 253 types of zeolite structures have been accepted by the Structural Committee and given the three-letter code by the International Zeolite Association (IZA)⁹.

The primary building units (PBUs) of a zeolite framework are the TO_4 tetrahedra (T = Si, Al, P, Ge, etc.) (**Figure 2-1**). PBUs are connected by sharing oxygen atoms to form special arrangements with simple geometric forms, which are named as the secondary building units (SBUs). Currently, about 23 types of SBUs are known and each zeolite unit cell can be built by combining several types of SBUs (**Figure 2-2**)⁹. A particularly interesting SBU considered in this thesis work is double-four-ring (D4R) unit, which is frequently found in germanosilicate zeolites^{8, 10, 11}. An alternative to SBUs, composite building units (CBUs) approach is used for comparison of zeolite frameworks which share one or several CBUs such as double rings, cancrinite cages and alpha cavities¹². Some of CBUs are shown in **Figure 2-3**.

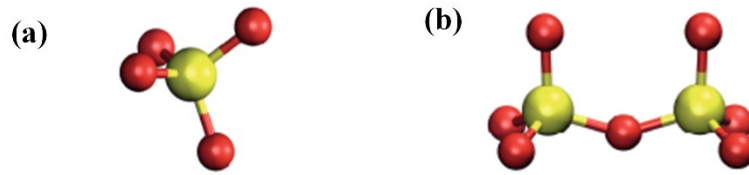


Figure 2-1. TO_4 tetrahedron (a) and two TO_4 tetrahedra sharing one oxygen atom (b). T and oxygen atoms are shown as yellow and red spheres, respectively.

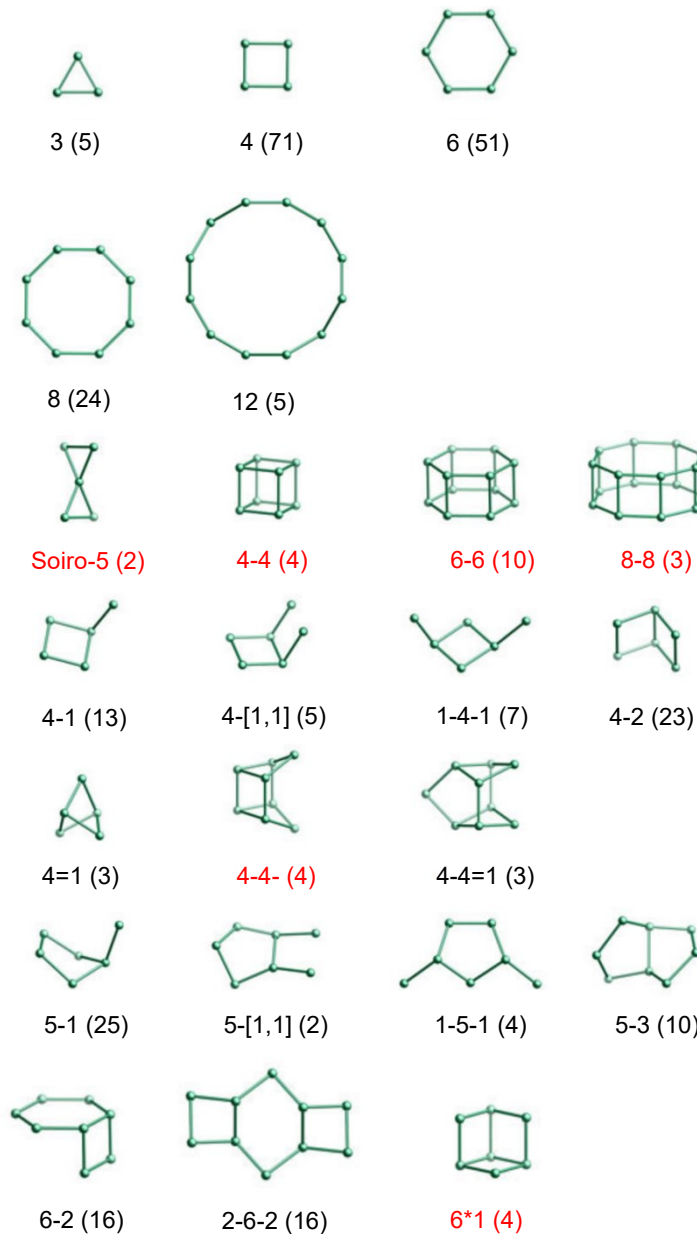


Figure 2-2. Secondary building units (for the ones highlighted with red color, CBUs of the same structure can be found, see **Figure 2-3**)⁹. T atoms are shown as spheres, oxygen atoms are not shown.

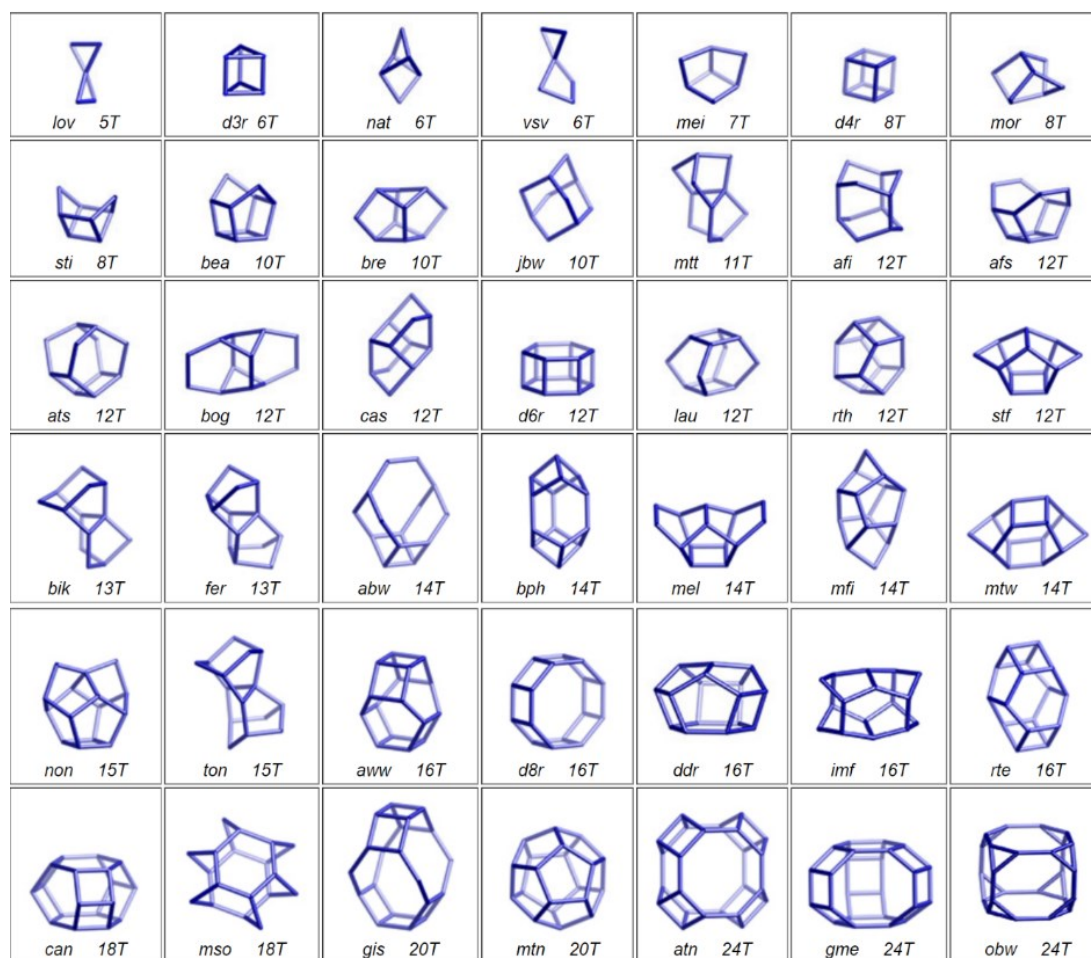


Figure 2-3. Composite building units⁹. Vertexes of polyhedra represent T atoms, oxygen atoms are not shown.

Zeolite channels are defined by the number of T-atoms forming the pore aperture (7-to-30-rings) (**Figure 2-4**). According to the size of pore openings, zeolites are generally classified as small pore (7 and 8-rings with diameter ~ 4.0 Å; e.g., **LTA**, **SOD**, **CHA**), medium pore (9- and 10-rings with diameter ~ 5.5 Å; e.g., **ITH**, **MFI**, **MWW**), large pore (11- and 12-rings with diameter ~ 7.0 Å; e.g., **IWW**, **UOV**, ***BEA**) and extra-large pore (> 12 -rings with diameter > 7.0 Å; e.g., **CFI**, **UTL**, ***CTH**)¹³. In addition, according to the channel interconnectivity, pore systems of zeolites are categorized into one-dimensional (1D) with no intersecting channels (e.g., **LTL**, **MTW**); 2D with intersections of two kinds of channels (e.g., **FER**, **UTL**); and 3D with (e.g., **FAU**) or without cavities (e.g., ***BEA**)¹³ at the channel intersections.

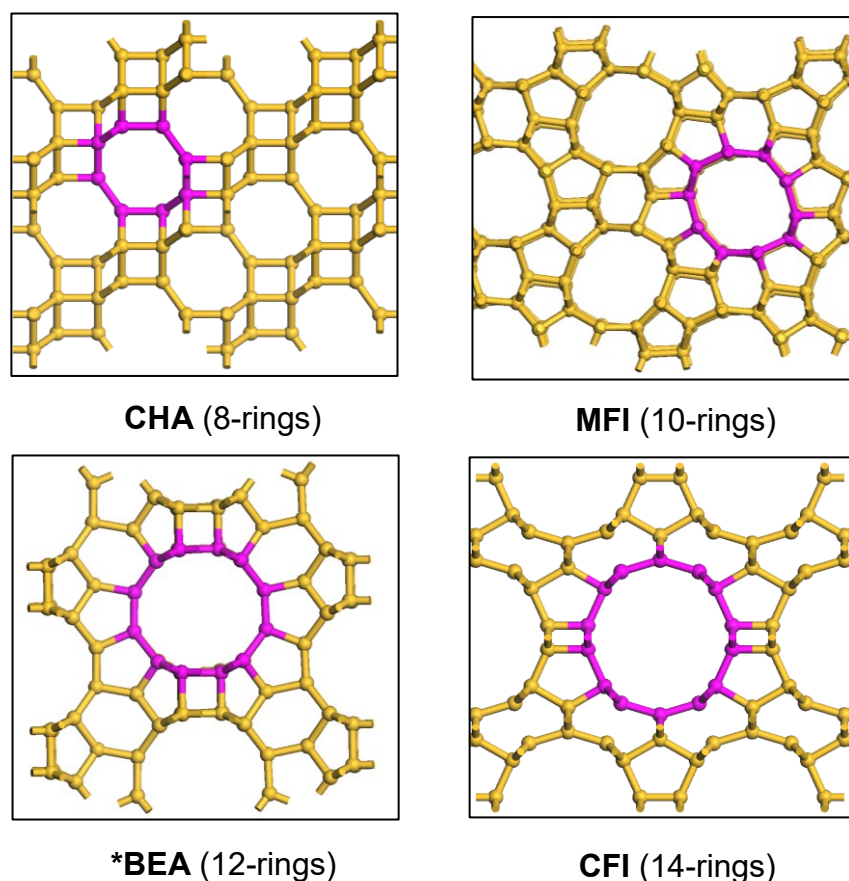


Figure 2-4. Zeolites with different pore sizes. T atoms are shown as spheres, oxygen atoms are not shown⁹.

Isomorphous incorporation of heteroelements is an important method to tune physico-chemical properties of zeolites, such as hydrophilicity/hydrophobicity, hydrothermal stability, the nature of acid sites and related catalytic activity. Incorporation of trivalent elements T^{3+} such as Al^{3+} , Fe^{3+} , Ga^{3+} , and B^{3+} imposes negative charge of a zeolite framework. When compensated by a proton, bridging hydroxyl groups ($\equiv Si(OH)T^{3+}\equiv$) are formed. These groups can donate a proton when interacting with reactants, thus acting as Brønsted acid sites (BAS) (**Figure 2-5a**). In turn, coordinatively unsaturated elements capable to accept an electron pair with their LUMO perform as Lewis acid sites (LAS), while being incorporated into zeolite framework. For example, in aluminosilicate zeolite, Lewis acid sites are formed *via* dehydroxylation of $\equiv Si(OH)T^{3+}\equiv$ Brønsted acid sites (**Figure 2-5a**)¹⁴, while isomorphous substitution of coordinatively unsaturated atoms of four valent T^{4+} elements (e.g., Ti, Sn, Zr)

results in formation of either ‘open’ or ‘closed’ Lewis acid centers performing differently as active sites in catalysis (**Figure 2-5b**)¹⁵⁻¹⁷.

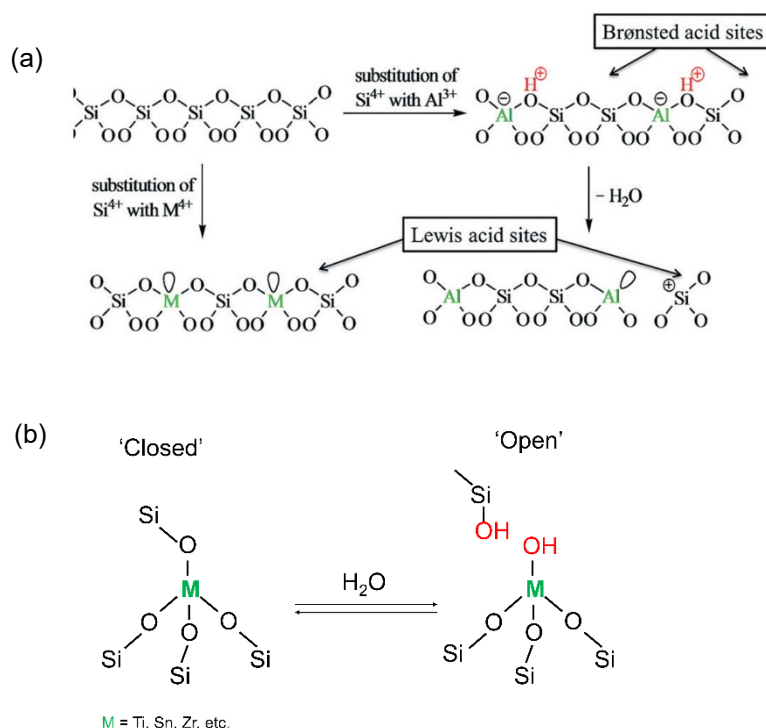


Figure 2-5. Two types of acid sites in a zeolite (a)¹⁴ and ‘closed’ and ‘open’ sites in Lewis acid zeolite (b)¹⁵⁻¹⁷.

Due to their acidic functionalities, uniform pore size, and high thermal stability, zeolites are widely applied as catalysts in a variety of industrial chemical processes (e.g., cracking, alkylation and isomerization of hydrocarbons) used for production of fuels, fine chemicals, polymer precursors and dyestuffs¹⁷⁻²⁵.

2.1.2. Hydrothermal synthesis, mechanism of crystallization

Zeolites are generally prepared by hydrothermal synthesis in aqueous media where sources of T-elements (Si, Al, Ge, Sn, Zr, etc.), inorganic and/or organic cations are mixed together in basic or fluoride media. In most cases, an organic compound acts as a structure-directing agent (SDA). The crystallization proceeds in a closed vessel (autoclave) at increased temperature

(usually 100 – 240 °C) under autogenous pressure for a period from few hours to several weeks².

The general mechanism of zeolite crystallization is described with a S-shaped curve (Figure 2-6), which includes three sequential steps: (i) induction period, pre-nucleation comprising depolymerization of a source of T-elements with a formation of oligomeric (element)-silicate anions, (ii) nucleation period comprising the rearrangement of oligomeric anions and SDA into clathrate-like primary units and the formation of nucleation centers by aggregation of the silicate clusters and (iii) crystal growth by aggregation of the nuclei²⁶⁻²⁸.

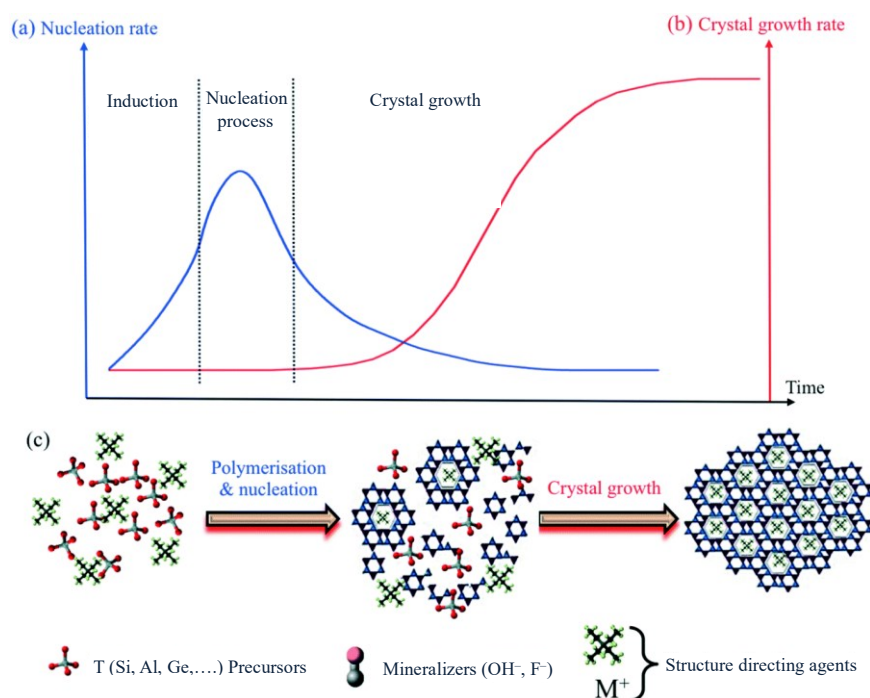


Figure 2-6. Mechanism of zeolite crystallization²⁸.

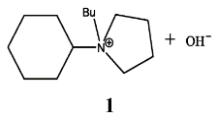
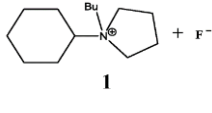
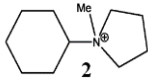
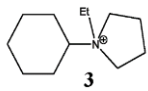
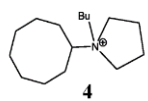
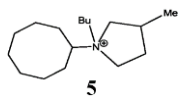
Variation of the composition of reaction mixture (e.g., Si/Al ratio, [OH⁻], structure directing agent, nature of charge compensating cation, among others) and reaction conditions (temperature, duration) usually leads to the formation of different types of zeolites.

2.1.3. Organic structure-directing agents, structure-directing propensity of germanium

The presence of organic structure-directing agent is essential to direct the crystallization

of a particular zeolite. A slight change in the structure of SDA may result in the formation of different types of zeolites, independently of the chemical composition (Si/T/H₂O ratio) and conditions of crystallization, due to a higher stabilization of targeted zeolite with typical SDA²⁹. For example, substitution of butyl group in SDA-1 (**Table 2-1**) with methyl or ethyl groups directs the crystallization towards the formation of **MTW** zeolite (1D channel system) rather than ***SFV** (3D) or **MEL** (3D) zeolites. In turn, changing the cyclo-hexyl ring to cyclo-octyl ring in SDA-1 results in the formation of **SFG** zeolite with 2D pore system. Further attaching a methyl group to the pyrrolidine ring in SDA-4 yields **MEL** zeolite (**Table 2-1**).

Table 2-1. Change in the selectivity of zeolite crystallization vs. the structure of SDA²⁹.

SDA	Zeolitic product	Framework composition	Channel system
 1	SSZ-57 (*SFV)	Si	3D, 12R×10R×10R
 1	ZSM-11 (MEL)	Si, Al	3D, 10R×10R×10R
 2	ZSM-12 (MTW)	Si, Al	1D, 12R
 3	ZSM-12 (MTW)	Si, Al	1D, 12R
 4	SSZ-58 (SFG)	Si, B	2D, 10R×10R
 5	ZSM-11 (MEL)	Si, Al	3D, 10R×10R×10R

In most cases, hydrothermal syntheses result in crystallization of three-dimensional (3D) zeolites, although the formation of 2D (layered) zeolites with layer thickness of 1 – 2 unit cells (typically, 2 – 3 nm) can be promoted by using specially designed surfactant SDAs (**Figure 2-**

7a)³⁰⁻³⁴, which contain both hydrophilic and hydrophobic parts. The hydrophilic part directs the zeolite crystallization while the hydrophobic part of the surfactant prevents crystal growing in one crystallographic direction. Therefore, zeolites with sheet-like crystals are formed (Figure 2-7b). An alternative approach for the synthesis of 2D zeolites³⁵ by post-synthesis of germanosilicates will be discussed in detail in Section 2.2.2.

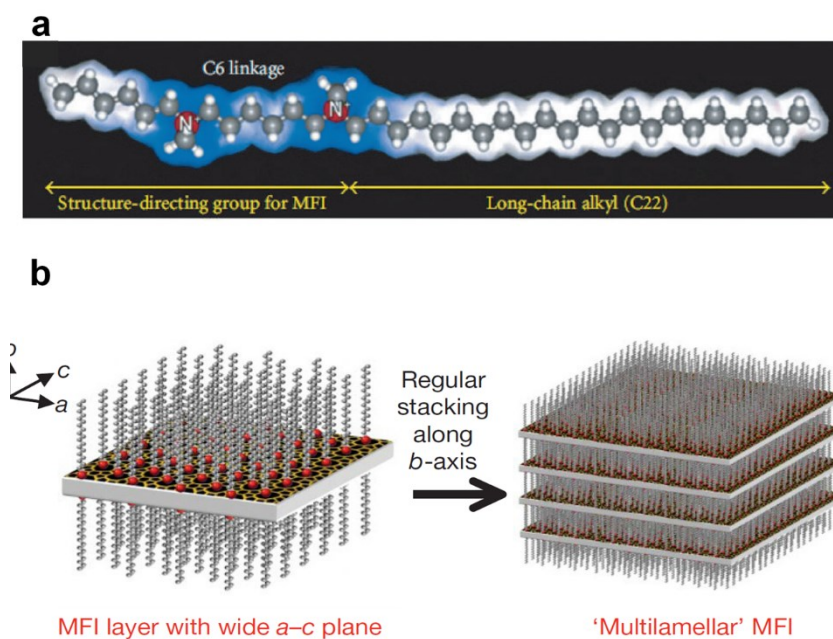
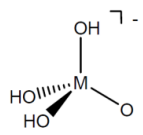
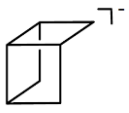
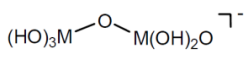
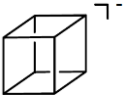
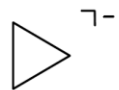

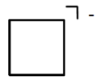
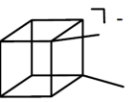
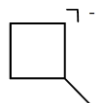
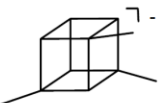
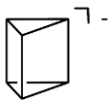
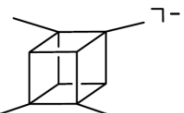


Figure 2-7. Surfactant molecules (a) and surfactant-templated synthesis of two-dimensional zeolite (b)³².

Not only organic SDA, but also framework-building elements, e.g., germanium, were reported to influence the structure of formed zeolite. The specific structure-directing propensity of germanium towards the formation of single-four-ring (S4R) and double-four-ring (D4R) germanate and mixed germanosilicate ions were revealed at the prenucleation step of crystallization process (Figure 2-6) using the ESI-MS technique³⁶⁻³⁸. The results shown in Table 2-2 demonstrate that, independently of the nature of SDA, the major species detected in Ge-containing pre-nucleating solutions were germanosilicate S4R- and D4R-type ions containing up to three Ge atoms (Table 2-2).

Table 2-2. List of species occurring in germanium-containing solutions with a molar composition of 1 TEOS : 1 GeO₂ : *x* TAAOH^a : 54 H₂O (with *x* = 2.2, 1.1, 0.55)³⁶.

Structure	Description & Formula	Ge atoms	Structure	Description & Formula	Ge atoms
	Monomer M ₁ O ₄ H ₃	0, 1		Open D4R M ₇ O ₁₉ H ₉	0,1
	Dimer M ₂ O ₇ H ₅	0, 1, 2		D4R M ₈ O ₂₀ H ₇	0,1,2
	3R M ₃ O ₉ H ₅	0, 1		D4R+M(OH) ₃ M ₉ O ₂₃ H ₉	0,1,2
	4R M ₄ O ₁₂ H ₇	0,1,2,3		D4R+2M(OH) ₃ M ₁₀ O ₂₆ H ₁₁	0,2,3
	4R+M(OH) ₃ M ₅ O ₁₅ H ₉	0,1,2,3		D4R+3M(OH) ₃ M ₁₁ O ₂₉ H ₁₃	0,3,4
	D3R M ₆ O ₁₅ H ₇	0		D4R+4M(OH) ₃ M ₁₂ O ₃₂ H ₁₅	0,3,4

^a: TPAOH, TMAOH, or TEAOH

In agreement with ESI-MS results showing the formation of D4Rs in Ge-containing solutions³⁸, a number of new D4R-containing zeolites was synthesized from germanate and germanosilicate reaction mixtures. During the last two decades, germanium has played a special role as an “inorganic structure director”³⁹, referred to (i) the selective location of Ge in the D4R domains of zeolites⁴⁰ and related (ii) tendency of Ge to stabilize such structures⁴¹ and (iii) the accelerated crystallization of zeolites containing D4R units in the presence of Ge in reaction mixtures⁴². The formation of Ge-containing small structural units (D4Rs or D3Rs)

allowed to synthesize a variety of new germanosilicate zeolites^{10, 39, 43-57}. Corma's group pioneered the design of germanosilicate zeolites and reported more than twenty new germanosilicates of ITQ-n family (Instituto de Tecnologia Quimica-n). Some examples of ITQ-n materials are shown in **Figure 2-8**⁵⁸.

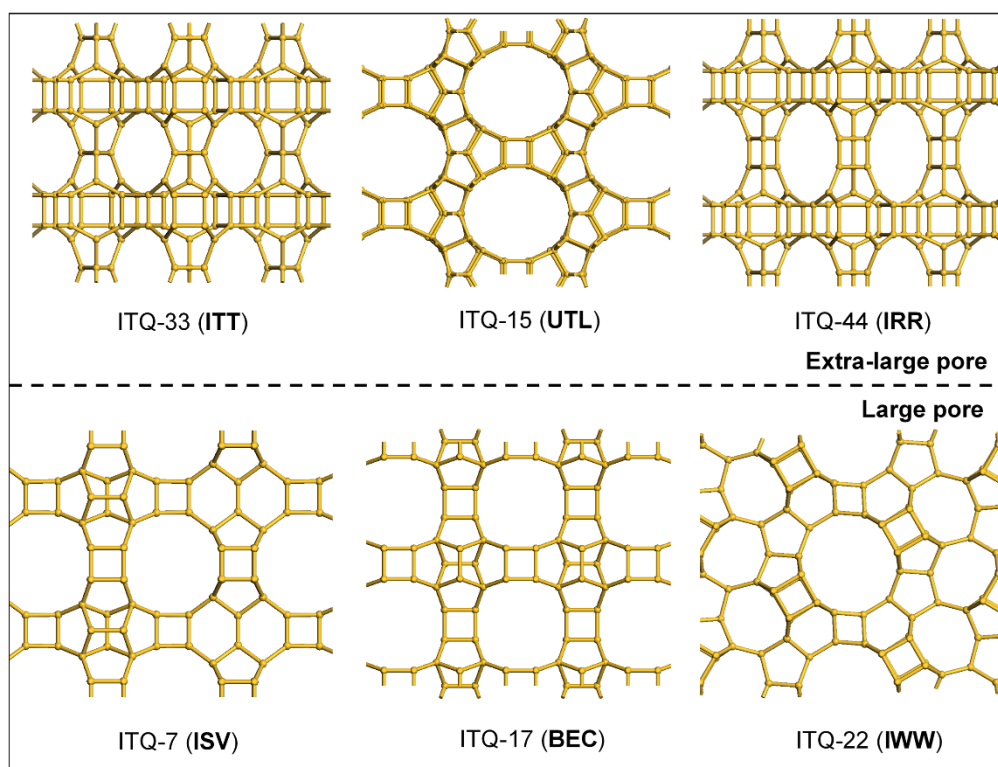


Figure 2-8. Large- and extra-large pore germanosilicate zeolites. T atoms are shown as spheres, oxygen atoms are not shown⁹.

D4R units have been rarely found in Ge-free zeolites. Among D4R-containing zeolites, only 2 were known as aluminosilicates (**UFI**⁵⁹, **LTA**⁶⁰), 5 are metallophosphates (**POR**⁶¹, **DFO**⁶², **ACO**⁶³, **-CLO**⁶⁴, **AFY**⁶⁵), 7 such zeolites were synthesized as purely silica materials in fluoride-containing medium (i.e., **AST**⁶⁶, **IFY**⁶⁷, **ISV**⁶⁸, **ITH**⁶⁹, **ITW**⁷⁰, **IWW**⁷¹, **STW**⁷²), and 25 were first discovered in germanate or germanosilicate forms. Thus, more than 90 % of the known germanosilicate zeolites contain D4R units (**Figure 2-9**), which is explained by a higher flexibility of the Si-O-Ge/Ge-O-Ge bond angles compared to Si-O-Si, which simplifies the formation of small D4R and D3R⁷³.

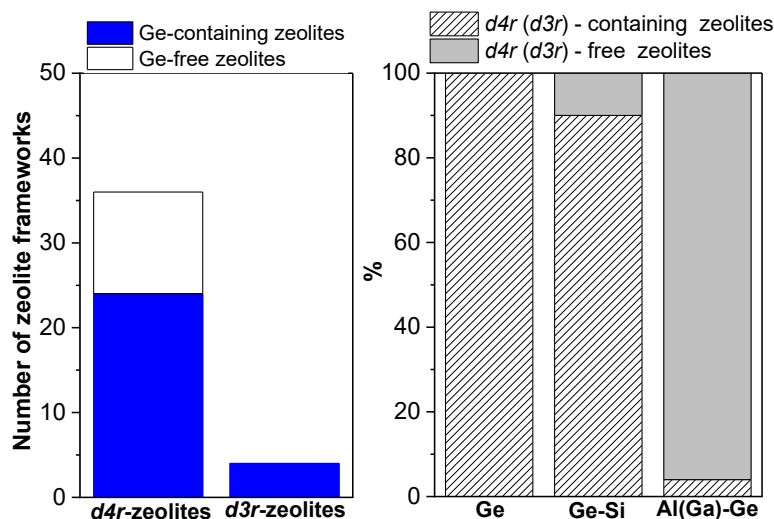


Figure 2-9. Overview of known D4R (D3R)- (left) and Ge-containing zeolites (right). The figure shows the relative fraction of Ge-containing (i.e., the sum of the number of known pure germanates, germanosilicates and alumino-/gallogermanates) and Ge-free zeolite having D4R/D3R units in the framework. Right figure shows the distribution of D4R-/D3R-containing and D4R-/D3R-free frameworks among germanate (Ge), germanosilicate (Ge-Si) and alumino-/gallogermanates (Al(Ga)-Ge)⁷³.

Owing to the existence of small rings (e.g., 3R, 4R), the frameworks of germanosilicate zeolites are normally characterized by high pore volumes (up to 40 % of total zeolite volume), low densities (up to 10.5 T/1000 Å³) and large pores, making them particularly suitable for transformations of bulky molecules⁷⁴. However, low hydrothermal stability and high costs of Ge significantly restrict practical application of Ge-containing zeolites. On the other hand, as it will be shown in Section 2.2, hydrolytic lability of Ge-O vs. Si-O bonds opens the way for a number of post-synthesis modifications allowing to tailor chemical composition, textural properties and even structure of germanosilicate zeolites.

2.2. Post-synthesis modification of germanosilicate zeolites

Post-synthetic modification of germanosilicate zeolites usually includes degermanation step (discussed in Section 2.2.1), which may be followed by metalation (discussed in Section 2.2.3) aimed at isomorphous incorporation of different metals for variation of acidic and catalytic properties of zeolites.

2.2.1. Tailoring textural properties

Post-synthesis demetallation is known as a facile method for the preparation of hierarchical zeolite materials, that is, zeolites containing transport mesopores. The most common demetallation methods involve dealumination⁷⁵, desilication⁷⁶, deboronation⁷⁷, detitanation⁷⁸, and recently degermanation⁷⁹, which are compared in this section.

Extraction of aluminum from the zeolite framework is conventional method for modification of both textural and acidic characteristics of a zeolite catalyst. Dealumination is generally achieved by liquid-phase acidic treatment (HCl, HNO₃) at temperatures between 50 – 100 °C or by steam treatment at relatively high temperatures around 550 °C. Both methods result in selective extraction of aluminum from zeolite framework, thereby increasing its Si/Al ratio and decreasing the concentration of Brønsted acid sites^{75, 80}. In turn, destruction of Al-containing fragments of a framework leads to the creation of intracrystalline (meso) pores. The textural characteristics can be adjusted depending on the chemical composition of a specific zeolite and the conditions of dealumination process (pH, temperature, the nature of acid, etc.)⁸¹⁻⁸³.

Another well-known approach to tailor textural properties of zeolites is desilication. Similarly to dealumination, desilication also produces hierarchical aluminosilicate zeolites and can be achieved in alkaline medium containing either organic or inorganic cations^{76, 84}. By changing the pH, temperature and duration of desilication treatment, the textural properties of a zeolite, such as mesopore volume, BET area, pore size distribution (PSD), can be tuned. In addition, Si/Al ratio of a zeolite and morphology of zeolite crystals strongly influence textural properties of desilicated materials. For Al-rich zeolites (Si/Al < 25), minor extraction of Si and limited mesopore formation were observed due to the “shielding effect” of Al species⁸⁵⁻⁸⁷. In contrast, Al-poor zeolites with Si/Al ratio of 25 – 50 are susceptible to desilication⁸⁸, which allowed to design hierarchical zeolite materials by alkaline treatment of ***BEA** (Si/Al = 35)⁸⁹, **FER** (27.5)⁹⁰, **MFI** (37)⁷⁶, **MOR** (45)⁷⁶.

In contrast to the already mentioned dealumination achieved under harsh conditions (e.g.,

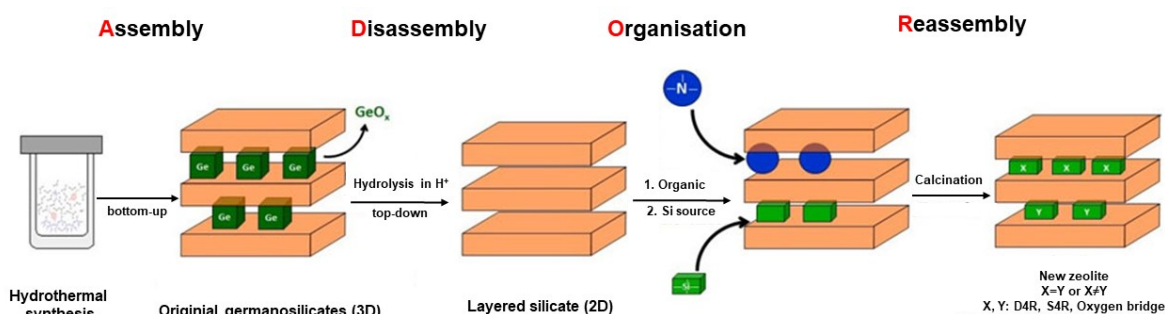
high temperature and concentration of acid or alkali), both deboronation and degermanation of a zeolite can be achieved in neutral medium at room temperature due to a higher hydrolytic lability of B-O/Ge-O bonds in comparison to Al-O^{73, 91, 92}. In particular, degermanation in mildly acidic or even aqueous medium has been shown as an efficient approach to adjust the textural properties of Ge-poor **IWW** and **ITH** zeolites⁷³. Layered materials (e.g., IPC-1P) can be formed upon the removal of Ge-rich D4R units from the **UTL** zeolite, as discussed in detail in Section 2.2.2. Tuel *et al.*⁹³ reported that the repetitive treatment of **IWW** zeolites with hydrochloric acid led to the extraction of the most of Ge and formation of mesopores without modifications of the framework topology. Kasneryk *et al.*⁷⁹ applied degermanation method for the preparation of micro-mesoporous zeolites **IWW** and **ITH** by changing the concentration of acid, duration and temperature of the treatment. The quantity of extracted Ge and volume of both micro and mesopores increased with the temperature of the treatment. Independently of the zeolite topology and chemical composition, the volumes of mesopores generated in **IWW** and **ITH** increased with the treatment time, while pH had negligible impact on the textural characteristics of micro-mesoporous **IWW** and **ITH** zeolites.

Thus, all demetallation methods, including degermanation, were proven as efficient for the formation of transport mesopores in zeolite catalysts. In turn, unlikely other demetallation approaches, degermanation appeared to be useful for the preparation of previously unknown 2D and 3D zeolites *via* ADOR strategy, as discussed in the next section.

2.2.2. Structure modification *via* ADOR strategy

The ADOR strategy for the preparation of new zeolites³⁵ includes several steps. At **Assembly** step, traditional hydrothermal synthesis of parent 3D germanosilicate zeolite is performed (see Section 2.1.2). **Disassembly** step includes the treatment of parent zeolite in neutral or acidic medium leading to degermanation (see Section 2.2.1). Disassembly of **UTL** germanosilicate with a framework constructed from Ge-rich D4Rs connecting silica slabs results in the formation of layered IPC-1P material. The next step involves the **Organization** of the layers formed at the second step upon treatment with organics such as amines or

dialkoxydialkylsilanes. Finally, at **Reassembly** step, the crystalline layers are condensed into new 3D zeolite. The steps of the ADOR process are shown in the **Scheme 2-1**.



Scheme 2-1. ADOR strategy for zeolite synthesis.

Studies⁹⁴⁻⁹⁶ on **UTL** zeolites showed that the disassembly step of the ADOR transformation involves two key processes: 1) “de-intercalation”, that is, bond-breaking of Ge-O(Si) or Ge-O(Ge) and leaching of the framework Ge from the interlayer area and 2) “rearrangement” of the leached species to form different interlayer-connecting units in a “daughter” zeolite.

It was also shown that the outcome of **UTL** zeolite disassembly is strongly affected by the acidity⁹¹. Under low acidic conditions ($[H^+] = 0 - 1.5 \text{ M}$), complete de-intercalation of interlayer units leads to the formation of layered precursor IPC-1P, giving **PCR** (10×8-ring pores) zeolite with interlayer O-bridge connectivities upon organization/reassembly⁹⁴. With the prolongation of the treatment in low-acidic medium, IPC-2P (precursor of **OKO** 12×10-ring pores zeolite containing -S4R- interlayer linkages) is formed. Meanwhile, the intermediate IPC-6P (precursor of the stage-structured ***PCS** zeolite containing both **OKO**- and **PCR**-type linkages in a 1:1 ratio) was found in the process of IPC-1P to IPC-2P transformation⁹⁶. In the medium acidic solutions (3 M of H⁺), IPC-7 (14×12- and 12×10-rings) with both D4Rs and S4Rs connections can be prepared⁹⁵, while high acidity (8 – 12 M of H⁺) favors disassembly of **UTL** into IPC-2P. Thus, various “isoreticular” zeolites with the same crystalline layers but different interlayer connectivities (**PCR**, **OKO**, ***PCS**, IPC-7) can be synthesized under the

control of the rate of “rearrangement” process by changing the pH of UTL disassembly (**Figure 2-10**)⁹⁷⁻⁹⁹.

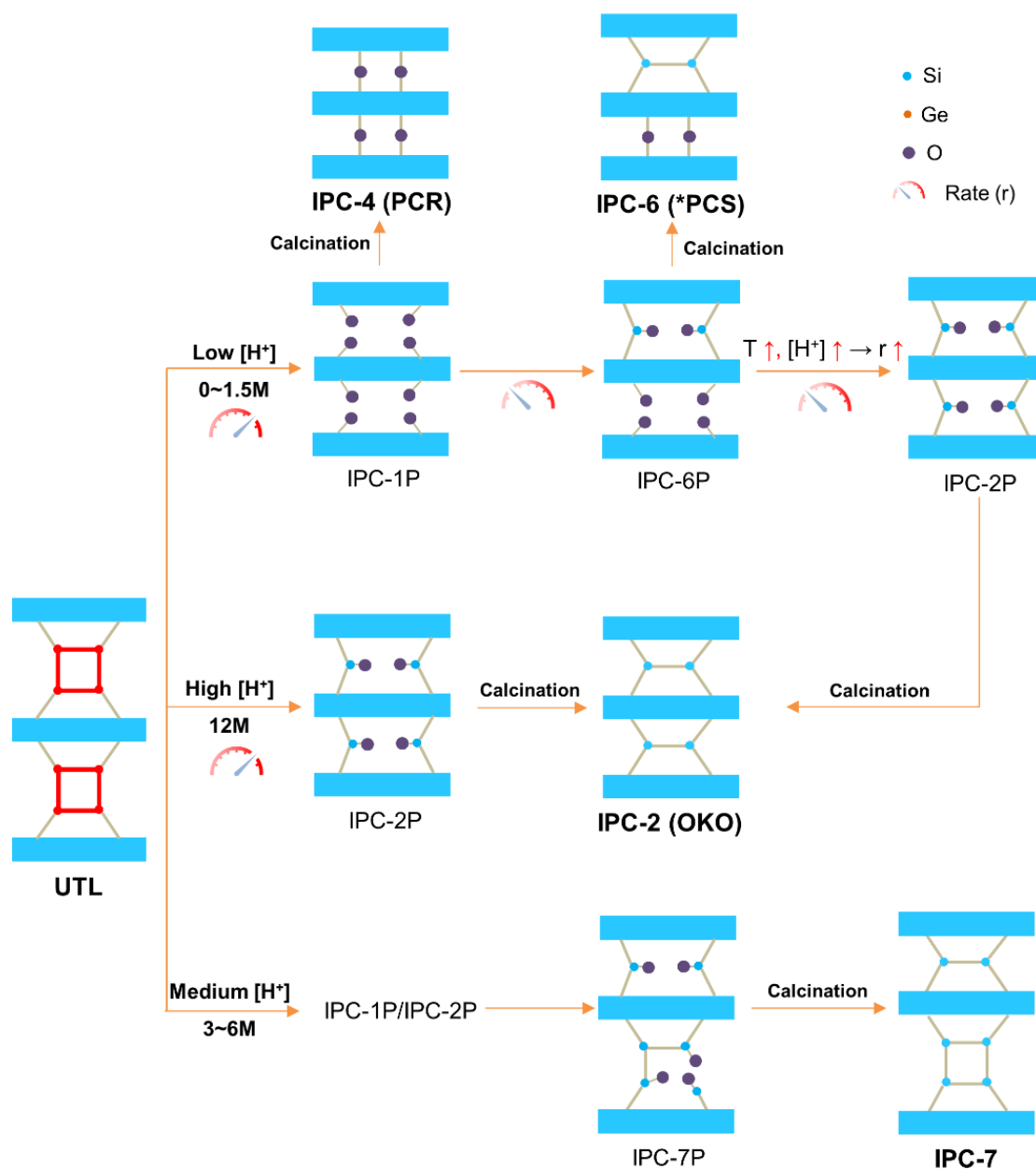


Figure 2-10. ADOR strategy for zeolite synthesis from germanosilicate zeolite UTL⁹⁷⁻⁹⁹.

While UTL was the first germanosilicate successfully subjected to the ADOR transformation, disassembly of another zeolite UOV into layered material (named IPC-12P and being a layered precursor of IPC-12 zeolite with -O- linkages between UOV-derived silica

layers) was recently reported proceeding in pure water or 0.1 M HCl aqueous solution^{44, 100}. However, the behavior of **UOV** zeolite producing IPC-12P material independently on pH and liquid-to-zeolite ratio apparently differs from that of **UTL**. This was explained by facile mass transport of the leached species, thus not participating in rearrangement process, off the interlayers space of IPC-12P through the pores perpendicular to **UOV** layers¹⁰⁰. In contrast to water-sensitive **UTL** and **UOV**, leaching of ~ 80 % of framework Ge in distilled water did not affect the structure ordering of two other germanosilicate zeolites **ITH** and **IWW**. To explain different hydrolytic stability of those zeolites, Tuel *et al.*¹⁰¹ attempted a detailed NMR study on the local structure of D4R units in Ge-rich **ITH** (Si/Ge = 4), **IWW** (Si/Ge = 6) and **UTL** zeolites (Si/Ge = 5). For that purpose, ¹H-²⁹Si CP/MAS NMR spectra of zeolites gently treated with water were analyzed respecting the signals of different (SiO)_{4-n}Si(OH)_n (0 ≤ n ≤ 4) groups. MAS NMR spectra of hydrolyzed materials revealed that D4R units in **UTL** zeolite possess four Ge atoms on the same face, resulting in the breakage of interlayer linkages in the presence of water. Conversely, in the case of **IWW** and **ITH** zeolites, the presence of Si-O-Si interlayer linkages in D4R is capable of maintaining zeolite structure against degradation by water. Nevertheless, water-stable **IWW** zeolite was recently successfully subjected to HCl-assisted disassembly under vapor-phase-transport conditions¹⁰². Similarly, ***CTH** zeolite containing a large quantity of Si-O-Si linkages was successfully disassembled through alkaline-assisted hydrolysis in the aqueous solution of 1 wt.% ammonia¹⁰³.

Application of the ADOR process in preparation of new germanosilicate zeolites has become an important milestone in materials design, as it enabled to prepare “isoreticular” zeolites with tuneable building units (i.e., -O-, -S4R-, -D4R-), connecting crystalline layers. None of those materials can be synthesized by hydrothermal synthesis method so far.

In addition to the synthesis of zeolites with hierarchical porosity and new zeolite structures, post-synthesis modification of germanosilicate zeolite opens the way for adjusting acidic properties and thus the catalytic performance of new zeolites by isomorphous substitution.

2.2.3. Alteration of chemical composition *via* isomorphous substitution

Recently, a number of T^{3+} and T^{4+} -substituted zeolites ($T = \text{Al, Ga, Fe, Ti, Sn, Zr, etc.}$) were synthesised by two-step post-synthesis demetallation-metalation method (**Figure 2-11**)⁷³,
83.

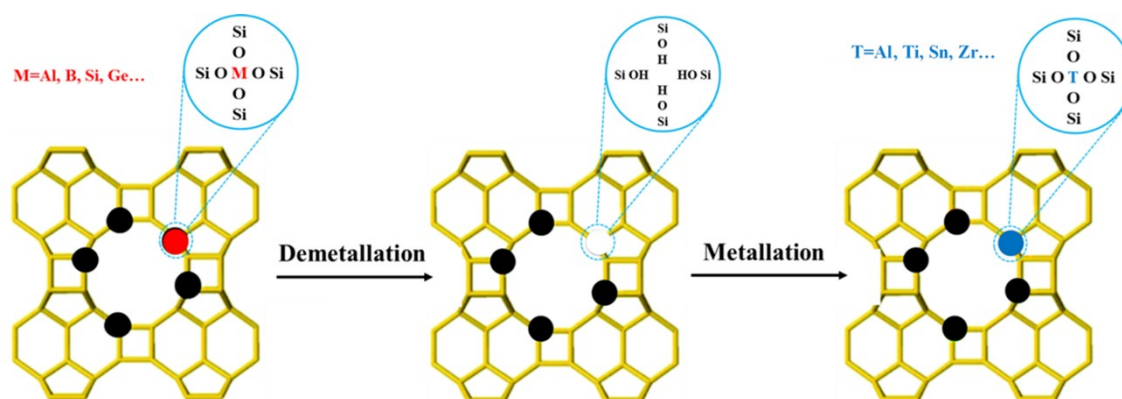


Figure 2-11. Schematic representation of post-synthetic demetallation-metalation method.

The methods used for post-synthesis incorporation of heteroelements into demetallated zeolite include: (i) gas-solid deposition (e.g., chemical vapor deposition) involving the treatment of a zeolite with volatile precursor of heteroelements at high temperature; (ii) liquid-phase routes (e.g., impregnation) involving the treatment of a zeolite with neutral, acidic or alkaline liquid source of heteroelements at moderate temperature; (iii) solid-state ion-exchange (SSIE) comprising a mechanical grinding of demetallized zeolite with the appropriate solid precursor followed by the treatment at high temperature (450 – 550 °C).

Post-synthetic incorporation of Al is the most frequently reported method to modify the acidic properties of boro-^{104, 105} and germanosilicate zeolites¹⁰⁶⁻¹¹⁰, in which liquid-phase route using $\text{Al}(\text{NO}_3)_3$ as an Al source is the most common one. Thus, Al was post-synthetically incorporated in a number of germanosilicate (e.g., **UTL, IWW, IWR, ITH**)¹⁰⁶⁻¹¹⁰ and borosilicate (e.g., **AFI, SFS, CON, *SFV**)¹⁰⁵ zeolites. This approach not only increases the

hydrothermal stability of zeolite frameworks but also generates strong Brønsted acid sites. Valtchev *et al.*¹¹¹ reported simultaneous degermanation and alumination of **BEC** zeolite by treatment of as-synthesized zeolite with polyaluminum hydroxide chloride solution allowing to incorporate Al into the framework and maintain zeolite structure. However, neither $\text{Al}(\text{NO}_3)_3$ nor polyaluminum hydroxide chloride solutions can be applied to small- and medium-pore zeolites (e.g., **MEL**) because the bulky Al^{3+} hexaquo complex is difficult to penetrate into \leq 10-ring pores¹¹². Sodium aluminate solution is another efficient Al source enabling simultaneous removal of framework Si and incorporation of Al instead¹¹³.

Recently, post-synthetic incorporation of Sn, Ti and Zr into zeolite frameworks to form isolated Lewis acid sites by demetallation-metalation method attracted significant attention due to the promising performance of respective materials in activation of oxygenated molecules¹¹⁴⁻¹²³.

Wu *et al.*¹²⁴ reported a gas phase metalation of dealuminated ***BEA** zeolites with tin tetrachloride at elevated temperatures *via* the reaction of the SnCl_4 molecules with the silanol defects. However, the formation of inactive extra-framework SnO_2 species could not be avoided. Alternatively, impregnation of Al-free ***BEA** zeolites with SnCl_4 in isopropanol was used to prepare an active Sn-substituted ***BEA** zeolite¹¹⁹.

Zr was grafted into ***BEA** zeolites *via* wet impregnation of dealuminated zeolites with ZrOCl_2 in DMSO solution. FTIR of absorbed pyridine and ^{29}Si MAS NMR spectroscopy revealed that Zr species were preferentially condensed with the terminal silanol groups on the external surface of the zeolite crystals rather than incorporated into internal silanol nests¹¹⁶. Solid-state ion exchange route was firstly reported by Hermans *et al.*¹²⁵ to prepare Sn- and Zr-***BEA** using Sn (II) acetate and Zr (IV) ethoxide as sources of Sn and Zr, respectively. Despite high metal loadings (10.1 and 7.7 wt.% for Sn- and Zr-***BEA**, respectively) were achieved, no bulk SnO_2 and ZrO_2 species were detected in the prepared materials.

Zr-substituted **BEC** zeolites were prepared by consecutive two-step procedure of zeolite degermanation/stabilization through solvothermal treatment with silica source (TEOS)

followed by the metalation with $ZrOCl_2$ in DMSO. Modified zeolite showed higher thermal stability and enhanced concentration of Lewis acid sites than the parent **BEC** zeolites, creating an active catalyst for Meerwein-Ponndorf-Verley (MPV) oxidation of 1,4-butanediol with levulinic acid¹²⁶.

Wu *et al.*¹²⁷ reported an effective method for post-synthesis isomorphous substitution of Ge for Sn in **UTL** zeolite. The treatment of SDA-containing **UTL** zeolite with 1 M HNO_3 allowed removal of Ge and resulted in partial destruction of the framework, restored upon further hydrothermal treatment with acidic solution of tin (IV) chloride pentahydrate. The most of Sn species were incorporated into the framework positions and showed coordination number 4 determined by UV-vis spectroscopy.

Recently, it has been reported that precise control of the acidic hydrolysis of **UTL** zeolites coupled with H_2TiF_6 -assisted isomorphous incorporation of Ti allowed to prepare Ti-containing IPC-2 (ECNU-14) and IPC-7 (ECNU-15) zeolites (**Figure 2-12**)¹²⁸.

Thus, the reported approaches for post-synthesis modification of porosity, structure and chemical composition of germanosilicate zeolites are based on degermanation or its combination with metalation. The post-synthetic degermanation can be considered as a facile route to zeolites with hierarchical micro-mesoporosity. The ADOR approach uses degermanation to transform the starting germanosilicate zeolite into new 2D or 3D zeolites. In turn, degermanation, followed by metalation is an easy and efficient method for tuning acidic characteristics of germanosilicate zeolites, thus, the hydrolytically stable zeolite catalysts can be prepared. Notwithstanding the efficiency of reported post-synthesis modification approaches for the enhancement of stability and tuning acidity of germanosilicate zeolites, they suffer from a loss of high cost of Ge since no recycling procedure was applied so far.

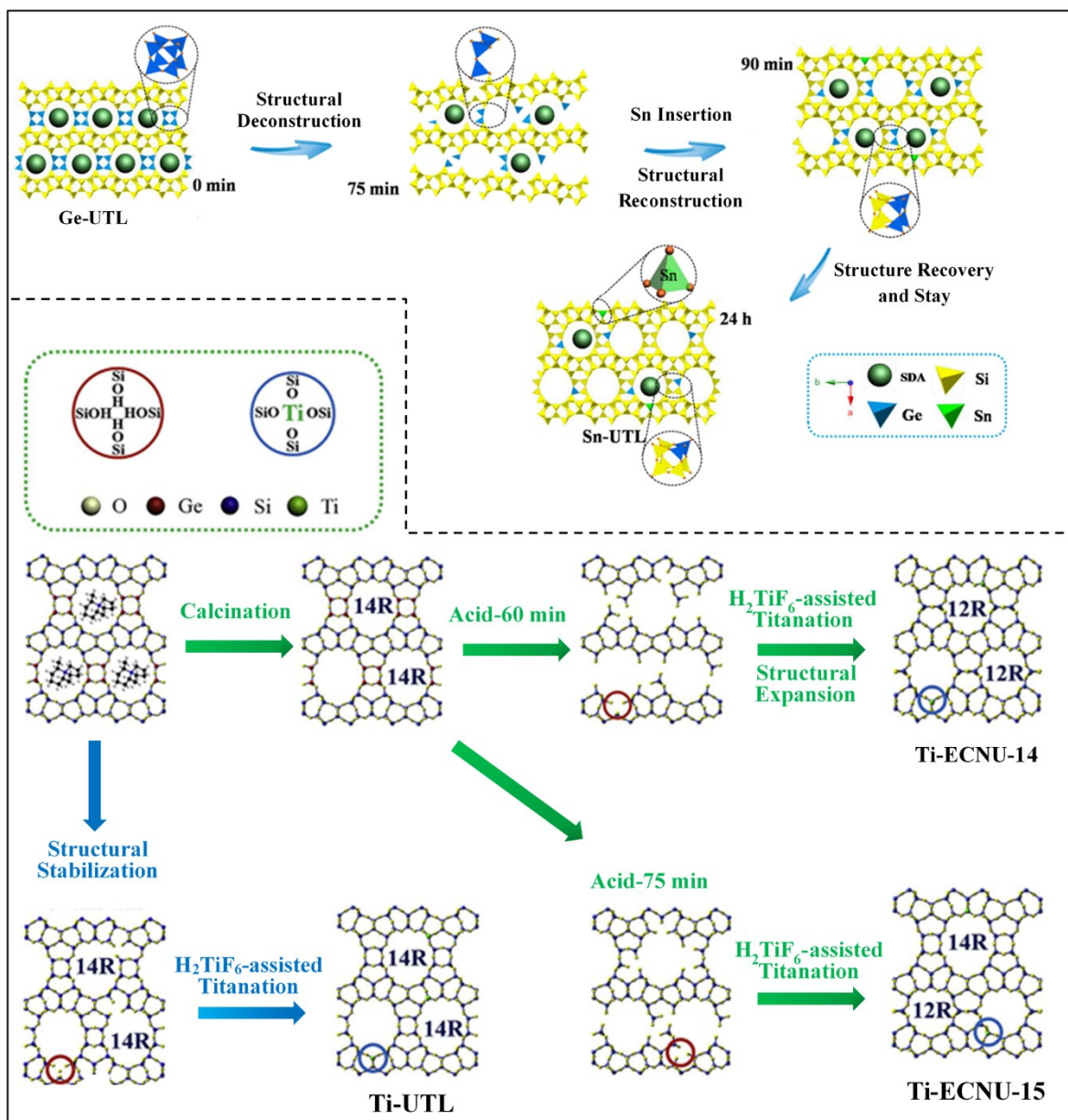


Figure 2-12. Post-synthesis functionalization of UTL zeolite by isomorphous incorporation of Sn (Ref.¹²⁷) and Ti (Ref.¹²⁸) atoms.

2.3. Zeolites as solid acid catalysts

Heterogeneous acid catalysis is one of the most important fields of catalysis. The tunability of acidic characteristics (nature and strength of acid sites) combined with uniform porosity and related shape-selectivity makes zeolites highly efficient solid acid catalysts. Both Brønsted and Lewis acid sites in zeolites are critical for chemical industry, while variation in the nature and characteristics of the acid site is essential to achieve high activity and selectivity of the zeolite

catalysts. Brønsted acid sites in zeolites can catalyze a variety of industrially important chemical reactions, such as fluid catalytic cracking (FCC), alkylation and isomerization of aromatics, isomerization of alkanes/alkenes, etc.¹²⁹⁻¹³³. Several specific zeolites are involved in these reactions, for instance, La-exchanged **FAU** zeolite is widely used for FCC¹³². Using ZSM-5 zeolite as additive in FCC allowed to increase propylene production¹³³. In industrially relevant acylation of anisole with acetic anhydride¹³⁴, the Brønsted acid sites of zeolite ***BEA** play a key role in the formation of an important acylium intermediate.

The first zeolite containing exclusively isolated Lewis acid sites was titanosilicate **MFI** (TS-1) prepared in 1983⁷. TS-1 is a major milestone in the field of oxidation catalytic reactions. The discovery of TS-1 made possible to perform numerous oxidation reactions (i.e., epoxidation of alkenes, oxidation of alkanes, hydroxylation of aromatics) under mild conditions using aqueous solution of H₂O₂ as the environmentally friendly oxidant rather than using homogeneous catalysts or expensive organic hydroperoxides or peracids^{129, 135, 136}.

Recently, modified germanosilicate zeolites were reported as promising catalysts of Brønsted (Section 2.3.1) and Lewis (Section 2.3.2) acid catalyzed reactions.

2.3.1. Brønsted acid catalysis

The important effect of acidic and structural properties of B-, Al-, Ga- and Fe-substituted germanosilicate zeolites was reported in several Brønsted acid catalyzed reactions^{79, 108, 109, 137}.

In the acylation of p-xylene with benzoyl chloride¹¹⁰, Ga-**UTL** with suitable strength of Brønsted acid centers, which enabled the efficient activation of substrate and facile desorption of the product, showed the highest selectivity and activity in this reaction. In turn, B- and Al-**UTL** materials with weak (i.e., not efficient in activation of reactants) and strong acid sites (i.e., strongly adsorbed the products) exhibited lower catalytic performance than Ga-**UTL**. Post-synthesis galliation and alumination of B-substituted **IWR** zeolite in acidic medium have been found to efficiently adjust its acidic and catalytic properties¹⁰⁶. Al- and Ga-substituted zeolites obtained under optimized conditions are characterized by a higher concentration of Brønsted

acid centers and superior catalytic performance (33 % and 99 % yield for Al- and Ga-**IWR** zeolites, respectively) in benzylation of p-xylene compared to the parent borogermanosilicate **IWR** zeolite (5 % yield).

In the Beckmann rearrangement of 1-indanone oxime¹¹⁰, B- and Fe-containing **UTL** materials with the weakest acidic sites showed higher conversion (100 % in 4 h) of the reactant than that of Al- and Ga-**UTL** with strong and medium acid centers, while high selectivity (100 %) of the targeted product was observed over all **UTL** samples.

In the transformation of aromatic hydrocarbons (e. g., disproportionation and alkylation of toluene, disproportionation/isomerization of trimethyl benzene), isomorphously substituted Al-, Ga-, Fe-containing **UTL** zeolites exhibited lower activity but higher selectivity in comparison to commercial aluminosilicate **MFI** and ***BEA** zeolites¹³⁸.

Post-synthesis Al-substituted germanosilicates differing in pore size were compared in the reaction of propanol tetrahydropyranylation in Ref.¹⁰⁹. Enhanced activity over the Al-substituted zeolites (up to 80 % yield of the product) due to the presence of Brønsted acid centers compared to the inactive germanosilicate zeolites was observed. The comparable yield (80 %) in large pore Al-**IWW** and extra-large pore Al-**UTL** zeolites has been explained by a smaller crystal size of the Al-**IWW** catalyst. On the other hand, both Al-**IWW** and Al-**UTL** showed 2 times higher yield than medium pore **ITH** zeolite (40 %). In turn, post-synthesis degermanation-alumination of Ge-rich **ITH** resulted in hierarchical micro-mesoporous materials. In comparison with traditional hydrothermally synthesized Al-**ITH** with similar chemical composition, post-synthetically aluminated hierarchical **ITH** exhibited a higher activity in the reaction of propanol tetrahydropyranylation (40 vs. 20 % yield)^{108, 137}.

Recently, the catalytic activity of a series of Al-containing IPC-n zeolites in liquid-phase tetrahydropyranylation of alcohols was correlated with the pore size of zeolite (**Figure 2-13**)¹³⁹. There was no difference in the activity (100 % yield) of Al-IPC-n zeolites when using ethanol as reactant, while for bulkier molecules (1-hexanol or 1-decanol) with a limited access to the internal active centers, the catalytic activity of Al-IPC-n zeolites increased with micropore

volume/size in the following sequence: IPC-4 (21 % of external acid sites, 36 %/6 % of 1-hexanol/1-decanol conversion) < IPC-6 (25 %, 42 %/18 %) < IPC-2 (29 %, 87 %/68 %) < IPC-7 (35 %, 95 %/78 %).

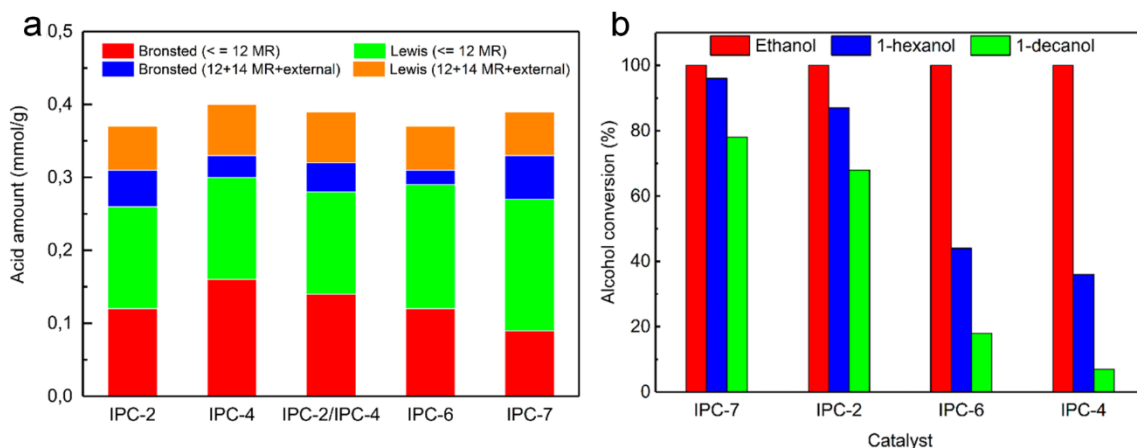


Figure 2-13. Distribution of acid sites in Al-IPC zeolites (a) and the conversion of alcohol in the tetrahydropyranylation of ethanol (b)¹³⁹.

2.3.2. Lewis acid catalysis

Lewis acid sites in zeolites are known as active centers in acid-catalyzed and oxidation transformations. Varying the nature of these sites (Ti, Sn, Zr, Hf, Ta and Nb, etc.) by isomorphous substitution allows one to tune the strength of Lewis acid centers and hence to design zeolite catalysts for particular process.

Germanosilicate zeolites were reported as active materials to catalyze the hydration of ethylene oxide to ethylene glycol¹⁰³, Baeyer-Villiger oxidation (BVO) of 2-adamantanone¹²⁷ and esterification of levulinic acid⁷⁹, although the nature of active centers in these materials remained controversial. For instance, Ref.¹⁴⁰ reported UTL as monofunctional Lewis acid zeolites while the existence of both Brønsted and Lewis acid centers in UTL was observed in Refs.^{45, 141}. Besides poorly understood acidic properties of germanosilicate zeolites, the hydrolytic lability of Ge-O bonds also limited their practical application.

In contrast to hydrolytically unstable germanosilicates, water-tolerant Ti- and Sn-, Zr-

containing zeolite catalysts are efficient in catalyzing epoxidation of alkenes and MPV reduction of carbonyl compounds with hydrogen peroxide and secondary alcohols, respectively. Isomerization of sugars, epoxidation of alkenes, and aldol condensation of biomass-derived oxygenates are among important reactions catalyzed with tetravalent element-substituted zeolites¹⁴.

Among T^{IV}-substituted zeolites, titanosilicates are exceptionally active and selective catalysts for the reaction of alkenes epoxidation²⁰. Corma *et al.*¹⁴² compared the catalytic behavior of octene epoxidation with H₂O₂ over Ti-, Sn-, Zr-containing *BEA zeolites. Only Ti-*BEA showed catalytic activity (initial rate: 11.0 mmol·h⁻¹) among different zeolites. Ti-substituted UTL zeolite with extra-large pores prepared *via* post-synthesis degermanation-metalation showed much higher activity (TOF: 29.3 h⁻¹) in the epoxidation of cyclohexene with bulky tert-butyl hydroperoxide (TBHP) than large pore Ti-*BEA (12.4 h⁻¹), Ti-MOR (2.2 h⁻¹), Ti-MWW (11.8 h⁻¹) and medium pore Ti-MFI (0.2 h⁻¹) zeolites with similar Si/Ti ratio¹²⁸. When small-size hydrogen peroxide was applied as the oxidant, Ti-*BEA and Ti-UTL exhibited similar catalytic performance in the epoxidation of cyclooctene, linalool and norbornene¹⁴³.

Sn-containing zeolites have been recognized for their excellent ability to selectively activate carbonyl groups, and therefore have been applied as catalysts for the BVO of aldehydes and ketones with H₂O₂. Among different T^{IV}-substituted *BEA (T = Ti, Sn, Zr) zeolites¹⁴², Sn-*BEA showed 5-times higher initial rate (26.8 mmol·h⁻¹) vs. Zr-*BEA (4.71 mmol·h⁻¹), while Ti-*BEA was inactive in this reaction. Wu *et al.*¹²⁷ investigated the BVO of cyclohexanone with H₂O₂ over Sn-substituted large- (*BEA) and extra-large pore (UTL) zeolites (**Figure 2-14a**). It was shown that germanosilicate UTL zeolites have a lower activity than Sn-containing UTL zeolites due to the lack of tetrahedrally coordinated Sn with stronger Lewis acidity than Ge. Post-synthesized nanocrystalline Sn-*BEA zeolites exhibited a higher activity compared to that of the hydrothermally synthesized microcrystalline Sn-*BEA zeolite, which was related to the higher accessibility of acid sites in zeolites with smaller crystal size. In addition, Sn-UTL zeolite with extra-large pores exhibited excellent catalytic performance in BVO of

ketones even using bulky TBHP as the oxidant (**Figure 2-14b**), which was explained by the fewer diffusion restrictions for bulky substrate in the extra-large pores. Sn-containing *BEA zeolite with strong Lewis acid sites was also shown to catalyze isomerization of glucose to fructose^{144, 145}. Comparable selectivity (~ 65 %) but higher activity (TOF = 500 vs. 305 h⁻¹) of post-synthesized vs. hydrothermally synthesized Sn-*BEA zeolite was observed¹⁴⁴.

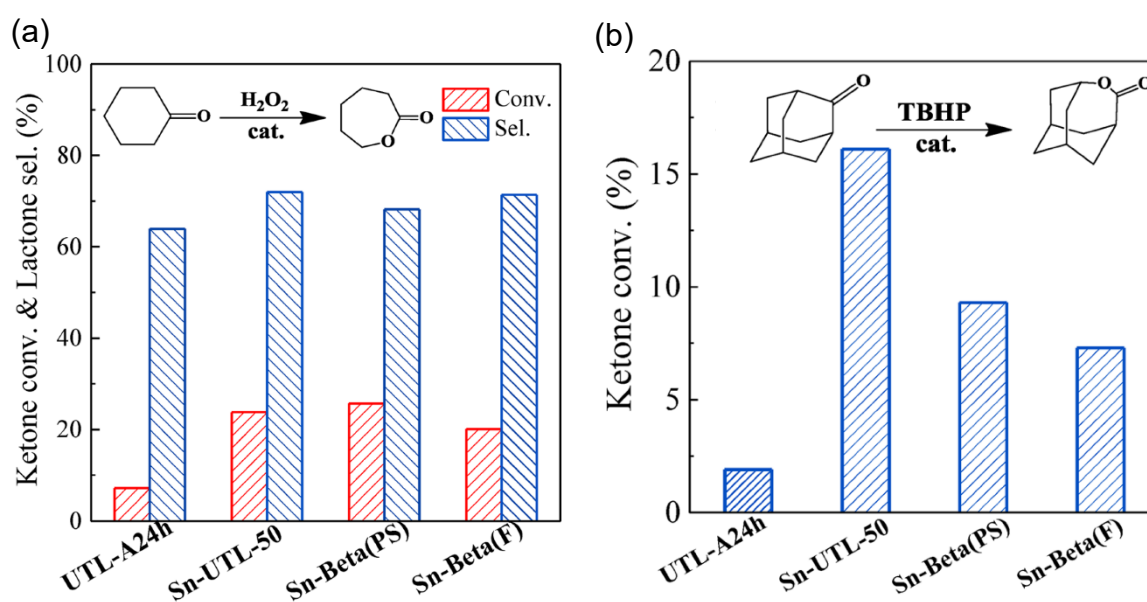


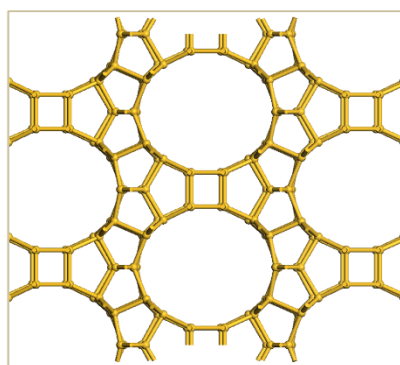
Figure 2-14. BVO of cyclohexanone with H₂O₂ (a) and TBHP (b) over UTL and *BEA zeolites. Sn-UTL-50 and Sn-Beta (PS) refer to the post-synthesized UTL and *BEA zeolite, respectively. Sn-Beta (F) refers to the hydrothermal synthesized *BEA zeolite in F-containing system. UTL-A24h refers to the calcined sample of as-synthesized UTL zeolite treated with 1 M HNO₃ (190 °C, 24 h) in a Teflon-lined stainless-steel autoclave¹²⁷.

Zr-containing zeolites showed distinctive catalytic performances in many Lewis acid-catalyzed reactions, such as MPV reduction^{126, 146-148} and aldol condensation^{149, 150}. MPV reduction of cinnamaldehyde to the cinnamyl alcohol was performed over both Al-containing and Al-free Zr-*BEA zeolites with the same Si/Zr ratio. Both materials showed a high selectivity (> 95 %) to the targeted product, while a higher conversion over Al-free Zr-*BEA (80.6 %) was reported in comparison with the corresponding Al-containing zeolite (59.1 %) ¹⁵¹.

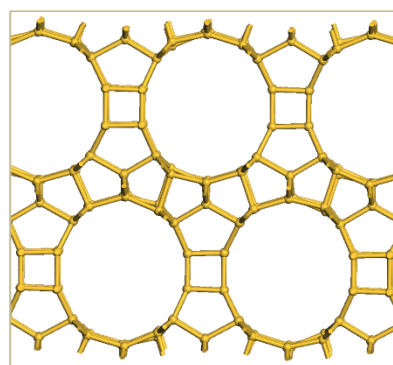
Zr-**BEC** zeolite prepared by post-synthesis degermanation-metalation exhibited a higher catalytic activity (initial rate: $12 \pm 2 \text{ mmol}\cdot\text{g}^{-1}\cdot\text{h}^{-1}$) in the MPVO reaction of 1,4-butanediol with levulinic acid in comparison with those of Zr-***BEA** (initial rate: $5.2 \pm 0.8 \text{ mmol}\cdot\text{g}^{-1}\cdot\text{h}^{-1}$) obtained by traditional hydrothermal synthesis¹²⁶. The aldol condensation of different aldehydes with acetone in toluene as a solvent was used to test the catalytic performance of Zr- and Sn-***BEA**. It was shown that Zr-***BEA** exhibited the highest activity with more than 90 % conversions and up to 97 % selectivity toward the targeted product¹⁴⁹. Zr- and Sn-containing ***BEA** zeolites were further applied in MPV reduction of furfural¹⁵². Zr-***BEA** showed a higher turnover frequency of 1.8 min^{-1} vs. Sn-***BEA** (0.5 min^{-1})¹⁵³.

Thus, germanosilicate zeolites with unusual structure/extra-large pores are promising for the transformation of bulky molecules, however, a lack of strong (Brønsted/Lewis) acidity and instability of germanosilicates limit their practical use in catalytic reactions, such as, acylation, alkylation, epoxidation, etc. Post-synthesis introduction of trivalent (Al, Ga, B etc.) and tetravalent (Ti, Sn, Zr, etc.) heteroelements into the framework of zeolites has been proven as an efficient approach to tailor the properties of acid sites in zeolite catalysts. However, there is still a need for improvement of cost-efficiency of the existing post-synthesis modification methods by their coupling with recovery and recycling of expensive Ge – one of the goals of this thesis. In this work, **ITH**, **IWW**, **UTL**, and ***CTH** germanosilicates were used as model zeolites (**Figure 2-15**).

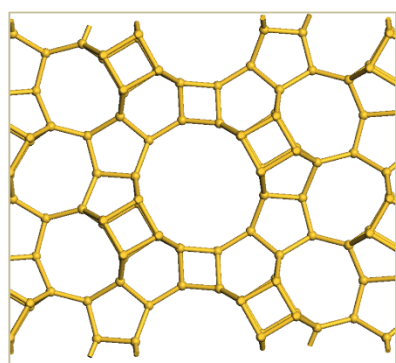
This thesis is arranged as follows: Section 3 describes the detailed protocols of zeolite synthesis and post-synthesis, characterization and catalytic tests; Section 4 outlines the experimental results related to (i) the catalytic activity and nature of active sites in germanosilicate **IWW** and **UTL** zeolites (Section 4.1); (ii) design of Lewis acid zeolites by post-synthesis of germanosilicates coupled with Ge recovery/recycling (Section 4.2); (iii) controlling primary stages of ADOR transformation of **UTL** zeolite (Section 4.3); Section 5 provides concluding remarks and some perspectives.



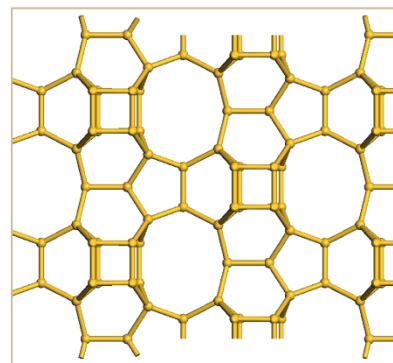
UTL (14×12)



***CTH** (14×10)



IWW (12×10×8)



ITH (10×10×9)

Figure 2-15. Germanosilicate zeolites with different topologies studied in the thesis.

3. Experimental part

3.1. Chemicals and materials

Chemical name	Quality	Company	Formula
1-octene	≥ 99.5 %	Sigma-Aldrich	CH ₃ (CH ₂) ₅ CH=CH ₂
1,2-dimethylimidazole	98 %	Sigma-Aldrich	C ₅ H ₈ N ₂
1,4-butanediol	99 %	Sigma-Aldrich	HO(CH ₂) ₄ OH
1,4-dibromobutane	99 %	Sigma-Aldrich	Br(CH ₂) ₄ Br
1,4-dioxane	99.8 %	Sigma-Aldrich	(CH ₂) ₄ O ₂
1,5-dibromopentane	97 %	Sigma-Aldrich	Br(CH ₂) ₅ Br
1,6-dibromohexane	96 %	Sigma-Aldrich	Br(CH ₂) ₆ Br
2-butanone	≥ 99.0 %	Sigma-Aldrich	C ₂ H ₅ COCH ₃
3-methylbenzyl chloride	98 %	Alfa Aesar	C ₈ H ₉ Cl
acetone	≥ 99.9 %	Sigma-Aldrich	CH ₃ COCH ₃
acetonitrile	≥ 99.9 %	Sigma-Aldrich	CH ₃ CN
aluminum nitrate nonahydrate	> 98 %	Sigma-Aldrich	Al(NO ₃) ₃ ·9H ₂ O
Ambersep® 900(OH), ion exchange resin		Alfa Aesar	
*BEA-12.5	CP814E	Zeolyst	Si/Al = 12.5
*BEA-25	CP814Q	Zeolyst	Si/Al = 25
*BEA-75	CZB-150	Clariant	Si/Al = 75
borosilicate glass filter		P-Lab	
chloroform	99.9 %	Lachner	CHCl ₃
cyclohexanone	≥ 99.9 %	Sigma-Aldrich	(CH ₂) ₅ CO
cis-(2,6)-dimethylpiperidine	98 %	Sigma-Aldrich	C ₇ H ₁₅ N
deuterium oxide	99.9 %	Sigma-Aldrich	D ₂ O
diethyl ether	99.9 %	Lachner	(C ₂ H ₅) ₂ O
ethanol	99.8 %	Penta	CH ₃ CH ₂ OH
ethyl acetate	99.9 %	VWR	CH ₃ COOC ₂ H ₅

		Chemicals	
ethylene glycol	99.8 %	Sigma-Aldrich	HOCH ₂ CH ₂ OH
furfural	99 %	Sigma-Aldrich	C ₄ H ₃ OCHO
germanium oxide	> 99.99 %	Alfa Aesar	GeO ₂
glycerol	≥ 99.5 %	Sigma-Aldrich	HOCH ₂ CH(OH)CH ₂ OH
heptane	99 %	Sigma-Aldrich	C ₇ H ₁₆
hydrogen peroxide	30 %	Sigma-Aldrich	H ₂ O ₂
hydrochloric acid	37 %	Sigma-Aldrich	HCl
hydrofluoric acid	48 %	VWR Chemicals	HF
isopropanol	≥ 99.5 %	LACHNER	(CH ₃) ₂ CHOH
mesitylene	98 %	Alfa Aesar	C ₆ H ₃ (CH ₃) ₃
methanol	99.8 %	Sigma-Aldrich	CH ₃ OH
n-dodecane	99 %	Sigma-Aldrich	CH ₃ (CH ₂) ₁₀ CH ₃
nitric acid	69 %	VWR Chemicals	HNO ₃
N-methylpyrrolidine	97 %	Sigma-Aldrich	C ₅ H ₁₁ N
N,N,N',N'-tetramethyl-1,6-hexanediamine	99 %	Sigma-Aldrich	C ₁₀ H ₂₄ N ₂
N,O-bis(trimethylsilyl)trifluoroacetamide	≥ 99.0 %	Sigma-Aldrich	CF ₃ C[=NSi(CH ₃) ₃]O Si(CH ₃) ₃
pyridine	≥ 99.5 %	Penta	C ₅ H ₅ N
silica, fumed		Sigma-Aldrich	SiO ₂
sodium hydroxide	98 %	Penta	NaOH
sodium sulfate	> 99 %	Sigma-Aldrich	Na ₂ SO ₄
tetraethoxysilane	98 %	Sigma-Aldrich	Si(OC ₂ H ₅) ₄
tin (IV) chloride solution, 1.0 M in heptane		Sigma-Aldrich	SnCl ₄

tin (IV) tetrachloride pentahydrate	98 %	Sigma-Aldrich	SnCl ₄ ·5H ₂ O
titanium (IV) chloride solution, 1.0 M in toluene		Sigma-Aldrich	TiCl ₄
toluene	99.8 %	Sigma-Aldrich	C ₆ H ₅ CH ₃
trimethylamine solution 31-35 wt.% in ethanol		Sigma-Aldrich	(CH ₃) ₃ N
trimethylchlorosilane	≥ 99.0 %	Sigma-Aldrich	(CH ₃) ₃ SiCl
zirconium (IV) chloride	≥ 99.5 %	Sigma-Aldrich	ZrCl ₄

3.2. Synthesis of organic structure directing agents

Hexamethonium (HM) dihydroxide, SDA for the synthesis of **ITH** zeolite was prepared according to the procedure reported in Ref.⁵⁰. Typically, 18.7 g 1,6-dibromohexane and 41.3 g of trimethylamine solution (31-35 wt.% in ethanol) were added into 100 ml ethanol and refluxed for 48 h. The solids were separated and washed with diethyl ether.

1,5-bis-(methylpyrrolidinium)pentane (MPP) dihydroxide, SDA for the preparation of zeolite **IWW** was prepared based on the procedure reported in Ref.⁴⁶. 18.8 g of 1,5-dibromopentane and 20.0 g N-methylpyrrolidine were mixed in 150 ml acetone and refluxed for 20 h. The obtained products were collected by filtration and washed with acetone.

(6R,10S)-6,10-dimethyl-5-azoniaspiro[4.5]decane hydroxide (DMAD), SDA of **UTL** zeolite was synthesized based on Ref.³⁹. Typically, 61.3 g 1,4-dibromobutane was added into the solution of sodium hydroxide (11.4 g NaOH in 280 ml H₂O) and then the mixture was heated up to 80 °C. After that, 32.1 g of cis-2,6-dimethylpiperidine was added dropwise under vigorous stirring. The mixture was kept stirring for 24 h at 100 °C. Subsequently, the solution was cooled down by immersing the flask into an ice bath. Then NaOH pellets were added slowly until forming the oily product on the top of solution. After complete crystallization, the solid product was participated and collected by filtration, followed by extraction with chloroform. The solution (SDA in chloroform) was dried in anhydrous sodium sulphate for overnight. After that, the solution was collected and partially evaporated (100 – 200 ml of

residual volume). The SDA was extracted from the solution and washed with diethyl ether for 3 times.

1,2-dimethyl-3-(3-methylbenzyl)imidazolium hydroxide (DMBI), SDA of *CTH was synthesized based on Ref.¹⁵⁴. 42.2 g of 3-methylbenzyl chloride was mixed with 28.8 g of 1,2-dimethylimidazole in toluene (300 ml). Subsequently, the mixture was refluxed under vigorous stirring for 48 h at 110 °C. After cooling, the products were collected by filtration and washed with ethyl acetate.

All obtained solid products were dried under vacuum overnight and ¹H NMR was used for the confirmation of SDA structure after dissolution in deuterium oxide.

The SDAs recovered in dihalogenide forms were ion-exchanged into hydroxide form using anionic exchange resin (OH-type of Ambersep® 900) (8 mmol SDA/g resin). After that, the excess of water in SDA solution was evaporated at pressure $p = 35$ Torr and temperature $T = 35$ °C until the concentration of hydroxide was equal to ~ 1.0 M.

3.3. Synthesis of zeolites

3.3.1. Zeolite ITH

Ge-rich ITH was synthesized using TMHDA as the SDA according to Ref.⁴⁸. Firstly, GeO₂ was dissolved in TMHDA solution (1 M), it was followed by the addition of silica source (TEOS). After evaporating the excess of water and ethanol (formed due to hydrolysis of TEOS), the obtained mixture with the composition of 0.67 SiO₂ : 0.33 GeO₂ : 7 TMHDA : 44 H₂O : 1.4 HF was heated in Teflon stainless-steel autoclave at 175 °C under static conditions for 3 days. Solid products were recovered by filtration, washed with deionized water and dried at 60 °C overnight. The as-synthesized zeolites were calcined at 650 °C for 6 h with a ramp of 1 °C·min⁻¹ under the air flow to eliminate the template.

Ge-poor ITH was synthesized using the same procedure as Ge-rich ITH but with a lower amount of Ge in the reaction mixture and using HM as SDA⁶⁹. The mixture with a composition

of 0.90 SiO₂ : 0.09 GeO₂ : 0.25 HM : 0.5 HF : 5 H₂O was heated at 175 °C with rotation (60 rpm) for 14 days. The final products were recovered by filtration, washed with deionized water, and dried at 60 °C for overnight. The obtained samples were calcined at 550 °C for 6 h with a heating rate 1 °C·min⁻¹ under air flow to remove the template.

Obtained **ITH** sample was designated as **ITH-n** (n refers to the Si/Ge ratio according to chemical analysis).

3.3.2. Zeolite IWW

IWW zeolites were synthesized using MPP(OH)₂ as SDA according to Ref.⁴⁶. For the synthesis of germanosilicate **IWW** zeolites, appropriate amounts of GeO₂ were dissolved in MPP(OH)₂ under stirring, it was followed by the addition of TEOS. After evaporating the excess water/ethanol, the reaction suspension with the composition of 0.8 SiO₂ : 0.2 GeO₂ : 0.25 MPP(OH)₂ : 10 H₂O was heated in Teflon stainless-steel autoclave at 175 °C for 7 days under static conditions.

Sn-substituted **IWW** zeolites were prepared from a gel with a composition 0.66 SiO₂ : 0.33 GeO₂ : 0.0083 SnO₂ : 0.25 MPP(OH)₂ : 3.5 H₂O as reported in Ref.¹⁵⁵. GeO₂ was firstly dissolved in MPP(OH)₂ followed by the addition of TEOS. After that, the required amount of tin (IV) tetrachloride pentahydrate was introduced. The reaction mixture was stirred for overnight at room temperature to evaporate the excess of water/ethanol. When the required molar composition was achieved, the mixture was heated in Teflon stainless-steel autoclave at 175 °C under static for 23 days.

Solid products were collected by filtration, washed with deionized water, dried at 60 °C for overnight and further calcined at 580 °C for 6 h under air flow. Obtained germanosilicate and Sn-substituted **IWW** samples were designated as **IWW-n** and **Sn-IWW_{hydro}**, respectively.

3.3.3. Zeolite UTL

Germanosilicate **UTL** zeolites were prepared as reported in Ref.³⁹. The composition of the starting mixture was (1.2 - x) SiO₂ : x GeO₂ : y DMAD : 30 H₂O (x = y = 0.4 for Ge-rich **UTL**,

$x = 0.24$, $y = 0.65$ for Ge-poor **UTL**). Firstly, GeO_2 was dissolved in the solution of DMAD under stirring. Then, fumed silica was introduced into the solution. Subsequently, the reaction mixture was crystallized at 175 °C under agitation for 7 days. It was followed by the filtration, washing with deionized water, drying at 60 °C for overnight, and calcination at 550 °C for 6 h in air flow. Obtained **UTL** zeolites were designated as **UTL-n**.

3.3.4. Zeolite *CTH

***CTH** zeolites were prepared as reported in Ref.¹⁵⁴ using DMBI as SDA. The reaction mixture (0.8 SiO_2 : 0.2 GeO_2 : 0.5 DMBI : 0.5 HF : 10 H_2O) was crystallized at 175 °C under static conditions for 30 days. Typically, GeO_2 was dissolved in the solution of SDA (~ 1 M), it was followed by the addition of silica source (TEOS). Subsequently, the reaction mixture was stirred at ambient environment for 8 h to hydrolyze TEOS and evaporate ethanol, HF was further added dropwise with additional stirring for 2 days until full evaporation of the excess water. After filtration, washing with deionized water and drying at 60 °C for overnight, the recovered samples were calcined at 580 °C for 6 h in air flow. Obtained ***CTH** samples were designated as ***CTH-n**.

3.4. Post-synthesis modification

3.4.1. Germanium leaching

Calcined germanosilicate zeolites were treated with nitric or hydrochloric acid (solid/liquid ratio is 20 g/l) of different concentrations (0, 0.1, 1, and 4 M) at various temperatures (25 or 80 °C) for 1 or 16 h. The hydrolyzed zeolites were separated from the leaching solution *via* microfiltration with MF-Millipore™ Membrane Filter paper (0.025 μm pore size) or filtration with Fisher Scientific qualitative filter paper (grade 601), washed subsequently with the same volume of the respective acid solution, and dried at room temperature for overnight. The leaching solution (solution of initial treatment + washing) was analyzed by chemical analysis to evaluate the fraction of extracted Ge, while degermanated samples were further subjected to

metalation (Section 3.4.5) for post-synthesis incorporation of hetero-elements (Ti, Sn, Zr). The hydrolyzed samples were designated as “**Zeolite- x - y M Acid- T °C- τ h**” or “**Zeolite- x -H₂O- T °C- τ h/ n ””, in which x and y refer to Si/Ge ratio in parent zeolite and the concentration of acid, respectively, T , τ and n refer to the temperature, duration and multiplicity of the treatment, respectively.**

3.4.2. Ge recovery/recycling

Calcined **IWW-5** zeolites (10 g) were hydrolyzed in distilled water (1000 ml) at room temperature for 3 times (16 h for each time). The leaching solution was obtained after the separation of degermanated zeolite by microfiltration or filtration. A solid product (GeO₂ according to XRD) was recovered from the leaching solution after the evaporation of excess water at $T = 65$ °C and $p = 30$ atm.

The recovered GeO₂ was subsequently used as a source of Ge for the hydrothermal synthesis of zeolite samples according to the procedures described in Section 2.1.2. Thus obtained zeolites were named as **Zeolite ^{x} -SDA _{n}** , wherein “zeolite” refers to the topology of formed zeolite based on XRD, x refers to the method of GeO₂ recovery, i.e., microfiltration or filtration, n refers to the type of added SDA and synthesis conditions, i.e., **IWW**, **ITH** or **UTL**.

3.4.3. ADOR transformation

3.4.3.1. Water-methanol medium

Calcined **UTL** zeolites (1 g) were added to water-methanol solutions with different compositions (**Table 3-1**) preheated to 60 °C. Samples were periodically collected for 24 h. The solid products were obtained by centrifugation, washed with anhydrous methanol, air-dried at ambient temperature and further calcined at 550 °C for 6 h.

Table 3-1. Water-methanol solutions used for a slow disassembly of the UTL zeolite.

Methanol concentration, wt.%	m (water), g	m (methanol), g
100	0	160
60	64	96
40	96	64
20	128	32
0	160	0

3.4.3.2. Al-containing water-methanol medium

1 g of calcined UTL zeolite was added to 160 ml of 1 M Al(NO₃)₃ water-methanol solution (methanol concentration = 40 wt.%) preheated to 60 °C. Samples were periodically collected for 60 days. The solid product was obtained by centrifugation, washed with anhydrous methanol, air-dried at ambient temperature and further calcined at 550 °C for 6 h.

3.4.4. Post-synthesis stabilization of germanosilicate zeolites

UTL stabilization. 0.3 g of calcined UTL zeolites were mixed with 30 ml of 1 M HCl ethanol solution. An additional silica source was introduced into the mixture (1 mmol TEOS/g zeolite)^{109, 156} with further stirring for 30 min, and then the mixture was treated under hydrothermal conditions at 175 °C for 24 h. Then, zeolites were obtained by filtration, washed with anhydrous ethanol, and dried at 60 °C. This treatment procedure was repeated 2 times.

***CTH stabilization.** 0.3 g of calcined *CTH zeolites were mixed with 30 ml of 6 M HCl and autoclaved at 100 °C for 10 h¹⁰³. Solid samples were recovered by filtration, washed with anhydrous ethanol and dried at 60 °C.

Both solid UTL and *CTH products were calcined at 550 °C for 6 h at a rate of 1 °C·min⁻¹. The final stabilized sample was denoted as **Zeolite(S)-n** (n is Si/Ge ratio according to chemical analysis).

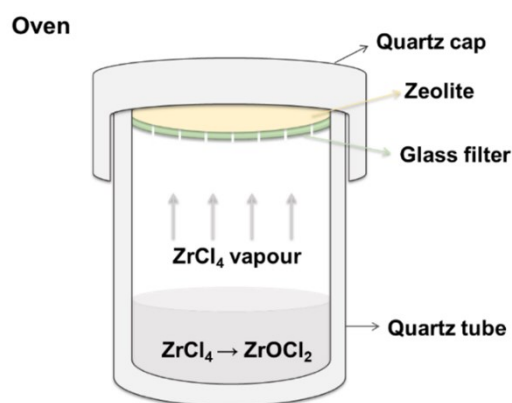
3.4.5. Lewis acid zeolites by post-synthesis treatment of germanosilicates

Titanium chloride (IV) (1 M solution in toluene), tin chloride (IV) (1 M solution in heptane)

and zirconium chloride (IV) were used as the Ti, Sn and Zr sources, respectively.

Ti- and Sn-containing zeolites were prepared by wet impregnation method. Degermanated zeolites were firstly dried at 450 °C for 4 h to remove the adsorbed water. The activated zeolites were treated with Ti- (0.25 M of TiCl_4 in toluene) or Sn- precursor (0.45 M of SnCl_4 in heptane) (solid/liquid ratio is 20 g/l) at 95 °C for 4 days in the nitrogen atmosphere. Solid products were obtained by filtration, washed sequentially with the respective solvent and anhydrous methanol to ensure the removal of all unreacted metal precursors. Further calcination at 450 °C for 4 h with $1\text{ °C}\cdot\text{min}^{-1}$ allowed to obtain Ti- and Sn-substituted samples, named as **Zeolite/Ti_{post}** and **Zeolite/Sn_{post}**.

Zr-substituted zeolites were prepared by means of vapour-state ion-exchange method^{157, 158}. The synthesis was carried out in a quartz crucible with self-sealing as shown in **Scheme 3-1**. Firstly, degermanated zeolites (0.25 g) were placed in the quartz cap of the crucible and activated at 450 °C for 4 h to remove adsorbed water. After the temperature decreased to 250 °C, the quartz tube with anhydrous ZrCl_4 powder (0.5 g) was placed into the oven. Zeolite sample and metal precursor were separated with the thermally stable borosilicate glass filter, which can withstand a temperature of 500 °C. The vapor-phase treatment of a zeolite took place at 300 °C for 10 h at a rate of $1\text{ °C}\cdot\text{min}^{-1}$. Finally, the glass filter and quartz tube were removed from the oven and samples were further calcined at 550 °C for 6 h to ensure completeness of metal incorporation. The samples were designated as **Zeolite/Zr_{post}**.



Scheme 3-1. Quartz crucible used for incorporation of Zr into zeolites.

3.4.6. Post-synthesis dealumination-metalation of commercial *BEA zeolite

Dealumination of *BEA zeolite (Si/Al = 12.5) was achieved by the treatment with 13 M HNO₃ at 373 K for 20 h (solid/liquid ratio is 50 g/l)¹⁵⁹, resulting in a highly siliceous zeolite (Si/Al = 96). Incorporation of Zr and Sn into dealuminated *BEA zeolite was performed using vapour-state ion-exchange procedure (Section 3.4.5) at 450 and 120 °C, respectively. ZrCl₄ and SnCl₄·5H₂O were used as the metal sources.

3.5. Characterization techniques

X-ray powder diffraction (XRD) was employed to examine the crystallinity of zeolite samples *via* Cu K α radiation ($\lambda = 0.154$ nm) at a scan rate of 0.25 $2\theta \cdot \text{min}^{-1}$, ranging from 3° to 40° on a Bruker AXS-D8 Advance diffractometer equipped with a Vantec-1 detector in the Bragg-Brentano geometry. Prior to measurement, samples were gently grinded and carefully loaded into the holder.

Scherrer equation was employed to estimate the mean crystallite size of crystals¹⁶⁰:

$$D = \frac{k\lambda}{\beta_{hkl} \cos\theta_{hkl}}$$

where k corresponds to the shape factor ($k_{\text{spherical nanoparticles}} = 0.94$); λ refers to the X-ray wavelength; β_{hkl} is full width at half the maximum intensity (FWHM); θ_{hkl} refers to the Bragg angle.

High-resolution transmission electron microscopy (HRTEM) images were taken by a JEOL NEOARM 200 F microscope with a Schottky-type field emission gun at 200 kV of accelerating voltage. Before the measurements, samples were uniformly dispersed in ethanol and then tinny drop was deposited onto the carbon-coated copper grids.

Scanning electron microscopy (SEM) (TESCAN Vega microscope) was used to assess the crystal morphology of zeolite. Si, Ge, Al, Ti, Sn, Zr contents in zeolite samples were determined by energy-dispersive X-ray spectroscopy (EDS) in the SEM.

Inductively coupled plasma optical emission spectroscopy (ICP-OES) measurements were

performed on ThermoScientific iCAP 7000 spectrometer, which was used to evaluate the Ge content in the leached solution.

Cary 300 ultraviolet-visible (UV-vis) spectrophotometer was employed to collect UV-vis spectra in the range of wavelength from 190 – 600 nm.

3Flex (Micromeritics) static volumetric apparatus was employed to measure Ar and N₂ adsorption/desorption isotherms at –186 and –196 °C, respectively. Before the measurements, zeolites were activated at 250 °C for 8 h under vacuum with a turbo molecular pump. BET method was applied to calculate the specific surface area in the relative pressure range (p/p^0) of 0.05 – 0.20¹⁶¹. Micropore volume (V_{micro})¹⁶² and pore size distribution¹⁶³ were evaluated *via* t-plot method and DFT model, respectively.

Fourier infrared spectroscopy (FTIR) measurements were performed on a Nicolet iS50 spectrometer with a transmission MCT/B detector, all spectra were collected by 128 scans with a resolution of 4 cm⁻¹ under ambient conditions.

The nature (i.e., Brønsted or Lewis), concentration and strength of acid sites were evaluated by FTIR of adsorbed pyridine^{164, 165}. Before the measurements, zeolites were pressed into self-supporting wafers with a density of 10 – 12 mg·cm⁻² and activated *in situ* at T = 450 °C under vacuum for 4 h. Adsorption of probe molecule was performed at partial pressure 3.5 Torr and T = 50 °C for 20 min, followed by desorption for 20 min at 50, 75, 100, 120, 150 and 200 °C. Py was degassed in freezing and thawing cycles prior to adsorption. The obtained spectra were analyzed, including normalization, baseline correction, integration, fitting, using Omnic 8.2 (Thermo Scientific) program.

For Sn-substituted zeolites, C_L at $T_{\text{des}} = 150 - 200$ °C were firstly evaluated using absorption band ca 1455 cm⁻¹ (ν_{19b} -LAS band) and molar absorption coefficient ϵ (L-Sn) = 1.42 cm· μmol^{-1} reported in Ref.¹⁶⁴. Furthermore, due to the overlap of H-bonded pyridine (ν_{19b} -H band at 1443 cm⁻¹) with ν_{19b} -LAS band at $T_{\text{des}} < 150$ °C, the application of ν_{19b} -LAS band for FTIR analysis of C_L in Sn-substituted zeolites is limited (details were shown in Section 4.2.3.2). In turn, using the intensity of ν_{8a} -LAS (1610 cm⁻¹) was shown sufficient for

quantification of C_L because the contribution of $\nu_{8a}\text{-H}$ (1596 cm^{-1}) can be eliminated even at lower temperature¹⁶⁶. Thus, C_L values for Sn-containing zeolites at $T_{\text{des}} < 150\text{ }^\circ\text{C}$ were calculated according to the equation¹⁶⁶:

$$C_L(T\text{ }^\circ\text{C}) = C_L(200\text{ }^\circ\text{C}) \cdot I_{1610}(T\text{ }^\circ\text{C}) / I_{1610}(200\text{ }^\circ\text{C})$$

where $C_L(T\text{ }^\circ\text{C})$ is the concentration of Lewis acid sites retaining pyridine after desorption at $T_{\text{des}} = T\text{ }^\circ\text{C}$ (T is 50, 75, 100, 120, 150 $^\circ\text{C}$); $I_{1610}(T\text{ }^\circ\text{C})$ is the intensity of a.b. at 1610 cm^{-1} after pyridine adsorption/desorption at $T\text{ }^\circ\text{C}$; $C_L(200\text{ }^\circ\text{C})$ is the concentration of Lewis acid sites determined based on a.b. at 1455 cm^{-1} at $T_{\text{des}} = 200\text{ }^\circ\text{C}$.

For Ti-, and Zr-substituted zeolites, the extinction coefficients for pyridine over LAS ($\sim 1608\text{ cm}^{-1}$) were determined in a separate experiment from the slope of a fitted straight line (x : total amount of adsorbed pyridine/cross sectional area of wafer ($\text{mmol}\cdot\text{cm}^{-2}$), y : integrated IR band area (cm^{-1})^{164, 167}. In order to evaluate the extinction coefficient, a specific dose of probe molecule (usually $0.15 - 0.45\text{ }\mu\text{mol}$) was stepwise inserted into the cell and after complete adsorption (monitored with Pfeiffer Vacuum CMR 363 gauge) spectrum was collected. Consecutive doses of probe molecule were adsorbed in zeolite wafer until reaching saturation of acid sites, i.e., a maintenance of the intensity of characteristic absorption band while adding new dose of a probe molecule.

²⁷Al MAS NMR spectra were used to identify the coordination of Al in zeolite samples, it was performed on a Bruker Advance III HD spectrometer ($B_0 = 9.4\text{ T}$, Larmor frequency of ²⁷Al is 104.2 MHz) using a thin-wall 3.2 mm zirconia rotor. The sample was packed into the rotor and rotated at a magic angle spinning rate of 15 kHz using a Bruker 3.2 mm HX CP-MAS probe. A pulse of $1.0\text{ }\mu\text{s}$ ($B1$ field approx. 95 kHz) with a relaxation delay of 1 s was applied, averaging 2048 transients. The spectra were referenced to a saturated solution of $\text{Al}(\text{NO}_3)_3$ in D_2O .

3.6. Catalytic tests

All catalytic reactions were performed in a multi-experiment workstation StarFish.

Catalysts were activated at 450 °C for 4 h before the catalytic testing. Samples of the reaction mixture were collected periodically, immediately centrifuged to separate the catalyst from the reaction mixture and analyzed using gas chromatography (GC, Agilent 7890B) equipped with HP-5 column (length: 30 m, diameter: 0.32 mm, film: 0.25 μm) FID detector and autosampler. The reaction products were identified by a Thermo Scientific® ISQ LT - TRACE 1310 GC/MS.

Conversion of a reactant (X), product yield (Y) and selectivity of a particular product at certain conversion (S) were calculated from the following equations:

$$X = \frac{n(\text{reactant})_0 - n(\text{reactant})_\tau}{n(\text{reactant})_0} \cdot 100 \%$$

$$Y = \frac{n(\text{product})_\tau}{n(\text{reactant})_0} \cdot 100 \%$$

$$S = \frac{Y}{X} \cdot 100 \% = \frac{n(\text{product})_\tau}{n(\text{reactant})_0 - n(\text{reactant})_\tau} \cdot 100 \%$$

where

$n(\text{reactant})_0$ and $n(\text{reactant})_\tau$ are amounts of reactant in reaction mixture at initial time and after specified time τ , respectively;

$n(\text{product})_\tau$ is an amount of a product formed in reaction mixture after specified time τ .

TOF values were calculated from the initial segment of conversion versus time plot ($t = 10 - 15$ min) as:

$$TOF = \frac{n(\text{reactant})_0 - n(\text{reactant})_\tau}{n(\text{acid sites}) \cdot \tau}$$

where

$n(\text{acid sites})$ is the amount of Sn-, Ti-, Zr-Lewis acid sites in the catalysts sample determined with FTIR spectroscopy of adsorbed pyridine or Ge sites determined by means of EDS.

Ketalization of polyols was performed by I. Podolean (Department of Organic Chemistry, Biochemistry and Catalysis, University of Bucharest) to study the catalytic properties of germanosilicate zeolites. 5 mg of catalyst, 1 mmol of polyols (i.e., ethylene glycol, glycerol or

1,4-butanediol) were added into the excess of acetone (5 or 25 mmol). The reactions were performed in glass vials equipped with magnetic stirrer at 25 or 80 °C for 3 h. Leaching test was performed as follows: the catalyst was removed from the reaction mixture by filtration after 1 h, the reaction solution was maintained under similar conditions for another 11 h and analyzed after 2 or 12 h of reaction as described below.

After specified time, the reaction mixture was cooled, followed by the addition of a small volume of ethanol (up to 1 ml) to solubilize the unreacted glycerol. The mixture was further centrifuged, filtered and dried with sodium sulphate to obtain the final solution (acetone + ethanol + products). Finally, reaction products were recovered by the slow evaporation of the final solution (200 µl) at 45 °C for overnight.

Before injection of products into the chromatographic column, it was necessary to perform silylation to enhance their volatility and to derivatize the free hydroxyls of polyols. With this purpose, the catalyst of pyridine (50 µl) was added into the derivatization agent (1 wt.% of trimethylchlorosilane in N,O-bis(trimethylsilyl) trifluoroacetamide, 150 µl) to start the derivatization reaction, which was carried out at 60 °C for half an hour. The molar ratio of substrate to derivatization agent was 1/3.

Ti-substituted zeolites were tested in **epoxidation of 1-octene** at 60 °C. In a typical run, 4.5 mmol of 1-octene, 0.25 g of mesitylene (internal standard), 8 ml of acetonitrile and 50 mg of catalyst were added into a three-necked vessel. The reaction was started by adding 2.3 mmol of hydrogen peroxide to the mixture.

Sn-substituted zeolites were tested in **BVO of cyclohexanone** at 80 °C. Typically, 50 mg of the catalyst was added to a solution consisting of cyclohexanone (2 mmol), mesitylene (internal standard, 0.16 g) and 1,4-dioxane (6 ml). The reaction was started by adding 2 mmol of hydrogen peroxide.

Sn-, and Zr-containing Lewis acid zeolites were tested in **MPV reduction of furfural**. 0.2 g of the catalyst and n-dodecane (internal standard) were added to 6 ml of isopropanol. The reaction mixture was heated to 80 °C and reaction was initiated by adding 96 mg of furfural.

4. Results and discussion

4.1. Structure-activity relationships for germanosilicate zeolite catalysts

To assess the nature of active sites in germanosilicate zeolite catalysts, the activity of large-pore **IWW** and extra-large pore **UTL** germanosilicate in ketalization of polyols was related to the number and strength of acid sites in studied zeolites.

4.1.1. Structural and acidic properties of IWW and UTL germanosilicates

XRD patterns (**Figure 4-1a**) confirmed the phase purity of **IWW** and **UTL** zeolite samples^{10, 46}. Both **IWW-7** and **UTL-4** zeolites exhibited type-I isotherms characteristic of microporous materials (**Figure 4-1b**). The micropore volume of the extra-large pore **UTL** ($0.21 \text{ cm}^3 \cdot \text{g}^{-1}$) was larger than that of the large-pore **IWW** zeolite ($0.11 \text{ cm}^3 \cdot \text{g}^{-1}$) in agreement with literature data^{10, 46}.

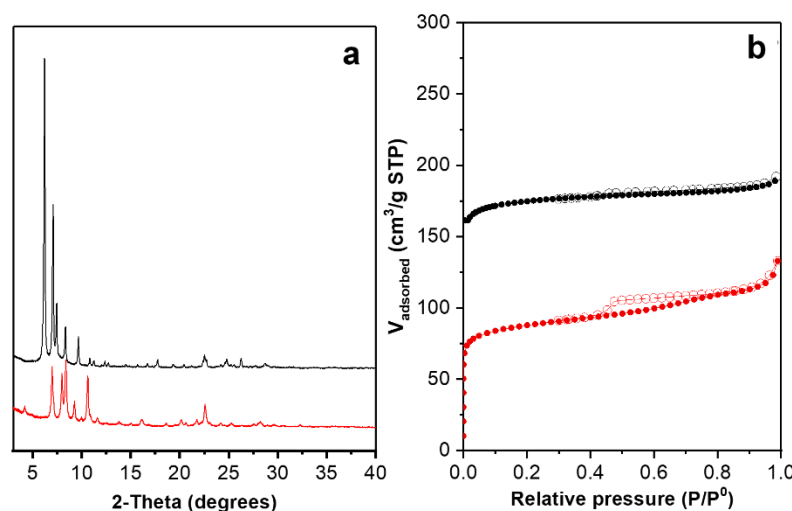


Figure 4-1. IWW-7 (—) and UTL-4 (—) zeolites: XRD patterns (a), N₂ adsorption (●) and desorption (○) isotherms (b).

SEM images indicated that **IWW-7** sample consists of agglomerated rectangular crystals with $0.5 \times 0.5 \times 0.5 \text{ }\mu\text{m}$ size (**Figure 4-2a**), while **UTL-4** zeolite is formed by uniform $30 \times 25 \times 1 \text{ }\mu\text{m}$ -size rectangular crystals (**Figure 4-2b**).

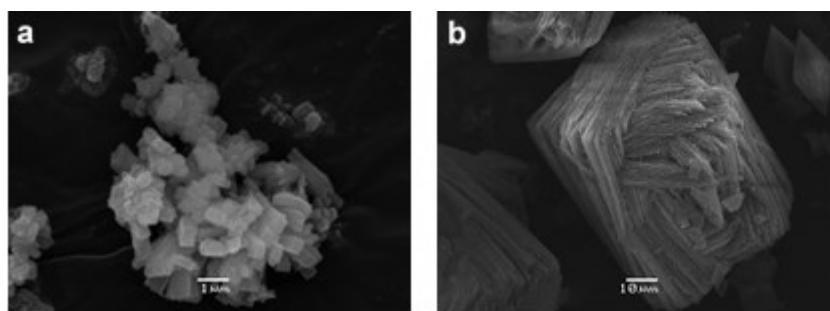


Figure 4-2. SEM images of germanosilicate zeolites: **IWW-7** (a) and **UTL-4** (b).

FTIR spectroscopy was employed to assess the acidity of germanosilicate zeolites. Consistent with the previous results^{137, 141, 168, 169}, both germanol (Ge-OH, 3660 – 3680 cm^{-1}) and silanol (Si-OH, 3740 cm^{-1}) groups were observed in **IWW** and **UTL** zeolites (**Figure 4-3a**). The band related to silanol groups in **IWW** zeolite is more intensive than that of **UTL**. This feature of **IWW** can be explained by a smaller crystal size and thus a higher external surface area accommodating terminal Si-OH groups (**Table 4-1**). The band at 3600 – 3400 cm^{-1} (H-bonded OH groups) is weaker and broader in the spectra of **IWW** and **UTL** zeolites activated at lower temperature (200 and 300 °C) than those activated at higher temperature (450 °C) evidencing the presence of residual adsorbed water at lower temperature.

Table 4-1. Chemical composition, textural properties, crystal sizes and acid sites concentrations of **IWW** and **UTL** zeolites.

Sample	Chemical composition, mol.%		Si/Ge	Textural properties		Crystal size, μm	Concentration of acid sites, $\text{mmol}\cdot\text{g}^{-1}$	
	Si	Ge		V_{micro} , $\text{cm}^3\cdot\text{g}^{-1}$	S_{ext} , $\text{m}^2\cdot\text{g}^{-1}$		C_B	C_L
	IWW-7	87.8	12.2	7	0.11	94	0.5×0.5×0.5	0.16 ^a 0.07 ^b 0.05 ^c
UTL-4	80.8	19.2	4	0.21	40	30×25×1	—	n.d. ^d

^a: $T_{\text{act}} = 200$ °C, ^b: $T_{\text{act}} = 300$ °C, ^c: $T_{\text{act}} = 450$ °C, ^d: n.d. - not determined due to the not-existing molar absorption coefficients

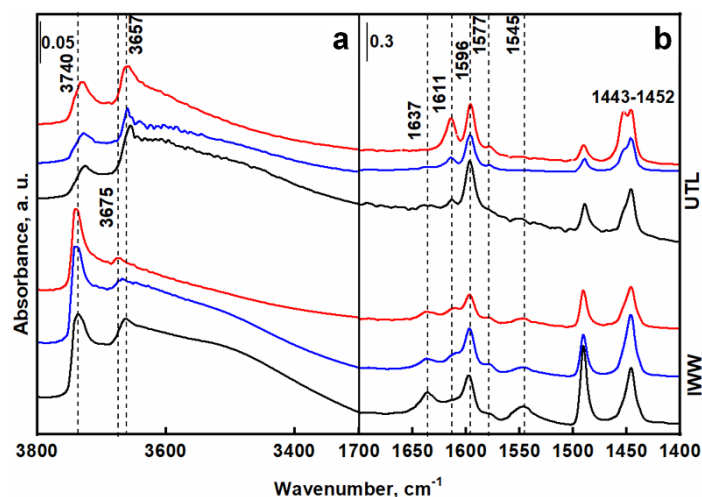


Figure 4-3. FTIR spectra of **IWW-7** and **UTL-4** zeolites upon activation at 450 (—), 300 (—), 200 °C (—) (a: region of OH- vibrations) and activation/adsorption of pyridine at 50 °C (b: region of Py-ring vibrations).

FTIR of adsorbed pyridine on both **IWW** and **UTL** samples showed three absorption bands (**Table 4-2**, **Figure 4-3b**): 1) physically adsorbed pyridine (Phys-Py), 2) H-bonded pyridine (H-Py), and 3) pyridine coordinatively bonded to Ge Lewis acid sites (LAS-Py).

Table 4-2. IR characteristic absorption bands of pyridine adsorbed in zeolites^{170, 171}.

Pyridine species	ν_{CCN} , cm^{-1}	
	ν_{8a}	ν_{19b}
Phys-Py	1577	1438
H-Py	1596	1443
LAS-Py	1600 – 1614	1445 – 1460
BAS-Py	1637	1545

Consistent with the reported results¹³⁷, the ν_{19b} absorption bands of LAS-Py (1445 – 1460 cm^{-1}) and H-Py (1443 cm^{-1}) overlapped, while their ν_{8a} bands (1600 – 1614 and 1596 cm^{-1}) were well-resolved in **IWW** and **UTL** zeolites. However, LAS in both zeolites were still hard to quantify as the molar absorption coefficient for the ν_{8a} band of LAS-Py cannot be determined due to the inevitable contribution of H-Py under various adsorption/desorption conditions (e.g., temperature, pyridine loading). Nevertheless, the ν_{8a} band of LAS-Py (1611 cm^{-1}) in **UTL** was

much more intensive than in **IWW** zeolite (**Figure 4-3b**), indicating a higher amount of LAS in the **UTL** germanosilicate. Although the Brønsted acidity in **UTL** zeolites was previously reported in Ref.¹⁴⁰, the characteristic bands of BAS-Py (**Table 4-2**) were not observed in FTIR-Py spectra of **UTL** zeolite upon activation at different temperatures (**Figure 4-3b**). In contrast to **UTL**, the spectra of **IWW** zeolite showed both ν_{19b} and ν_{8a} bands of BAS-Py (at 1545 and 1637 cm^{-1} , respectively, **Table 4-2** and **Figure 4-3b**). The concentration of Brønsted acid sites (calculated from ν_{19b} band at 1545 cm^{-1}) in **IWW** zeolites substantially decreased when pyridine desorption took place at $T_{\text{des}} = 100$ °C (**Figure 4-4a**). Thus, **IWW** germanosilicate showed a significantly weaker Brønsted acidity than commercial Al-containing ***BEA** zeolites reported to hold adsorbed pyridine up to $T_{\text{des}} = 350 - 400$ °C¹⁴¹.

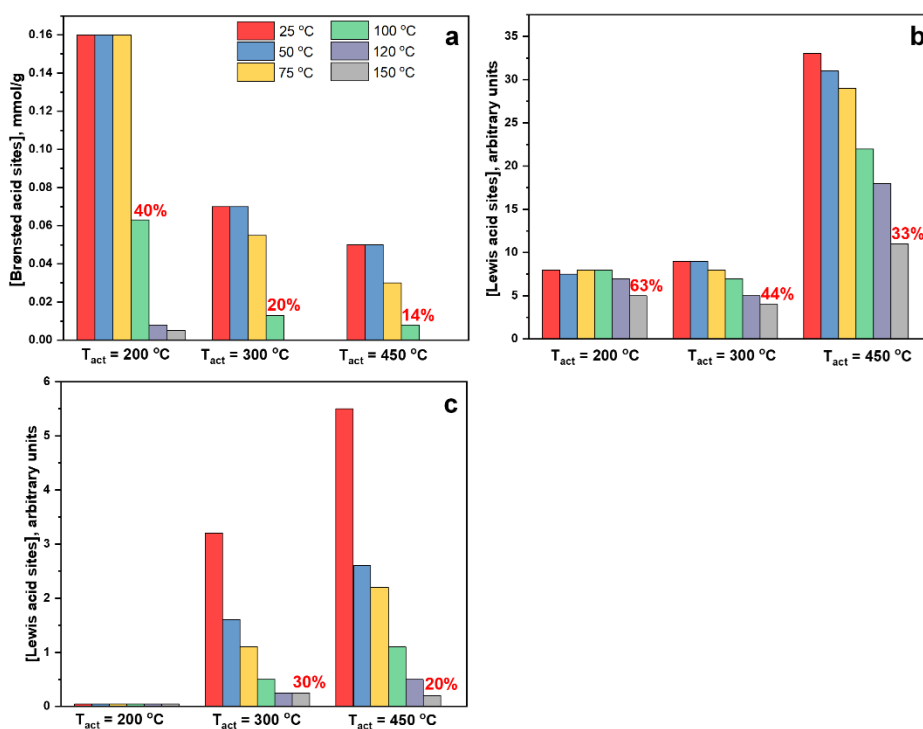


Figure 4-4. Concentration of acid sites in germanosilicate zeolites vs. T_{act} : C_B in **IWW** zeolite (a), C_L in **UTL** zeolite (b) and C_L in **IWW** zeolite (c). % numbers show the fraction of acid centers holding pyridine after desorption at $T = 100$ °C (a) or $T = 150$ °C (b, c).

In addition to a weak acid strength of Ge-BAS, their concentration in **IWW** zeolite decreases ($0.16 \text{ mmol} \cdot \text{g}^{-1}$ ($T_{\text{act}} = 200$ °C) \rightarrow $0.07 \text{ mmol} \cdot \text{g}^{-1}$ (300 °C) \rightarrow $0.05 \text{ mmol} \cdot \text{g}^{-1}$ (450

°C)) as the activation temperature increases (**Figure 4-4a**). The weakness of Brønsted acid sites associated with Ge and the alteration of concentration with the activation temperatures could be related to the H₂O-induced origin of BAS in germanosilicate, that is, the formation of BAS due to the adsorption of water molecules on LAS. In order to verify this hypothesis, FTIR spectroscopy was firstly employed to monitor dose-by-dose water adsorption over the activated ($T_{act} = 450\text{ °C}$) **IWW** zeolite, followed by the saturation with pyridine. Gradual increase in the amount of adsorbed water contributed to the progressive enhancing intensity of the BAS-Py band ($\nu_{19b} = 1545\text{ cm}^{-1}$) with simultaneously decreasing intensity of LAS-Py band ($\nu_{8a} = 1611\text{ cm}^{-1}$) (**Figure 4-5**).

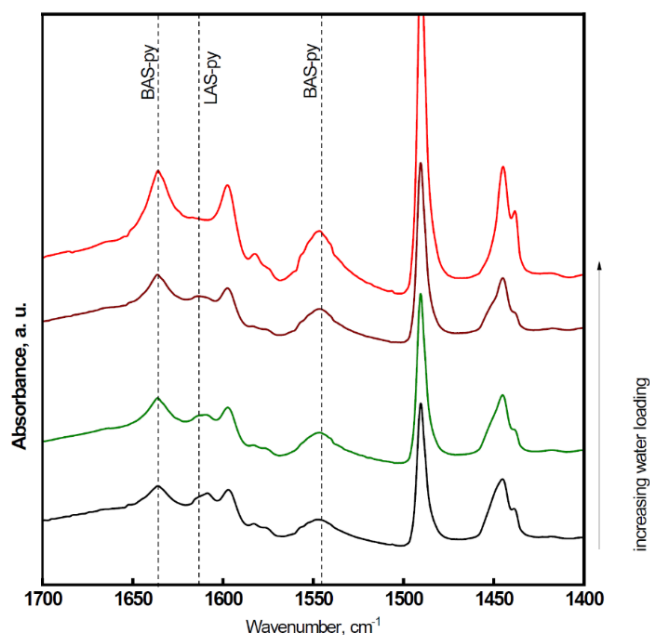


Figure 4-5. FTIR spectra of **IWW-7** zeolite after water (dose-by-dose) adsorption and further saturation with pyridine.

Similarly, it has been reported that the H₂O-induced formation of Brønsted acid centers takes place in Sn-containing ***BEA** zeolite¹⁷². By analogy with Sn-substituted ***BEA**, increasing intensity of BAS-Py coupled with decreasing intensity of LAS-Py in the FTIR spectra (**Figures 4-3b** and **4-5**) could imply similar mechanism for the conversion of Lewis-to-Brønsted acid site in Ge-containing **IWW** zeolite: 1) H₂O molecules are adsorbed on the

framework Ge atoms forming 5- or 6-coordinated Ge centers (e.g., LAS, $\equiv\text{Si-O-Ge(OSi)}_3 \rightarrow \equiv\text{Si-O-Ge(OSi)}_3(\text{H}_2\text{O}) \rightarrow \equiv\text{Si-O-Ge(OSi)}_3(\text{H}_2\text{O})_2$), 2) the adsorbed water molecule is polarized and deprotonated to form OH group with a hydroxonium nearby (e.g., $\equiv\text{Si-O-Ge(OSi)}_3(\text{H}_2\text{O})_2 \rightarrow \equiv\text{Si-(OH)-Ge(OSi)}_3(\text{OH})(\text{H}_2\text{O})$, BAS).

In turn, enhancing the activation temperature had a positive effect on the concentration of Lewis acid sites in UTL zeolite, e.g., the intensity of ν_{8a} at 1611 cm^{-1} (after desorption at $50\text{ }^\circ\text{C}$) for the sample activated at $450\text{ }^\circ\text{C}$ was approximately four times higher than that for the sample activated at $200\text{ }^\circ\text{C}$ (33 vs. 8, **Figure 4-4b**).

The result is consistent with the higher hydrolytic lability of UTL zeolite in comparison with IWW zeolite, Ge-O-Ge bonds in UTL zeolite are prone to hydrolyze rather than to form the acidic bridging groups at lower activation temperatures^{102, 173}. Therefore, the concentration of Lewis acid sites in UTL zeolite activated at $450\text{ }^\circ\text{C}$ (**Figure 4-3a**) reflects the number of 4-coordinated Ge atoms, which are accessible for pyridine adsorption. Conversely, after the activation at $200 - 300\text{ }^\circ\text{C}$ (**Figure 4-3a**), the residual adsorbed H_2O in UTL zeolite may lead to the hydrolysis of Ge-O(Si) bonds, thereby reducing the number of Ge atoms in the framework of zeolite and the concentration of LAS. It is worth noting that the number of acid centers (**Figure 4-4**) is almost independent of the chemical composition of the IWW and UTL zeolites (**Table 4-1**). This result may be explained by the spatial limitations of the interaction between pyridine and the adjacent acid sites (Ge) preferentially located in D4Rs⁷³.

4.1.2. Catalytic performance of IWW and UTL zeolites in ketalization of polyols

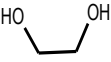
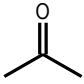
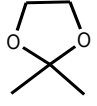
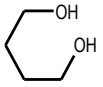
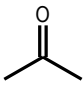
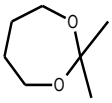
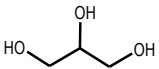
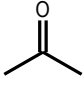
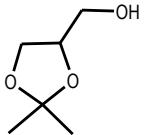
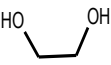
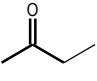
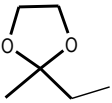
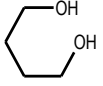
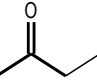
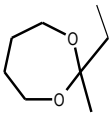
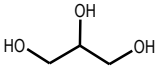
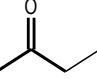
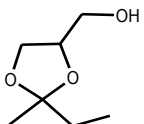
For reversible ketalization reaction (**Scheme 4-1**), the main limitation is the low equilibrium constant (2.66 under standard conditions¹⁷⁴).



Scheme 4-1. Ketalization of glycerol with acetone.

In order to solve this issue, it is necessary to shift the chemical equilibrium towards the formation of targeted ketal either by removing the product (H₂O) or by adding an excessive amount of reactant (ketone). In the current study, the second method was used. **Table 4-3** summarized the catalytic results of ketalization reaction of acetone or 2-butanone with a variety of polyols over **IWW** and **UTL** zeolites catalysts.

Table 4-3. Catalytic performance of **IWW** and **UTL** zeolites in polyols ketalization reactions.

Nr.	Polyol	Ketone	Main product	IWW		UTL	
				Conversion, %	Selectivity, %	Conversion, %	Selectivity, %
1				> 99	> 99	> 99	> 99
2				69	> 99	59	99
3				63	97	56	> 98
4				96	> 99	98	> 99
5				51	98	49	> 99
6				19	96	7	98

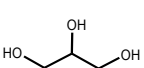
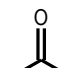
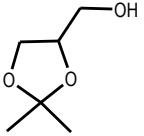
Reaction conditions: solvent-free, 5 mg catalyst, 5 mmol ketone, 1 mmol polyol, RT, T_{act} = 300 °C

The conversion of polyols ranged from 7 to > 99 %, while the selectivity for both zeolite catalysts was higher than 96 %. Meanwhile, increasing the size of polyol (ethylene glycol → glycerol → 1,4-butanediol) or ketone (acetone → 2-butanone) reduced the conversion of polyol

for both zeolites (**Table 4-3**). The results may indicate diffusion-controlled regime of the reaction for bulky reagents.

Table 4-4 compares the catalytic performance of germanosilicate zeolites with that of commercial large-pore aluminosilicate ***BEA** zeolites with Si/Al = 12.5, 25 and 75, possessing strong Brønsted and Lewis acid sites as reported in Ref.¹⁷⁵. In the case of **UTL**, which has the crystals (**Figure 4-2b**) elongated along 12- and 14-ring channels, the influence of diffusion limitations on the catalytic performance is especially pronounced. In ketalization of glycerol with acetone (**Table 4-4**), **UTL** showed the lowest conversions of glycerol (17 – 36 %) among germano- and aluminosilicates under the study. In turn, **IWW** germanosilicate showed glycerol conversions (41 – 56 %) comparable with ***BEA** aluminosilicate (49 – 53 %).

Table 4-4. Catalytic performance of **IWW**, **UTL** and ***BEA** zeolites activated at different temperatures.

Nr.	Polyol	Ketone	Main product	Catalyst (T_{act} , n_{ketone}/n_{polyol})	Conversion, %	Selectivity, %
1				UTL (450, 5)	17	96
2				IWW (450, 5)	41	96
3				IWW (450, 25)	> 99	> 99
4				UTL (300, 5)	27	97
5				IWW (300, 5)	56	98
6				UTL (200, 5)	36	97
7				IWW (200, 5)	46	98
8				*BEA-12.5 (450, 5)	53	98
9				*BEA-25 (450, 5)	57	96
10				*BEA-75 (450, 5)	49	96

Reaction conditions: solvent-free, 5 mg catalyst, 5/25 mmol ketone, 1 mmol polyol, RT, 3 h

The results show that even the weak acid sites in germanosilicate zeolites can catalyze the ketalization reaction.

Noticeably, as the activation temperature decreased, the conversion of glycerol over **IWW** and **UTL** zeolites increased. This result can be correlated with the decreasing concentration of Brønsted acid sites in **IWW** zeolite (**Figure 4-4a**) and the declining strength of Lewis acid sites in **UTL** zeolite (**Figure 4-4b**) at increased activation temperature, discussed in Section 4.1.1. Thus, the suitable temperatures for **IWW** and **UTL** activation were 300 and 200 °C, respectively. The yield of targeted solketal over ***BEA** zeolites decreased with increasing of Al concentration (**Table 4-4**). This result can be explained by increasing hydrophilicity of zeolite framework with Al concentration, which favors the adsorption of H₂O generated in the ketalization reaction (**Scheme 4-1**) and competing with ketone for the active sites¹⁷⁶. In fact, it has recently been reported that the hydrophobization treatment of aluminum-rich HY zeolite by organosilane surfactant can improve the efficiency of glycerol conversion in ketalization reaction¹⁷⁷. Similarly, hydrophobization of **MFI** zeolites also resulted in a higher activity¹⁷⁸. Conversely, the incorporation of Ge into some silicate zeolite frameworks allows to prepare zeolite catalysts with a weak acidity and moderate affinity towards water^{179, 180}. In addition, the adsorption of H₂O molecules on the Ge Lewis centers of Ge-containing zeolite may facilitate the *in situ* formation of more active Brønsted acid sites¹⁸¹ in agreement with results of FTIR spectroscopy (**Figure 4-5**) and evolution of the conversion of glycerol and selectivity to solketal versus reaction time (**Figure 4-6**). In the case of the germanosilicate zeolite catalysts, the conversion of glycerol increased obviously in the first 2 hours (from 32 to 53 % for **IWW** and from 18 to 32 % for **UTL** zeolite). In contrast to germanosilicates, ***BEA** zeolite showed the conversion around 52 % maintained it for the whole catalytic run (**Figure 4-6**). Importantly, when **IWW**, **UTL** or commercial zeolite catalysts were tested in glycerol ketalization under the same reaction conditions, no by-products, i.e., dioxane or mesityl oxide (formed upon condensation of acetone) are formed^{182, 183}. Moreover, over 99 % yield of solketal was achieved over **IWW** zeolite when the molar ratio of ketone/alcohol increased from 5 (39 % yield, **Table 4-4**, row 2) to 25 even at ambient conditions (**Table 4-4**, row 3).

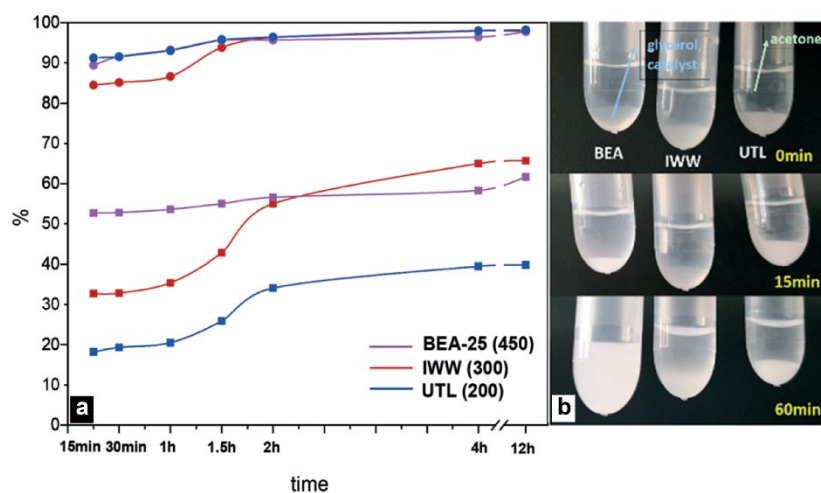


Figure 4-6. The variation of solketal selectivity (●) and glycerol conversion (■) with time (a). Appearance of the reaction mixtures after 15 and 60 minutes of reaction (b). Reaction conditions: solvent-free, 5 mg catalyst, 5 mmol acetone, 1 mmol glycerol, RT.

The results of the recycling test indicated that both **IWW** and **UTL** zeolite catalysts could be reused at least six times without significant changing in the conversion and selectivity (**Figure 4-7**).

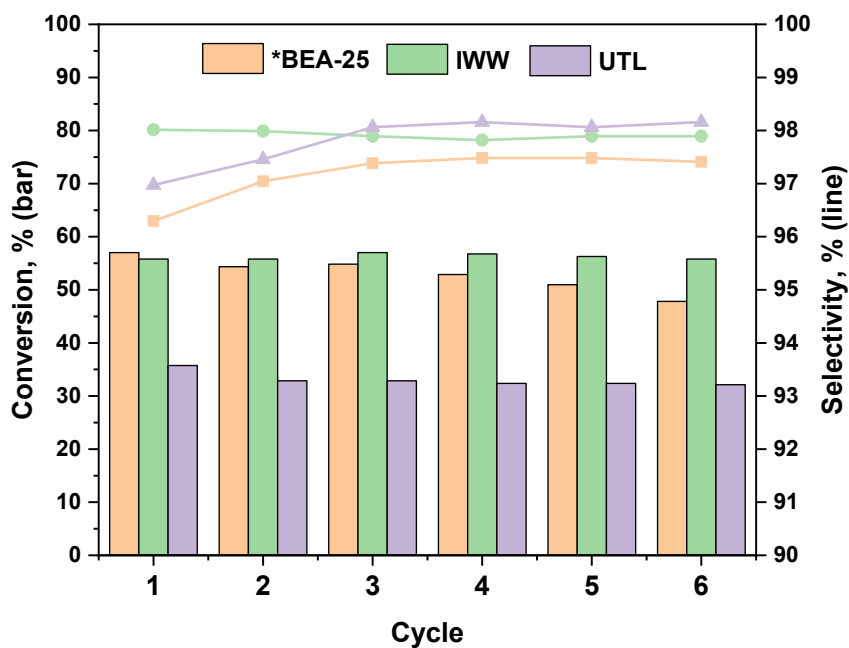


Figure 4-7. Catalyst recycling test for the synthesis of solketal. Reaction conditions: solvent-free, 5 mg catalyst, 5 mmol ketone, 1 mmol polyol, RT, 3 h.

In the ketalization reaction, Ge atoms in the framework of germanosilicate zeolite may not only adsorb the formed H₂O to transform from LAS to BAS, but also be extracted from zeolite framework to the reaction mixture. Thus, the concentration of extracted Ge in the reaction mixture was verified using ICP-OES measurement and was found less than 0.1 ppm. Importantly, the extracted Ge was not able to catalyze the ketalization reactions, as was confirmed with the results of the leaching test (**Figure 4-8**).

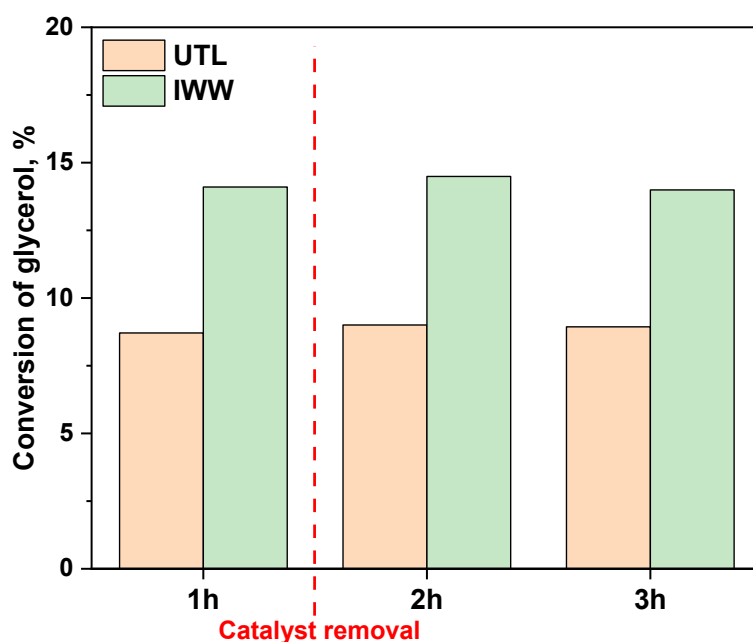


Figure 4-8. Leaching test over UTL and IWW zeolite catalysts. Reaction conditions: solvent-free, 5 mg catalyst, 5 mmol acetone, 1 mmol glycerol, RT, $T_{act} = 300\text{ }^{\circ}\text{C}$.

Germanosilicate zeolites showed similar glycerol conversion and solketal selectivity in comparison with other homogeneous or composite heterogeneous catalysts, i.e., ZrO₂/SO₄¹⁸⁴, MoPO/SBA-15SiO₂¹⁸⁵, Re/SiO₂¹⁸⁶, or MOR¹⁸⁷, MFI¹⁷⁸, *BEA zeolites^{183, 187, 188}, for some of those catalysts, the reaction must run at higher temperatures to achieve comparable yields¹⁸⁹.

All in all, the results discussed in this section show that incorporation of Ge into siliceous framework enables the preparation of zeolites with weak acidity and appropriate affinity towards H₂O^{179, 180} to be active and selective catalysts of glycerol ketalization. Noticeably, H₂O

adsorption on the Lewis acid sites (tetrahedrally coordinated framework Ge atoms) of germanosilicate zeolite **IWW** promotes the formation of weak Brønsted acid centers, which are more active than Lewis acid sites in the ketalization of glycerol¹⁸¹.

4.2. Zeolite catalysts by degermanation-metalation coupled with Ge recycling

Ge is a special framework-building element promoting the formation of D4R-containing zeolites (Section 2.1.3) with extra-large pores and unusual pore systems, which have high potential in catalysis. Although some reactions can be catalyzed by weakly acidic germanosilicate zeolites (Section 4.1), the high cost, low strength of acid sites and hydrolytic instability still limit their practical use in a variety of catalytic reactions. In this section, post-synthesis degermanation/metalation approach coupled with Ge recovery/recycling is described. The method was developed to prepare Lewis acid zeolite catalysts with targeted chemical compositions in a cost-efficient way.

4.2.1. Degermanation and germanium recovery

Germanosilicate zeolites **ITH**, **IWW** and **UTL** (Si/Ge = 3 – 5) (**Table 4-5**) were synthesized to study the influence of zeolite topology on the kinetics of Ge leaching. Meanwhile, two **ITH** samples with different crystal sizes were prepared to evaluate the effect of crystal size on the degree of Ge extraction (i.e., the amount of leached Ge/total Ge).

Table 4-5. Chemical composition and crystal size of germanosilicate zeolites.

Sample	Chemical composition,		Si/Ge	Crystal size, μm
	mol.%			
	Si	Ge		
ITH-10	90.9	9.1	10	2×0.5×0.5
ITH-3	75.6	24.4	3	40×10×5
IWW-5	84.1	15.9	5	0.5×5×5/0.5×0.5×0.5
UTL-3	76.2	23.8	3	50×30×<0.5

Varying the temperature (80 vs. 25 °C) and duration of the treatment (16 vs. 1 h), the nature (HCl vs. HNO₃) and concentration of the acid (4 vs. 1 vs. 0.1 M), the influence of the treatment conditions on the leaching of Ge was addressed. Upon the 16 h-treatment of different zeolites with 0.1 M acid solutions, the use of HNO₃ allowed to extract less Ge (40 – 75 %) than that when applying HCl (45 – 88 %, **Figure 4-9**). This result can be explained by a higher ability of Cl⁻ vs. NO₃⁻ anions in complexation of Ge after hydrolysis of Ge-O(Si) bonds¹⁹⁰.

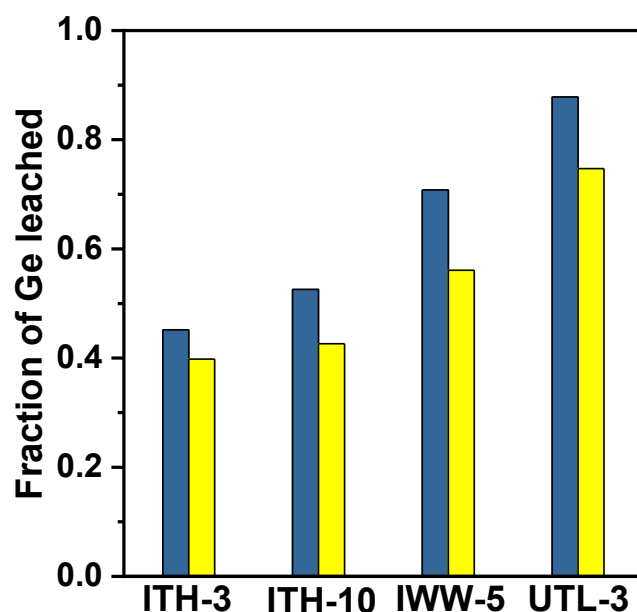


Figure 4-9. Fraction of Ge leached from the parent zeolites after acidic treatment with 0.1 M HNO₃ (■) vs. HCl (■) at RT for 16 h.

The efficiency of degermanation was not significantly affected by the temperature since the degree of extracted Ge was almost the same upon the treatment with 0.1 M HCl at 25 and 80 °C for all zeolites (**Figure 4-10a**). Extending the duration of the treatment (1 to 16 h) allowed the removal of a larger quantity of Ge (25 % to 45 %) from medium-pore **ITH-3** with bigger size of crystals, whereas no obvious effect of duration on the leaching efficiency was observed for either **ITH-10** with smaller size of crystals or **IWW-5** and **UTL-3** zeolites with larger pores (**Figure 4-10a**). This result indicates that germanosilicate zeolites with small pores or large size of crystals experience diffusion limitations during the hydrolysis process.

It is worth noting that more Ge was leached from zeolite framework with decreasing concentration of HCl (4 to 0.1 M, **Figure 4-10b**), which is consistent with the published results⁹⁷. At the first glance, this abnormal result may be explained by the H⁺-promoted condensation reaction between silanol defects in zeolite framework (formed by Ge leaching) and extracted Ge species [Ge(OH)_xO_(2-0.5x)] from leaching solution. As a result, Ge is re-incorporated into zeolite framework. Nevertheless, no further increase in the degree of leached Ge was observed with reducing of [H⁺] to 0 (e.g., water, **Figure 4-11a**), since the cleavage of Ge-O bond may be slowed down due to the decrease of [H⁺]. As the degree of Ge leaching is a trade-off of the relative rates of both H⁺-involved processes, pH = 2 appeared as the optimal pH value for the most productive Ge leaching.

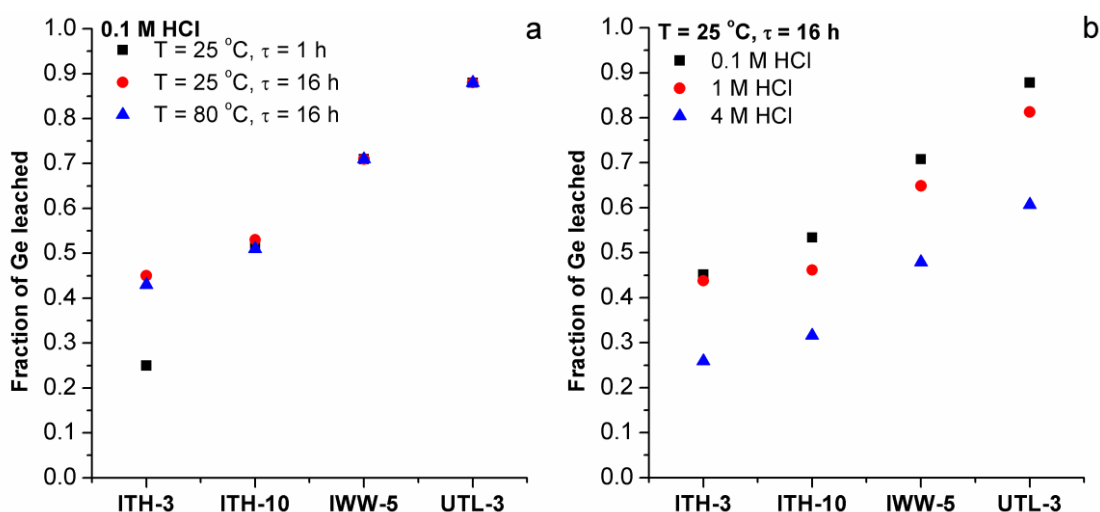


Figure 4-10. Fraction of Ge leached from the parent zeolites after treatment with: 0.1 M HCl under variable conditions (a) and HCl of different concentrations at RT for 16 h (b).

Noticeably, repetitive treatment of germanosilicate zeolites with water can significantly increase the degree of the leached Ge (**Figure 4-11b**). As a result, as much as 78 to 94 % of Ge was recovered after three-fold treatment of germanosilicate zeolites with water. Importantly, the maximum degree of Ge leached was closely related to the nature of the parent zeolite.

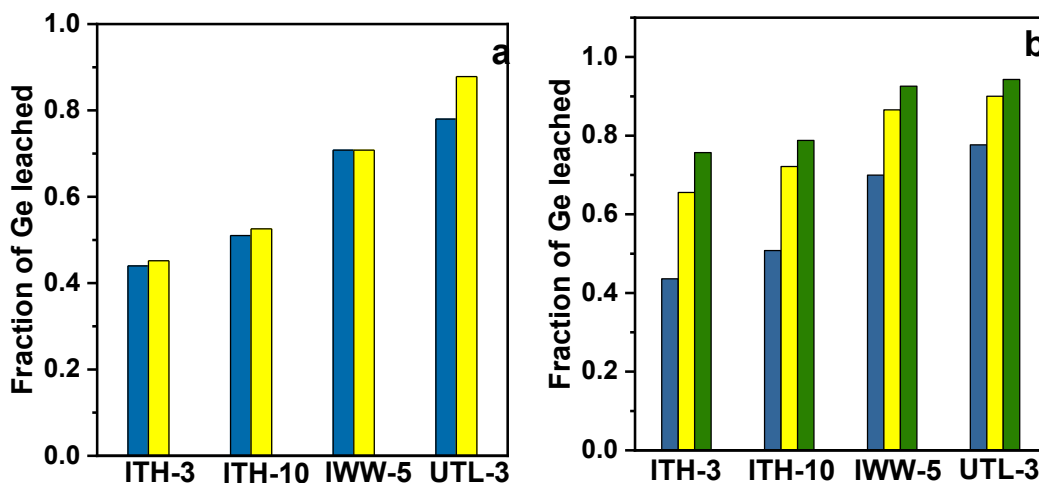
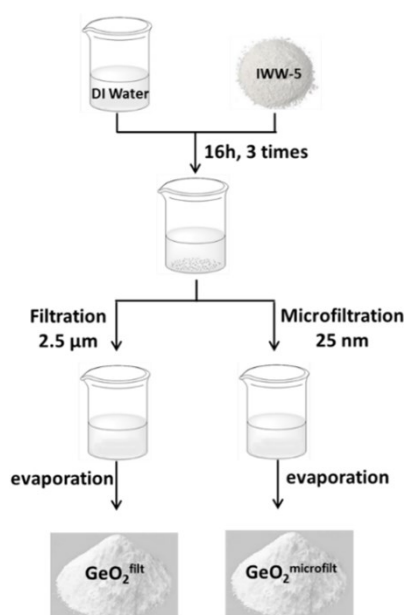


Figure 4-11. Fraction of Ge leached from the parent zeolites after treatment with: 0.1 M HCl (■) vs. H₂O (■) (a) and repetitive treatment with H₂O (1 time: ■, 2 times: ■, 3 times: ■) for 16 h at RT.

Further Ge recovery included two sequential steps (**Scheme 4-2**): 1) separation of the degermanated zeolite from the leached solution by *filtration* or *microfiltration*, 2) evaporation of the excess of water from the leached solution. Finally, two forms of recovered GeO₂ were collected (GeO₂^{filt} or GeO₂^{microfilt}). The results obtained for IWW-5 zeolite are discussed further to exemplify general trends.



Scheme 4-2. Two ways of GeO₂ recovery after hydrolysis of IWW zeolite.

The XRD patterns of both forms, $\text{GeO}_2^{\text{filt}}$ or $\text{GeO}_2^{\text{microfilt}}$, showed the characteristic diffraction lines, all observed for reference commercial germanium oxide (IV) sample ($\text{GeO}_2^{\text{commer}}$, **Figure 4-12a**). Meanwhile in contrast to $\text{GeO}_2^{\text{commer}}$, the FTIR spectra of $\text{GeO}_2^{\text{filt}}$ and $\text{GeO}_2^{\text{microfilt}}$ showed the vibrational bands (1100 – 1000 cm^{-1}) of Si-O bond (**Figure 4-12b**). These results indicate that there exist residual zeolite species in both recovered GeO_2 samples, although the content was less than 3 wt.% (according to ICP-OES analysis). The average size of GeO_2 crystals was calculated from the broadening (011) peak using the Scherrer equation. The obtained results revealed a much higher crystal sizes for $\text{GeO}_2^{\text{filt}}$ and $\text{GeO}_2^{\text{commer}}$ (77 nm) than those for $\text{GeO}_2^{\text{microfilt}}$ (35 nm). Subsequently, the result was also confirmed with HRTEM (**Figure 4-13**). Noticeably, in the case of $\text{GeO}_2^{\text{filt}}$, HRTEM detected the large and visible zeolite species (**Figure 4-14**).

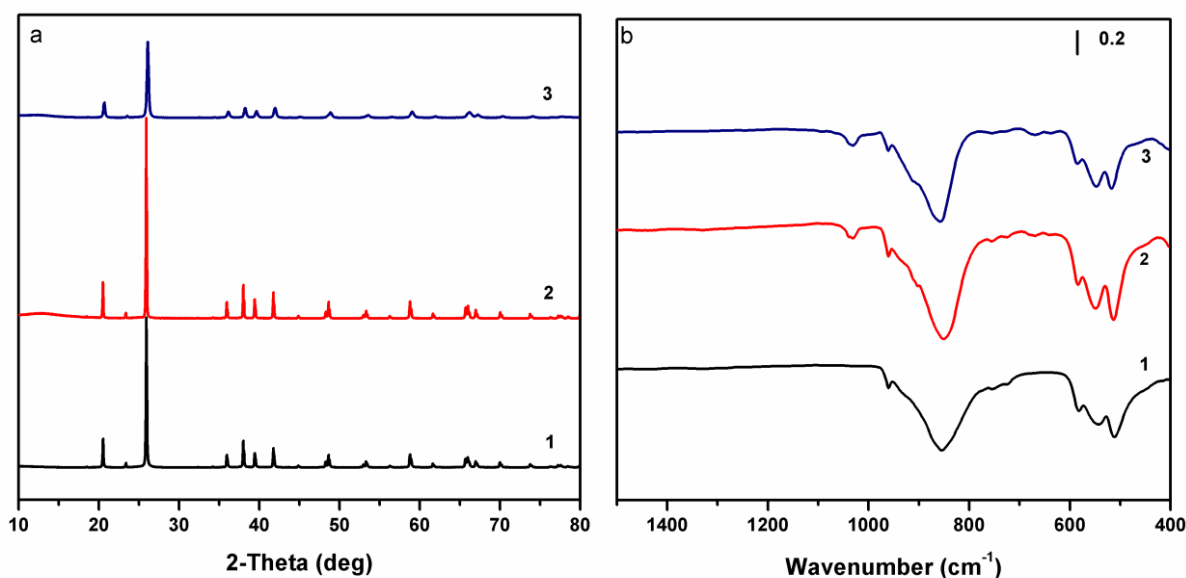


Figure 4-12. XRD patterns (a) and FTIR spectra (b) of $\text{GeO}_2^{\text{commer}}$ (1), $\text{GeO}_2^{\text{filt}}$ (2) and $\text{GeO}_2^{\text{microfilt}}$ (3).

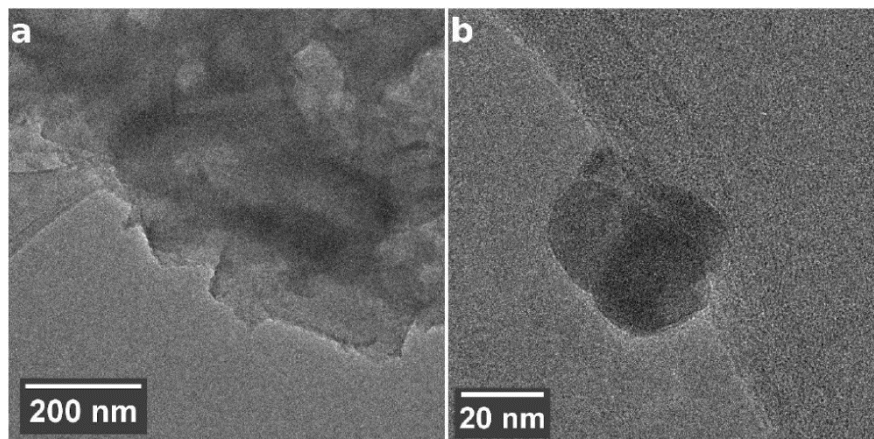


Figure 4-13. HRTEM images showing typical size of particles in $\text{GeO}_2^{\text{filt}}$ (a) and $\text{GeO}_2^{\text{microfilt}}$ samples (b).

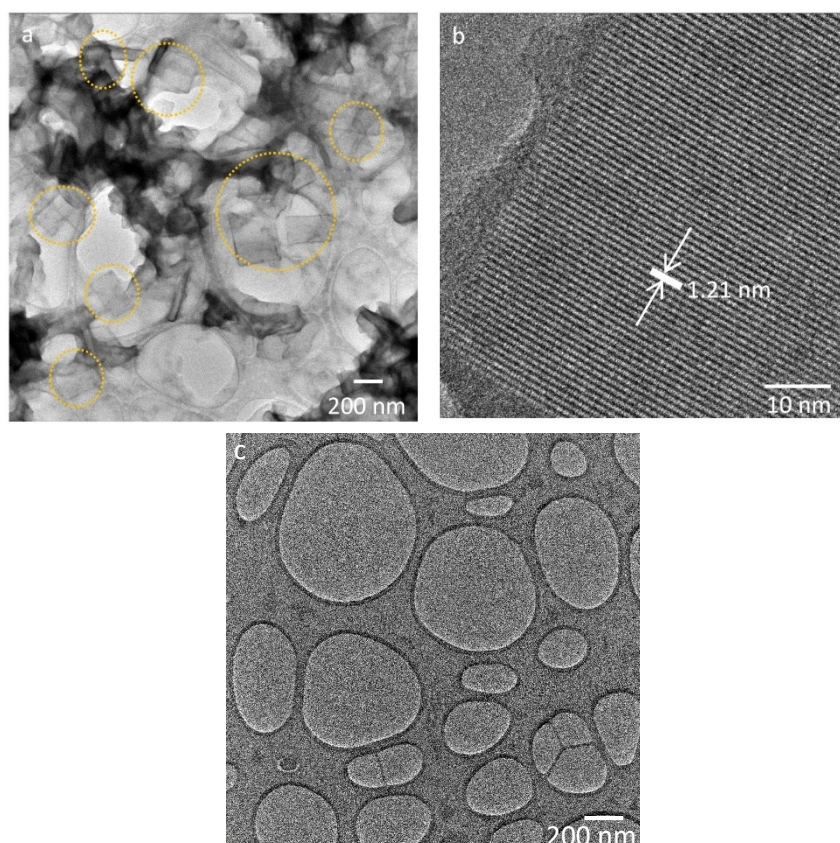


Figure 4-14. TEM images of the leaching solution obtained by the treatment of IWW-5 with H_2O at RT for 16 h, followed by filtration (a, b) or microfiltration (c).

4.2.2. Germanium recycling

$\text{GeO}_2^{\text{filt}}$ and $\text{GeO}_2^{\text{microfilt}}$ recovered from IWW zeolite were used as the germanium source

for the preparation of germanosilicate zeolites, using three different SDAs, i.e., SDA_{ITH} , SDA_{IWW} and SDA_{UTL} facilitating the formation of **ITH**, **IWW** or **UTL** zeolites, respectively, when using standard synthesis procedures. Noticeably, the mother liquor separation method for GeO_2 recovery determines the phase selectivity of zeolite crystallization. $\text{GeO}_2^{\text{filt}}$ always directed the crystallization process towards the formation of parent **IWW** zeolites, no matter which SDA and crystallization conditions were used (**Figure 4-15a**).

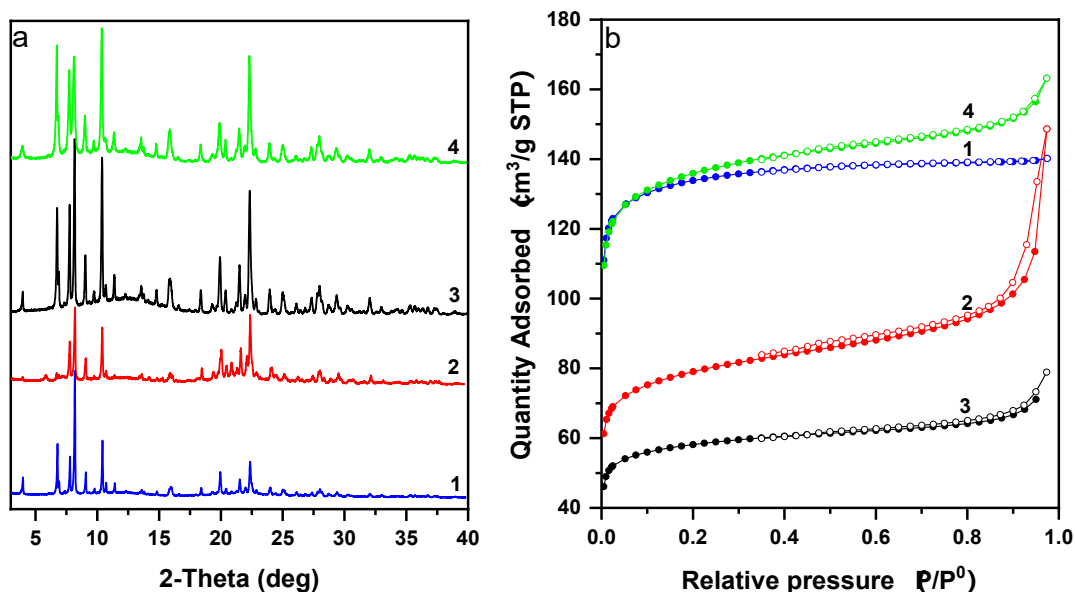


Figure 4-15. XRD patterns (a), N_2 adsorption (\bullet) and desorption (\circ) isotherms (b) of $\text{IWW}^{\text{filt}}\text{-SDA}_{\text{IWW}}$ (1), $\text{IWW}^{\text{filt}}\text{-SDA}_{\text{UTL}}$ (2), $\text{IWW}^{\text{filt}}\text{-SDA}_{\text{ITH}}$ (3) and parent **IWW**-5 (4).

More to that, SEM images of both samples showed the similar morphology with **IWW** zeolite (**Figure 4-16**). $\text{GeO}_2^{\text{filt}}$ in combination with SDA_{IWW} promoted the formation of $\text{IWW}^{\text{filt}}\text{-SDA}_{\text{IWW}}$ sample, which showed larger and more uniform crystals than those of the parent **IWW** zeolite, but both **IWW** samples showed same chemical composition ($\text{Si}/\text{Ge} = 4 - 5$) and textural characteristics ($V_{\text{micro}} = 0.17 - 0.18 \text{ cm}^3 \cdot \text{g}^{-1}$, $S_{\text{BET}} = 454 - 474 \text{ m}^2 \cdot \text{g}^{-1}$, **Table 4-6**).

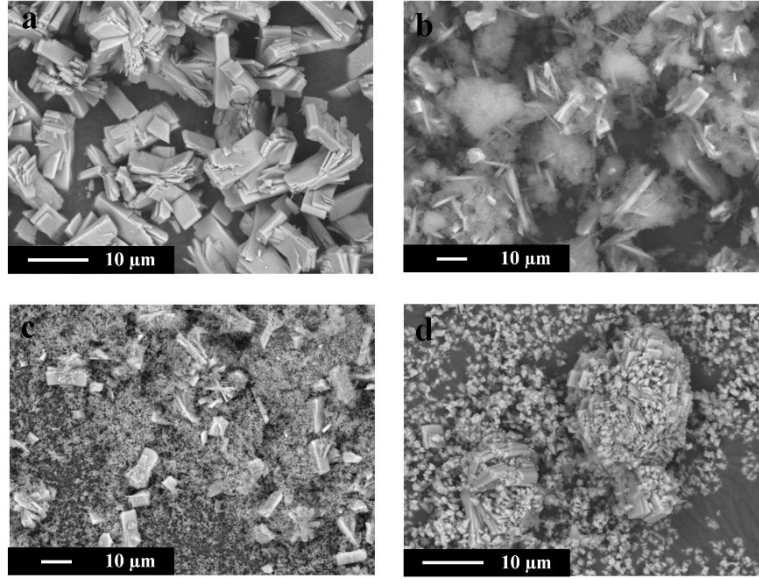


Figure 4-16. SEM images of $IWW^{filt}\text{-SDA}_{IWW}$ (a), $IWW^{filt}\text{-SDA}_{UTL}$ (b), $IWW^{filt}\text{-SDA}_{ITH}$ (c) and parent IWW-5 (d).

Table 4-6. Textural properties and chemical composition of parent IWW-5 and recycled zeolite samples.

Sample	Phase composition	Textural properties		Crystal size, μm	Si/Ge
		$V_{\text{micro}}, \text{cm}^3 \cdot \text{g}^{-1}$	$S_{\text{BET}}, \text{m}^2 \cdot \text{g}^{-1}$		
IWW-5		0.17	474	$0.5 \times 5 \times 5$ $/0.5 \times 0.5 \times 0.5$	5
$IWW^{filt}\text{-SDA}_{IWW}$	IWW	0.18	454	$10 \times 3 \times 1.5$	4
$IWW^{filt}\text{-SDA}_{UTL}$		0.09	276	n.d.	22
$IWW^{filt}\text{-SDA}_{ITH}$		0.07	203	n.d.	21
$IWW^{\text{microfilt}}\text{-SDA}_{IWW}$		0.17	451	$<0.5 \times <0.5 \times <0.5$	5
UTL-3	UTL	0.19	450	$50 \times 30 \times <0.5$	3
$UTL^{\text{microfilt}}\text{-SDA}_{UTL}$		0.18	427	$40 \times 30 \times <0.5$	4
ITH-3	ITH	0.12	271	$40 \times 10 \times 5$	3
$ITH^{\text{microfilt}}\text{-SDA}_{ITH}$		0.13	319	$40 \times 6 \times 5$	3

In contrast to GeO_2^{filt} , $\text{GeO}_2^{\text{microfilt}}$ appeared to be a versatile source of Ge for the preparation of recycled IWW, ITH and UTL zeolites under the respective crystallization conditions typical for each zeolite (Table 4-6). In particular, recycled zeolites ($\text{GeO}_2^{\text{microfilt}}$ as Ge source) exhibited similar XRD patterns (Figure 4-17a, c), N_2 ad-/desorption isotherms (Figure 4-17b, d) and morphology of crystals (Figure 4-18) as the respective zeolites prepared

using $\text{GeO}_2^{\text{commer}}$ as Ge source. A smaller crystal size of recycled samples was observed in comparison with the parent zeolites (**Table 4-6**). Therefore, the isotherms of parent and recycled zeolites revealed a different quantity of N_2 adsorbed at $p/p^0 > 0.95$ (**Figure 4-17b, d**). Particularly, in contrast to the isotherm of parent **IWW** sample, which showed the H3-type hysteresis loop, a visible capillary condensation was observed in the desorption branch of **IWW^{microfilt}-SDA_{IWW}** sample, indicating the presence of inter-particle mesopores (**Figure 4-17b**).

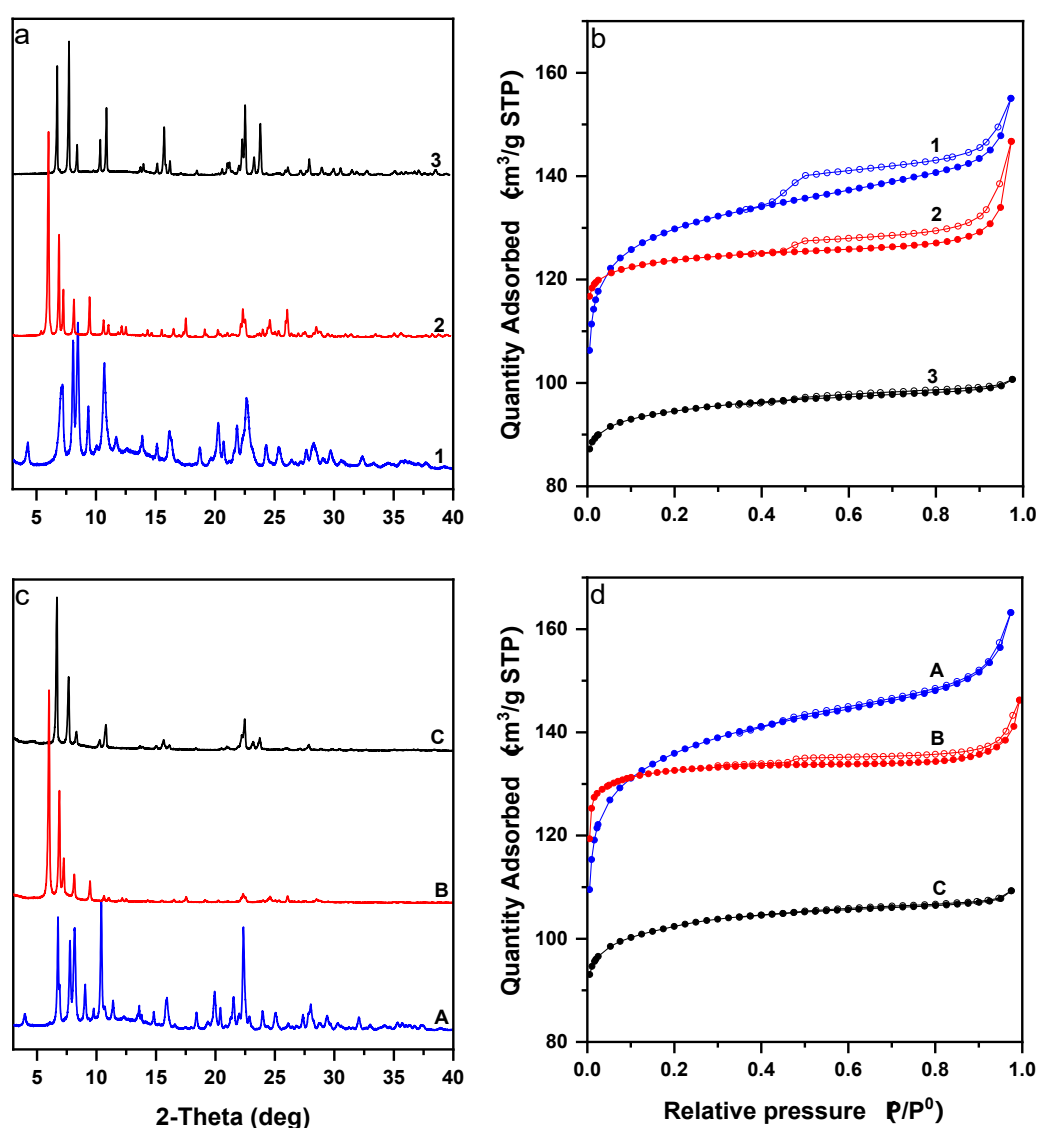


Figure 4-17. XRD patterns (a, c) and N_2 adsorption (\bullet) and desorption (\circ) isotherms (b, d) of **IWW^{microfilt}-SDA_{IWW}** (1) vs. parent **IWW-5** (A), **UTL^{microfilt}-SDA_{UTL}** (2) vs. parent **UTL-3** (B), and **ITH^{microfilt}-SDA_{ITH}** (3) vs. parent **ITH-3** (C).

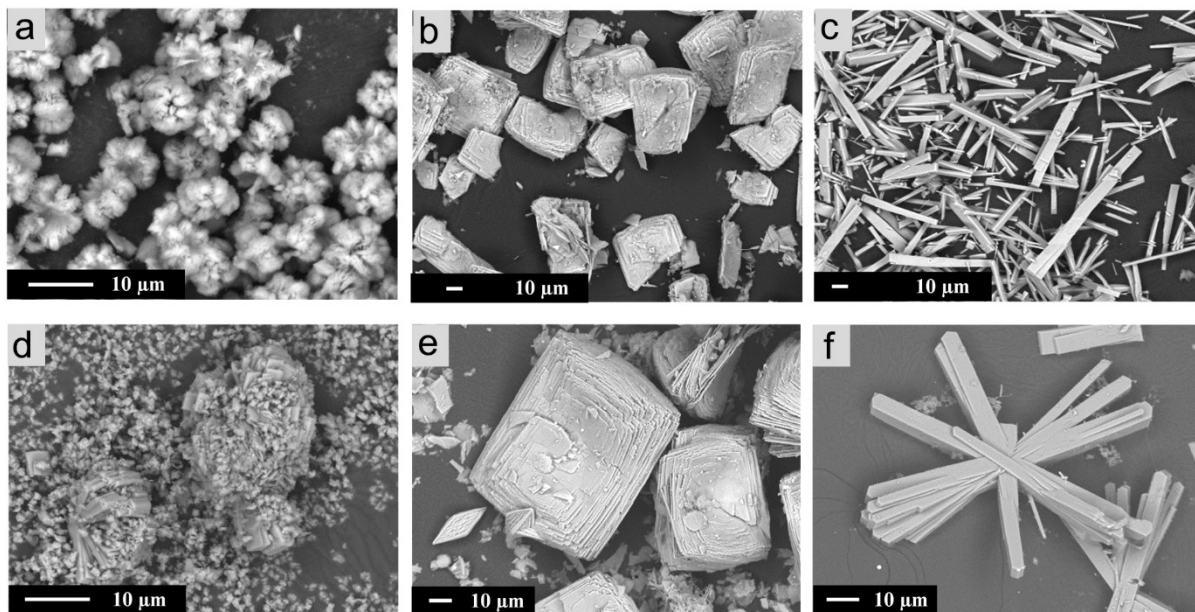
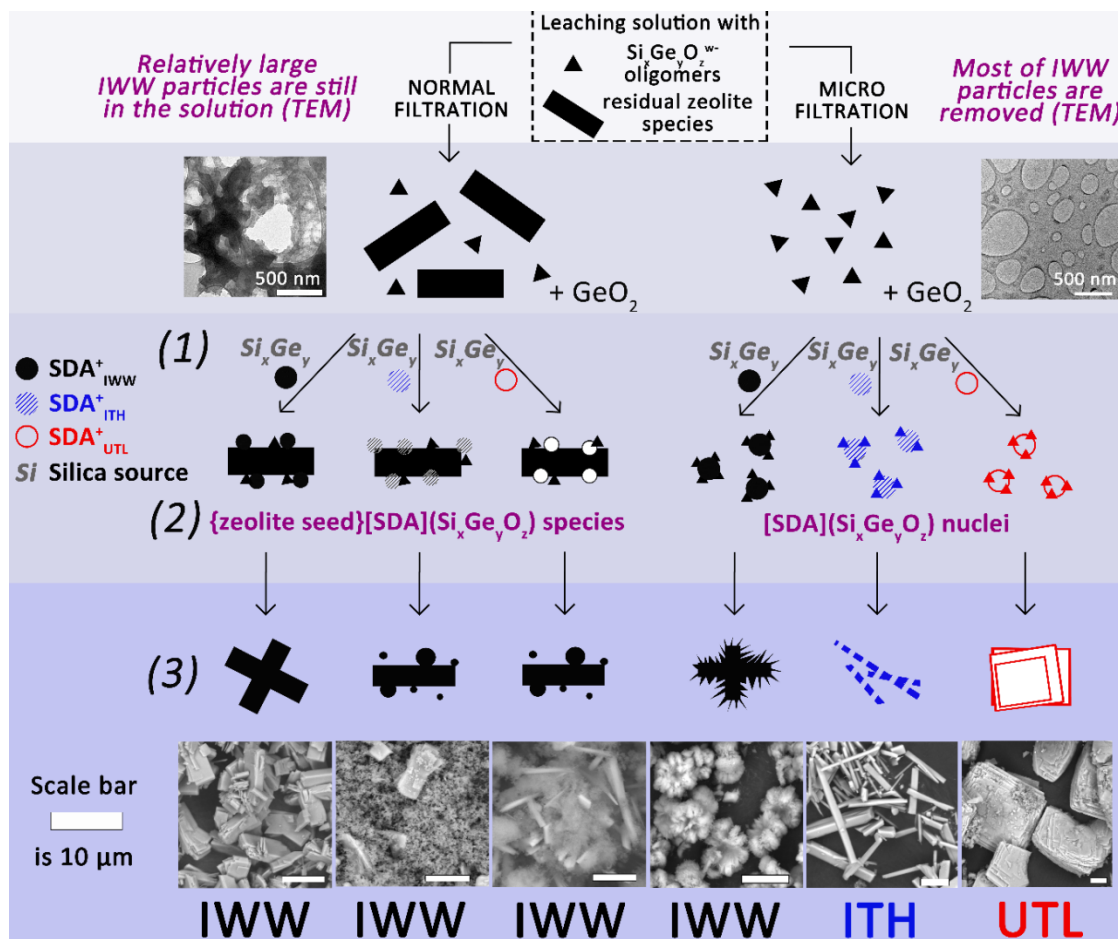


Figure 4-18. SEM images of $\text{IWW}^{\text{microfilt}}\text{-SDA}_{\text{IWW}}$ (a) vs. parent IWW-5 (d), $\text{UTL}^{\text{microfilt}}\text{-SDA}_{\text{UTL}}$ (b) vs. parent UTL-3 (e), and $\text{ITH}^{\text{microfilt}}\text{-SDA}_{\text{ITH}}$ (c) vs. parent ITH-3 (f).

Taking into account the general mechanism of zeolite crystallization (Section 2.1.2)⁸³, the effect of the method of Ge recovery (filtration or microfiltration) on the phase selectivity of zeolite crystallization was clarified as it is artistically shown on **Scheme 4-3**. Three sequential steps constitute the process of germanosilicate zeolite crystallization assisted by SDA: 1) *induction period* – pre-nucleation comprising depolymerization of Si and Ge sources with a formation of $\text{Si}_x\text{Ge}_y\text{O}_z^{\text{w-}}$ polyanions (Si_xGe_y in **Scheme 4-3**); Si_xGe_y structure is determined by the nature of SDA, pH and Si/Ge in reaction mixture and is similar to SBUs found in the formed zeolite framework¹⁹¹, 2) *nucleation period* comprising the generation of nucleation centers by rearrangement of Si_xGe_y and SDA^+ , 3) *crystal growth* by aggregation of the $[\text{SDA}](\text{Si}_x\text{Ge}_y)$ nuclei. In addition to the Si_xGe_y species formed upon standard crystallization, nanoparticles (zeolite seeds) detected in $\text{GeO}_2^{\text{filt}}$ (**Figures 4-12b, 4-13 and 4-14**) can affect the process of zeolite crystallization. Thus, when $\text{GeO}_2^{\text{filt}}$ was used as Ge source, the reaction system comprised a mixture of IWW seeds (nanoparticles), $\text{Si}_x\text{Ge}_y^{\text{IWW}}$ sub-nano fragments of IWW as the products of seeds dissolution, SDA and T-element (Si, Ge) sources. In this case, relative concentration of different nuclei may determine the structure of a zeolite product. 1) IWW seeds direct the crystallization towards IWW phase, 2) $[\text{SDA}](\text{Si}_x\text{Ge}_y)$ directs the

crystallization towards ITH, IWW, or UTL using their respective SDA. The nature of SDA did not influence the phase selectivity of zeolite, hence indicating a lower stability of $[\text{SDA}](\text{Si}_x\text{Ge}_y)$ nuclei compared to IWW seeds.



Scheme 4-3. Plausible mechanism of seed-SDA-assisted crystallization of germanosilicate zeolites using recovered GeO_2 as a source of Ge: $\text{GeO}_2^{\text{filt}}$ (left), $\text{GeO}_2^{\text{microfilt}}$ (right).

Moreover, $\text{IWW}^{\text{filt}}\text{-SDA}_{\text{IWW}}$ sample showed more uniform and bigger crystals than parent IWW-5 zeolite, which can be correlated with the synergistic effect of seed- and SDA-assisted crystallization, which eliminated the induction period and thus it is characterized by a rapid crystal growth (Figure 4-16a, Scheme 4-3). In turn, although the presence of $[\text{SDA}_{\text{UTL}}](\text{Si}_x\text{Ge}_y)$ and $[\text{SDA}_{\text{ITH}}](\text{Si}_x\text{Ge}_y)$ did not affect the type of formed zeolite phase, it obviously limited the rate of crystal growth of IWW zeolites (Scheme 4-3, Figure 4-16b, c).

In contrast to $\text{GeO}_2^{\text{filt}}$, the existence of only $\text{Si}_x\text{Ge}_y^{\text{IWW}}$ in $\text{GeO}_2^{\text{microfilt}}$ obviously had a negligible effect on the phase selectivity of zeolite crystallization when using SDA of **UTL** and **ITH**. The most probable explanation of this result is the low stability of the sub-nano **IWW** fragments, which are prone to depolymerization and degradation during the induction period and nucleation. The generated $\text{Si}_x\text{Ge}_y\text{O}_z^{\text{w-}}$ polyanions species can further participate in the formation of $[\text{SDA}](\text{Si}_x\text{Ge}_y)$ nuclei, resulting in **UTL** and **ITH** zeolites using respective SDAs (**Scheme 4-3, Figure 4-18b, c**).

4.2.3. Metalation: synthesis of Ti-, Sn-, Zr-substituted zeolite catalysts

In order to achieve the full cycle of [zeolite synthesis] \rightarrow [Ge leaching and recovery] \rightarrow [zeolite re-synthesis using recovered GeO_2]/[generation of acid sites], metalation by the post-synthesis incorporation of Ti, Sn and Zr to the degermanated large-pore **IWW** sample (**IWW-5-H₂O-25 °C-16 h/3**, denoted as **IWW-hydro** in the following text) was applied. Meanwhile, extra-large pore **UTL** and ***CTH** zeolites were also subjected to post-synthesis metalation for Sn and Zr incorporation.

4.2.3.1. Structural and textural characteristics

Consistent with the published results^{79, 173}, the structural maintenance of **IWW** zeolite framework during the neutral or acidic treatment was proved with XRD patterns (**Figure 4-19a**) – although decreasing in intensity, the characteristic diffraction lines retain their 2-theta positions. In contrast to the large-pore **IWW** zeolite, the frameworks of extra-large pore **UTL** and ***CTH** zeolites were transformed upon the treatment with water or acid (**Figure 4-19b-d**), which apparently limited functionalization of respective germanosilicates *via* degermanation/metalation approach. Therefore, partial post-synthesis Ge-for-Si substitution by the treatment of **UTL** and ***CTH** zeolites with silica source in ethanolic acid solutions or with highly concentrated acid solution, respectively, was used to prepare stabilized Ge-poor zeolites^{103, 109, 156}, further subjected to degermanation treatment.

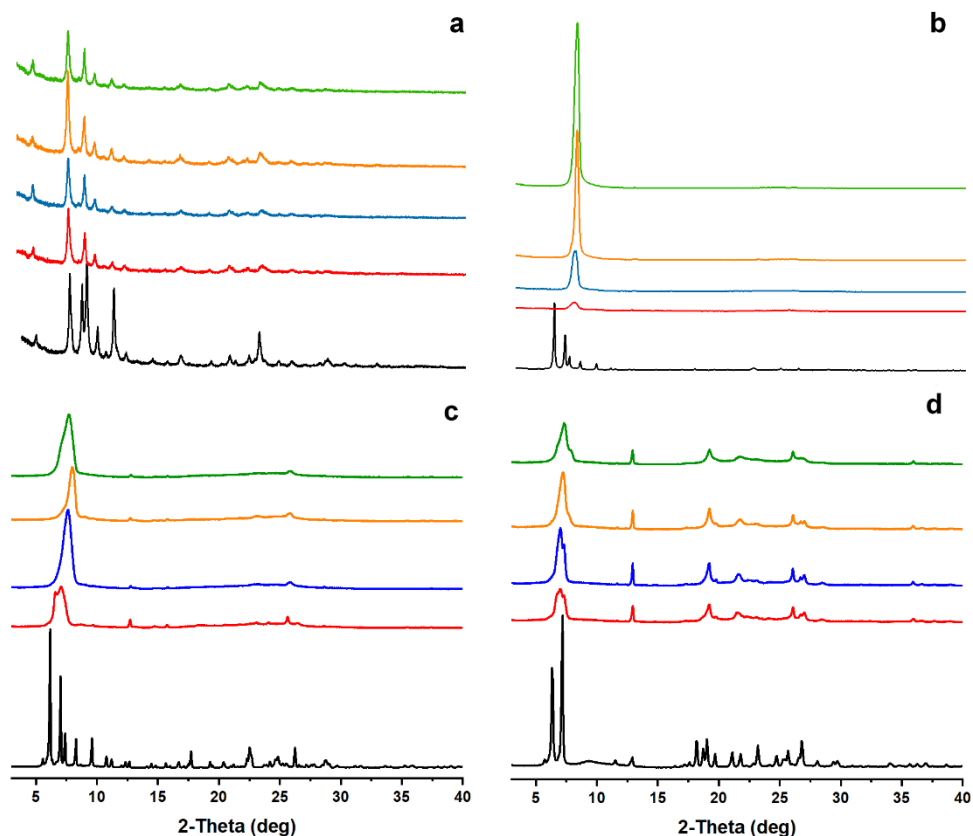


Figure 4-19. XRD patterns of IWW-5 (a), UTL-3 (b), UTL-5 (c) and *CTH-4 (d) before and after acidic treatment: Calcined zeolites (—), zeolite-0.1 M HCl-25 °C-1 h (—), zeolite-0.1 M HCl-25 °C-16 h (—), zeolite-0.1 M HCl-80 °C-16 h (—), zeolite-H₂O-25 °C-16 h/3 (—).

XRD patterns (**Figure 4-20b, c**) and chemical analysis (**Table 4-7**) of prepared stabilized UTL and *CTH zeolites revealed the maintenance of the structure but increase in the Si/Ge ratio (UTL: 12 vs. 5, *CTH: 12 vs. 4), which confirmed the substitution of Ge with Si. Noticeably, N₂ adsorption showed an enhanced BET area (UTL: 534 vs. 470 m²·g⁻¹, *CTH: 402 vs. 388 m²·g⁻¹) and comparable micropore volume (UTL: 0.22 vs. 0.20 cm³·g⁻¹, *CTH: 0.15 vs. 0.16 cm³·g⁻¹) between stabilized and the parent zeolites (**Figure 4-21b, c**). This result can be explained by the generation of additional bigger pores upon the extraction of Ge under acidic treatment due to the merge of several neighboring micropores^{79, 93}. Further hydrolysis of UTL(S) and *CTH(S) in aqueous medium led to an increase in Si/Ge ratio from 12 to 30 – 34 due to Ge leaching and to some decrease in the micropore volume and BET area in UTL(S)-hydro and *CTH(S)-hydro samples (**Table 4-7**). The latter result can be related to the distortion

of D4R units, effecting the geometry of the pore system upon Ge leaching. Noticeably, textural characteristics of non-stabilized **IWW-5** sample were greatly reduced upon hydrolysis, and 14-fold increase in Si/Ge ratio was observed in **IWW-hydro** vs. **IWW-5** (Table 4-7). Considering decreased intensities of diffraction lines in XRD pattern of respective **IWW-hydro**, it is reasonable to assume that deep degermanation of **IWW-5** sample removed some D4R units, which not only resulted in distortion of zeolite framework but also eliminated a fraction of 10-ring micropores parallel to silica layers.

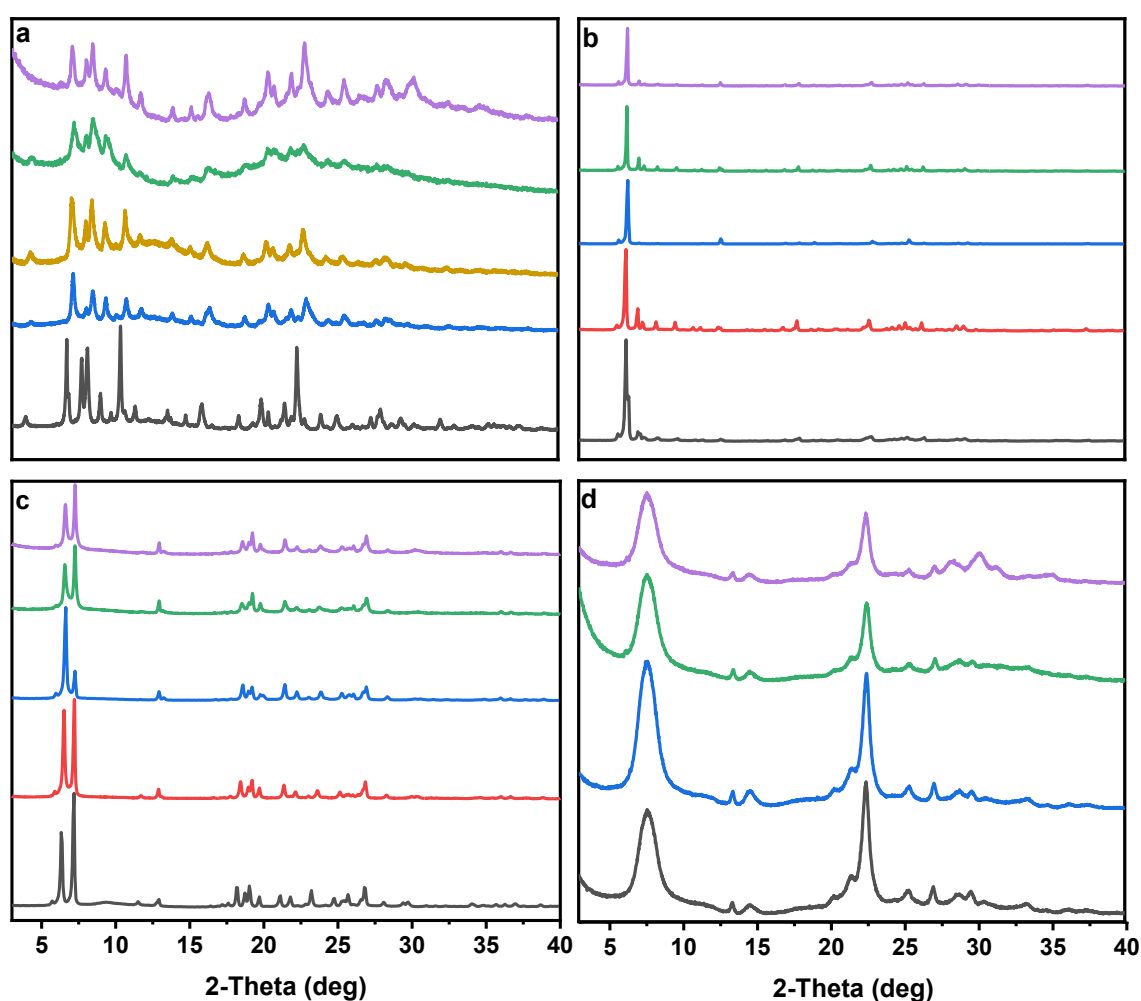


Figure 4-20. XRD patterns **IWW** (a), **UTL** (b), ***CTH** (c) and reference ***BEA** (d) zeolites: parent zeolite (—), post-stabilized zeolite (—), demetalated zeolite (—), **Zeolite/Ti_{post}** (—), **Zeolite/Sn_{post}** (—) and **Zeolite/Zr_{post}** (—).

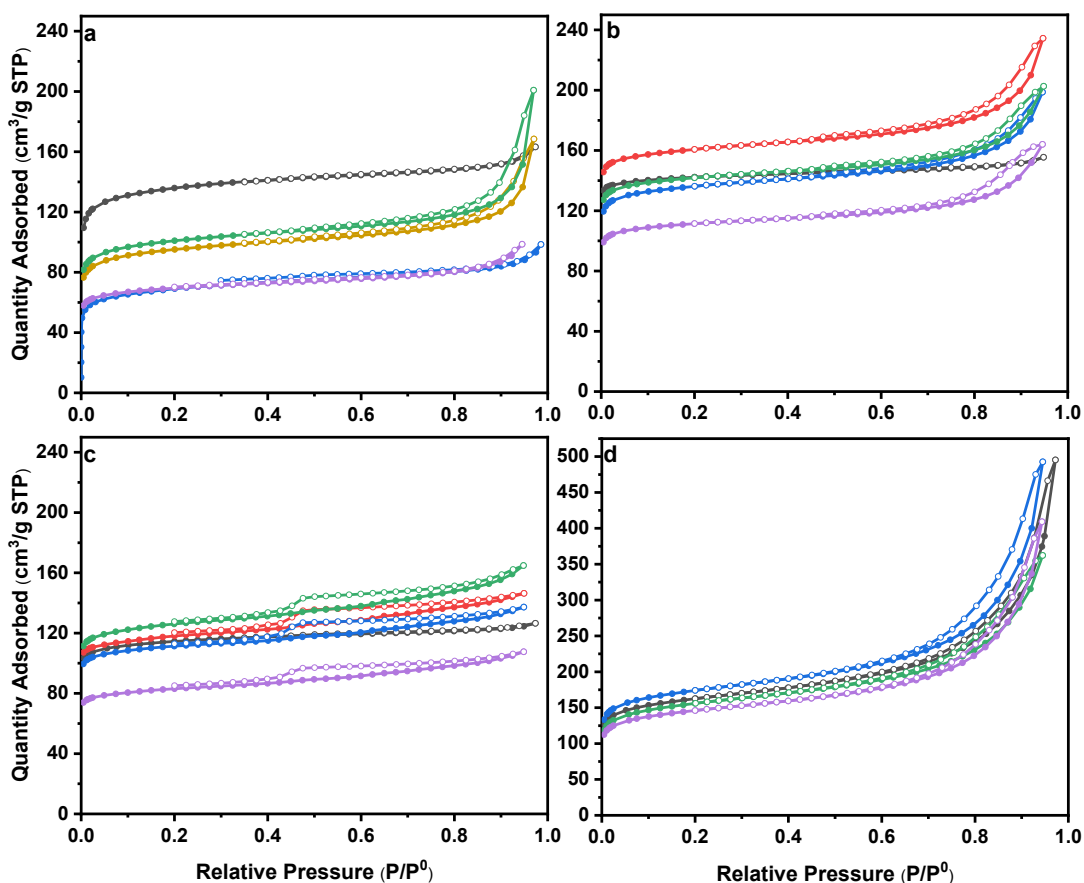


Figure 4-21. N₂ adsorption (●) and desorption (○) isotherms of IWW (a), UTL (b), *CTH (c) and reference *BEA (d) zeolites: parent zeolite (—), post-stabilized zeolite (—), demetalated zeolite (—), Zeolite/Ti_{post} (—), Zeolite/Sn_{post} (—) and Zeolite/Zr_{post} (—).

IWW-hydro, UTL(S)-hydro and *CTH(S)-hydro samples were further used for the incorporation of Ti, Sn and Zr either by impregnation (Ti, Sn) or vapor-phase ion-exchange (Zr). For the sake of better understanding of the features of germanosilicates under applied post-synthesis modifications, dealuminated commercial *BEA-12.5 zeolite¹⁵⁹ was also subjected to the metalation treatments and respective Sn- and Zr-containing *BEA samples were used as benchmark Lewis acid zeolites.

Although post-synthesized T^{IV}-substituted IWW, UTL, *CTH zeolite samples showed a lower intensity of diffraction lines than the parent germanosilicate zeolites, XRD patterns revealed their phase purity (Figure 4-20a-c). N₂ ad-/desorption isotherms of post-synthesized T^{IV}-substituted IWW samples showed typical microporous character (type I isotherm) as

parent **IWW** zeolite (**Figure 4-21a**), while the isotherms of T^{IV}-substituted **UTL** and ***CTH** zeolites correspond to those of stabilized samples, indicating the presence of mesopores (**Figure 4-21b, c**).

In the case of Ti and Sn incorporation, metalation does not significantly affect BET area and micropore volume of degermanated zeolites (**Table 4-7**). In contrast, a decrease in both characteristics was observed in the case of Zr incorporation due to a partial blockage of zeolite pores by the extra-framework Zr species supported by the results of FTIR spectroscopy and chemical analysis (Section 4.2.3.2). Importantly, UV-vis confirmed a dominated fraction of tetrahedrally coordinated Ti, Sn and Zr species in the zeolite framework (absorption band at 205 – 230 nm, **Figure 4-24**).

Table 4-7. Chemical composition and textural properties of zeolite catalysts under study.

Sample	Textural properties		Si/Me
	V _{micro} , cm ³ ·g ⁻¹	S _{BET} , m ² ·g ⁻¹	EDS
IWW-5	0.17	474	5 ^a
IWW-hydro	0.10	249	70 ^a
IWW/Ti_{post}	0.11	322	20 ^b
TS-1	0.10	510	28 ^b
IWW/Sn_{post}	0.12	352	33 ^c
Sn-IWW_{hydro}	0.15	420	101 ^c
IWW/Zr_{post}	0.10	233	13 ^d
UTL-5	0.20	470	5 ^a
UTL(S)	0.22	534	12 ^a
UTL(S)-hydro	0.18	459	30 ^a
UTL/Sn_{post}	0.19	478	33 ^c
UTL/Zr_{post}	0.16	384	9 ^d
*CTH-4	0.16	388	4 ^a
*CTH(S)	0.15	402	12 ^a
*CTH(S)-hydro	0.15	371	34 ^a
*CTH/Sn_{post}	0.16	421	30 ^c
*CTH/Zr_{post}	0.11	277	12 ^d
*BEA-12.5	0.16	558	10 ^e
*BEA-deAl	0.18	597	96 ^e
*BEA/Sn_{post}	0.16	536	14 ^c
*BEA/Zr_{post}	0.15	501	16 ^d

^a: Si/Ge, ^b: Si/Ti, ^c: Si/Sn, ^d: Si/Zr, ^e: Si/Al

Thus, post-synthesis functionalization of germanosilicate zeolites featuring regioselective location of hydrolytically instable domains may alter both structural (**Figure 4-20a-c**) and textural properties (**Figure 4-21a-c**) of zeolites. In contrast, post-synthesis demetallation/metalation does not significantly affect either structure ordering (**Figure 4-20d**) or adsorption characteristics (**Figure 4-21d**) of commercial large-pore zeolite *BEA, with random distribution of Al atoms in the framework. The results suggest an importance of careful optimization of post-synthesis conditions for designing germanosilicate zeolite-based catalysts with tunable chemical composition, but maintained structure.

4.2.3.2. Acidic properties

FTIR spectroscopy of adsorbed pyridine was employed to determine the nature (Lewis or Brønsted), concentration, and strength of acid sites in T^{IV}-substituted IWW, *CTH, UTL and reference *BEA zeolites.

Normally, for aluminosilicate zeolite with strong acid sites, the Lewis acidity is analyzed *via* FTIR spectroscopy of adsorbed pyridine, which includes the following steps: (i) pyridine adsorption at T = 150 – 200 °C followed by desorption at the same temperature; and (ii) evaluating the intensity of ν_{19b} -LAS band (1450 – 1452 cm⁻¹)¹⁷¹ and applying the Beer-Lambert law using the reported molar absorption coefficients¹⁶⁴. In contrast to Al-containing zeolites, the molar absorption coefficients are seldom reported for T^{IV}-zeolites, being, in particular, unavailable for Zr-containing zeolites. More to that, due to the lower acid strength of Ti-associated Lewis acid sites¹⁴⁸, the band of H-bonded pyridine (ν_{19b} band at 1443 cm⁻¹) is overlapped with ν_{19b} -LAS band (1445 – 1460 cm⁻¹)¹⁹². Hence the application of ν_{19b} -LAS band for FTIR analysis of the number of LAS in Ti-substituted zeolites is limited (**Figure 4-22**). Thus, an alternative approach based on the evaluation of the intensity of ν_{8a} -LAS at 1605 and 1608 cm⁻¹ bands to quantify the LAS in T^{IV}-zeolites was elaborated in this work for Ti- and Zr-containing zeolites. During the adsorption of pyridine, only ν_{8a} -LAS was observed upon the introduction of the first doses of pyridine while the band of ν_{8a} -H at 1596 cm⁻¹ appeared when adding more amount of pyridine (**Figure 4-22a, d**). Therefore, the proposed approach allows

to control the concentration of introduced pyridine ($< 2.5 \text{ mmol}\cdot\text{cm}^{-2}$, **Figure 4-22a, d**), to eliminate the contribution of H-bonded probe molecule, and to determine the molar absorption coefficient ε (LAS): 0.71 (for Ti LAS) and 0.73 (for Zr LAS) $\text{cm}\cdot\mu\text{mol}^{-1}$ by correlating the band area of ν_{8a} -LAS at 1605 or 1608 cm^{-1} with the amount of probe molecule, respectively.

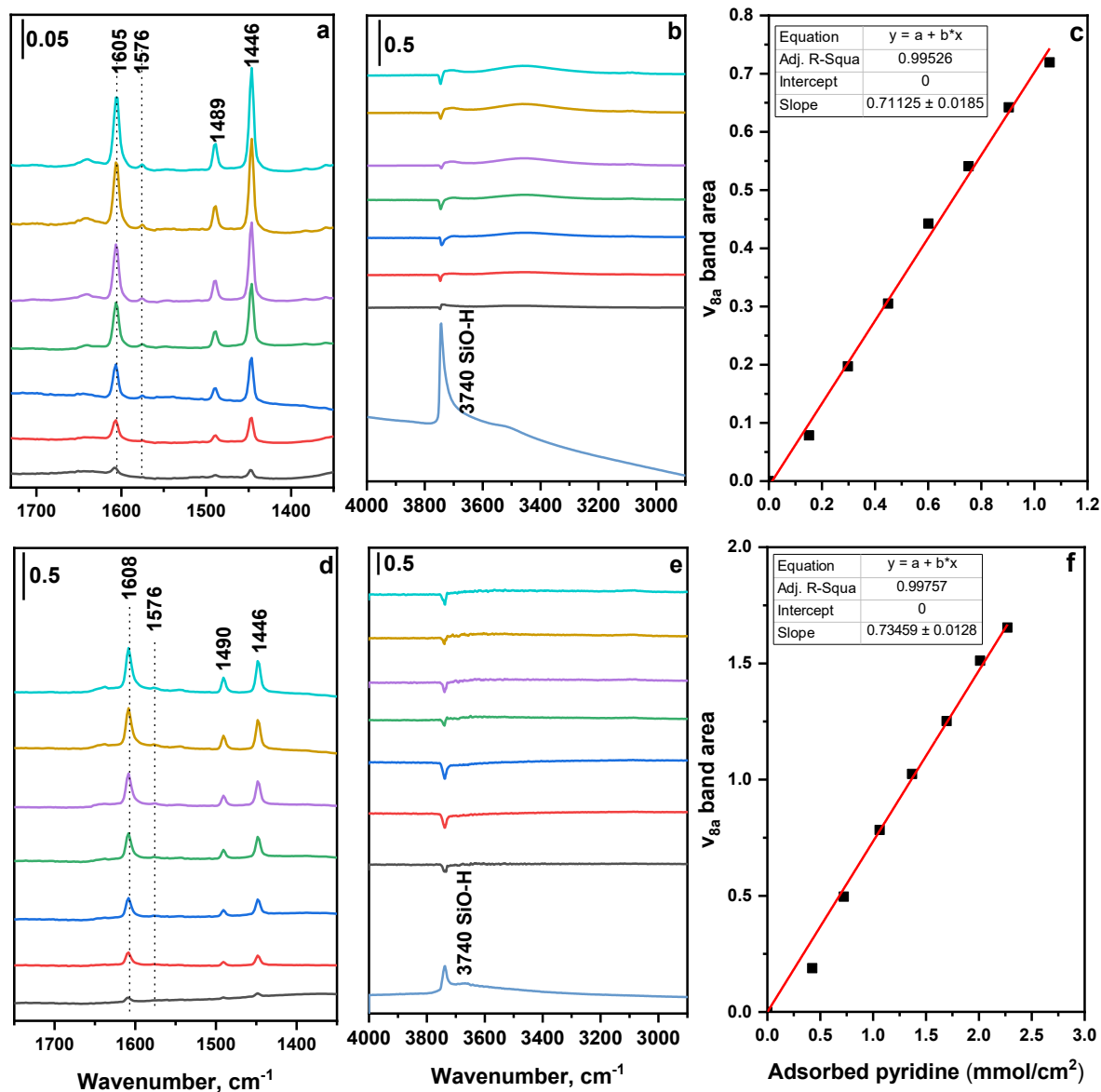


Figure 4-22. FTIR spectra (region of Py-ring vibrations) of IWW/Ti_{post} (a) and UTL/Zr_{post} (d) zeolites collected after dose-by-dose adsorption of pyridine. FTIR spectra (region of OH-vibrations) collected after dose-by-dose adsorption of pyridine in IWW/Ti_{post} (b) and UTL/Zr_{post} (e). Variation of ν_{8a} -LAS (Ti-: 1605 cm^{-1} , Zr-: 1608 cm^{-1}) band area with the concentration of pyridine adsorption over IWW/Ti_{post} (c) and UTL/Zr_{post} (f).

Once determining the values of ϵ (LAS), the adsorption of an excess of pyridine (~ 3.5 torr) followed by the thermo-desorption at 50, 75, 100, 120, 150, 200 °C allowed to calculate the concentrations (**Figure 4-23, Table 4-8**) of Lewis acid sites in designed T^{IV}-substituted zeolites and to estimate their strength.

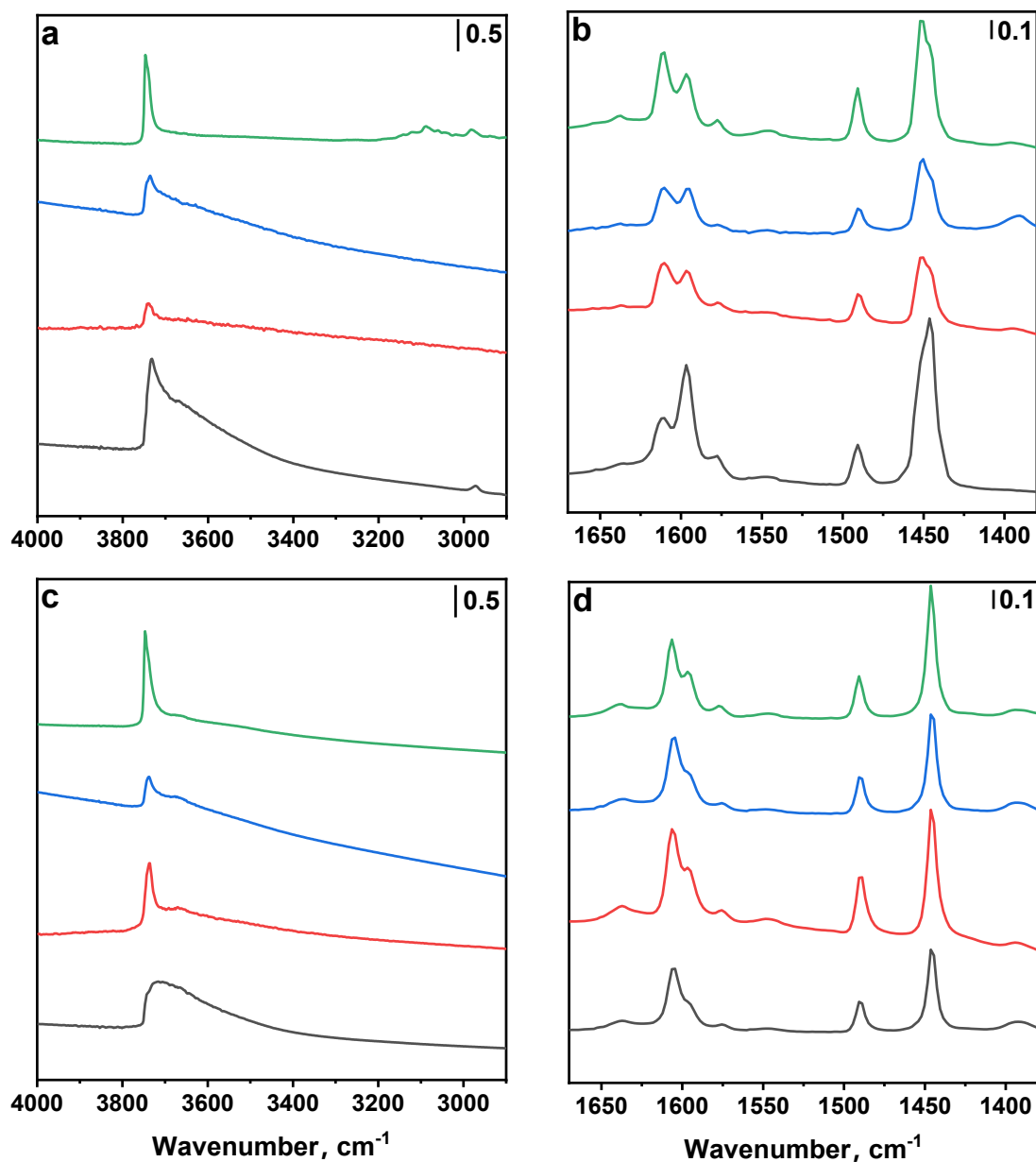


Figure 4-23. FTIR spectra of Sn- (a, b) and Zr-substituted (c, d) IWW (—), UTL (—), *CTH (—), *BEA (—) zeolites: region of OH- vibrations (a, c) and Py-ring vibrations collected after desorption of pyridine at 50 °C (b, d).

Table 4-8. Acidic properties of T^{IV}-substituted zeolite catalysts under study.

Sample	Acidic properties, $\mu\text{mol}\cdot\text{g}^{-1}$			Si/Me	
	C _L	C _B	C _Σ	EDS	FTIR-Py
IWW/Ti _{post}	612	0	612	20 ^a	26 ^a
TS-1	550	0	550	28 ^a	29 ^a
IWW/Sn _{post}	231	0	231	33 ^b	70 ^b
Sn-IWW _{hydro}	97	0	97	101 ^b	17 ^b
IWW/Zr _{post}	312	0	312	13 ^c	5 ^c
UTL/Sn _{post}	210	0	210	33 ^b	77 ^b
UTL/Zr _{post}	586	0	586	9 ^c	26 ^c
*CTH/Sn _{post}	183	0	183	30 ^b	88 ^b
*CTH/Zr _{post}	474	0	474	12 ^c	33 ^c
*BEA/Sn _{post}	261	29	290	14 ^b	62 ^b
*BEA/Zr _{post}	465	29	494	16 ^c	34 ^c

^a: Si/Ti, ^b: Si/Sn, ^c: Si/Zr

The formation of Lewis acid centers in T^{IV}-substituted zeolites agrees with the results of UV-vis spectroscopy (**Figure 4-24**) revealing a strong absorption band at about 230, 225 and 205 nm, which indicates ligand-to-metal charge transitions from oxygen to tetrahedrally coordinated Ti, Sn and Zr species, respectively^{115, 124, 193, 194}. The shoulder bands at ca. 265 (Ti-) and 255 nm (Sn-) may appear due to the presence of TiO₂ or SnO₂ in the extra-framework positions^{118, 194}. On the other hand, no bands related to the bulk ZrO₂ crystallites (triplet bands at 207, 214 and 227 nm¹⁹⁵) were found in the Zr-containing zeolite, confirming the avoidance of the aggregated ZrO₂ species. However, both tetrahedrally coordinated Zr species in zeolite framework and bulk ZrOCl₂ showed a dominant band at ca. 205 nm¹⁹⁶, thereby, the presence of ZrOCl₂ phase in Zr-containing zeolite cannot be completely ruled out based on UV-vis results. Moreover, a lower number of Zr atoms associated with Lewis acid sites determined by FTIR of adsorbed pyridine was observed in comparison with EDS results (e.g., UTL/Zr_{post}: Si/Zr_{EDS} = 9 vs. Si/Zr_{FTIR-Py} = 26, **Table 4-8**), revealing the potential presence of ZrOCl₂ phase.

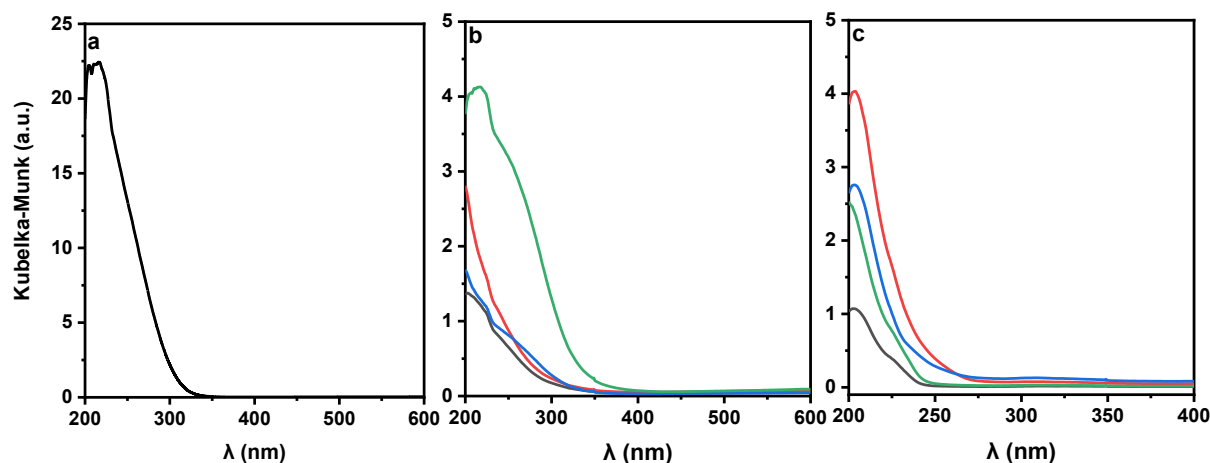


Figure 4-24. UV-vis spectra of **Zeolite/Ti_{post}** (a), **Zeolite/Sn_{post}** (b) and **Zeolite/Zr_{post}** (c): **IWW** (—), **UTL** (—), ***CTH** (—), reference ***BEA** zeolites (—).

According to the results of pyridine thermodesorption (**Figure 4-25**), Ge-for-T^{IV} substitution in **IWW**, **UTL**, ***CTH** zeolites were shown to generate Lewis acid centers with different strength determined by the nature of tetravalent element. The acid strength, estimated as the fraction of acid sites retaining the adsorbed pyridine after desorption at 200 °C (x % values in **Figure 4-25**) decreased in the following sequence independently on the structural type of zeolite framework: Sn- > Zr- > Ti-. As an example, for **IWW** zeolites, x % values decreased as follows: 51 % (**IWW/Sn_{post}**) > 47 % (**IWW/Zr_{post}**) > 17 % (**IWW/Ti_{post}**). This sequence is consistent with the results previously reported for isomorphously substituted zeolite ***BEA** in Refs.¹⁹⁷⁻¹⁹⁹.

Thus, post-synthesis degermanation/metalation of germanosilicates allowed to tailor a set of large- and extra-large pore zeolites with variable nature of Lewis acid sites, known to catalyze such redox reactions as epoxidation of olefins and BVO of cyclic ketones to lactones with hydrogen peroxide, MPV reduction of ketones to alcohols. The synthesis-structure-activity relationships of designed catalysts in the above-mentioned reactions is further discussed.

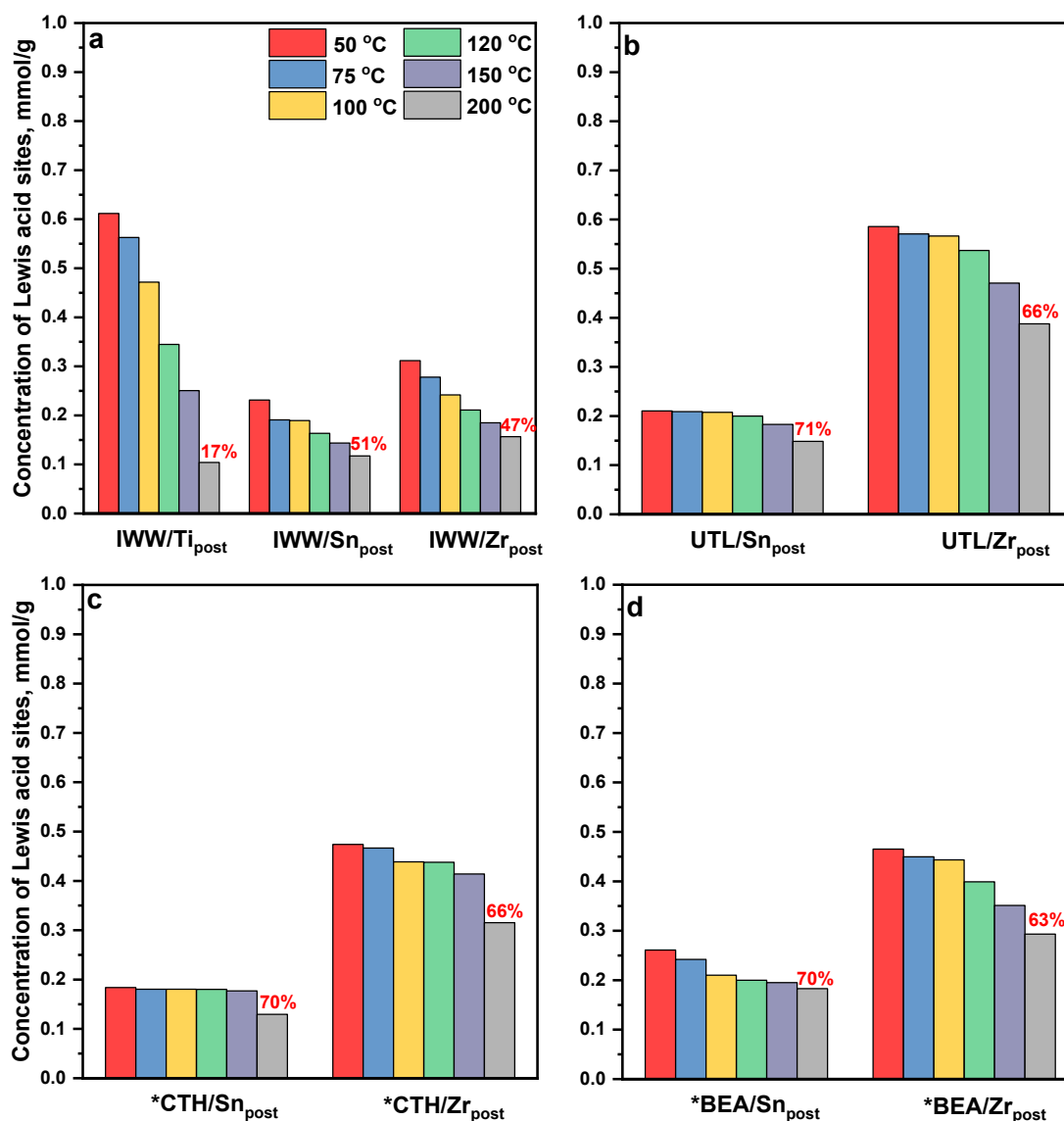


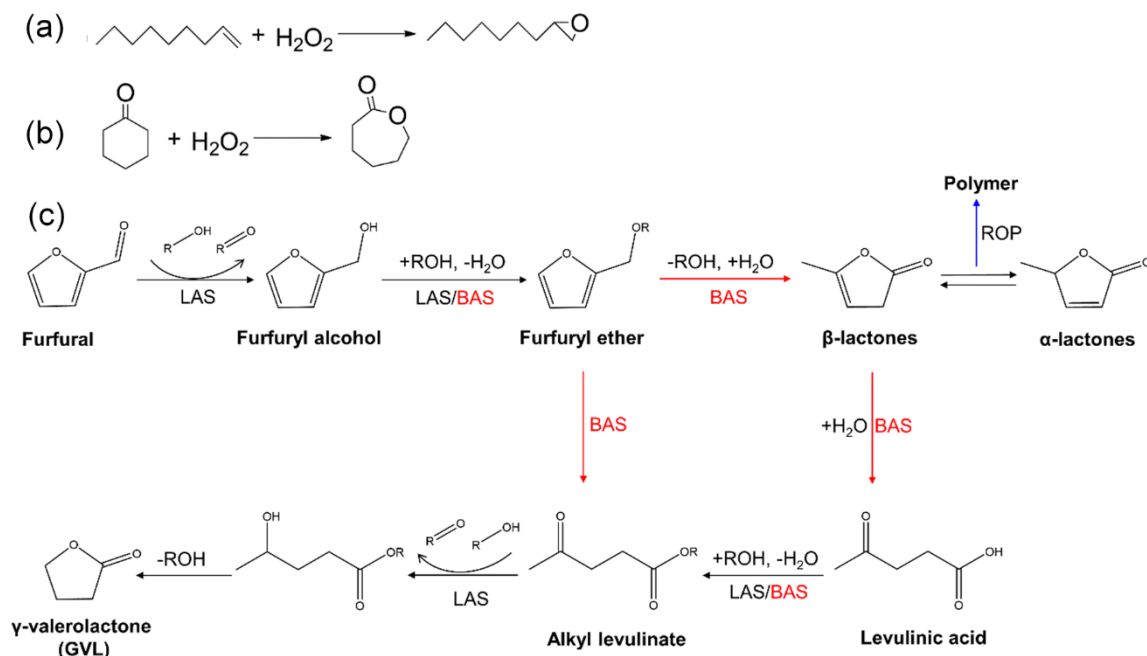
Figure 4-25. Concentration of acid sites in T^{IV}-substituted IWW (a), UTL (b), *CTH (c) and *BEA (d) zeolites retaining adsorbed pyridine at variable temperatures. *x* % refers to the fraction of acid sites retaining the adsorbed pyridine after desorption at 200 °C.

4.2.3.3. Catalytic performance

Three model reactions were used to test the catalytic performance of Ti-, Sn- and Zr-substituted Lewis acid zeolite catalysts.

- 1) Epoxidation of 1-octene (**Scheme 4-4a**) proceeding on Ti Lewis acid sites was tested over IWW/Ti_{post} vs. commercial TS-1;
- 2) BVO of cyclohexanone with hydrogen peroxide (**Scheme 4-4b**) efficiently catalyzed by Sn Lewis acid sites was tested over IWW/Sn_{post} vs. Sn-IWW_{hydro};

3) MPV reduction of furfural (**Scheme 4-4c**) catalyzed by Sn- and Zr- Lewis acid centers was tested over Sn- and Zr-substituted large (**IWW**) and extra-large pore (***CTH**, **UTL**) zeolites vs. post-synthetically dealuminated-metalated commercial ***BEA** zeolite.



Scheme 4-4. Catalytic reactions: epoxidation of 1-octene (a), BVO of cyclohexanone (b) and MPV reduction of furfural opening the way to valuable lactones (c). ROP: ring opening polymerization.

In contrast to the germanosilicate **IWW-5** zeolite inactive in epoxidation, **IWW/Ti_{post}** showed a highly selective conversion of 1-octene to 1,2-epoxyoctane (**Table 4-9**, selectivity: 94 %). This result supports the formation of acid centers active in epoxidation reaction upon post-synthesis incorporation of Ti atoms into the framework of **IWW** zeolite. **Figure 4-26** shows the profiles of conversion versus time for each zeolite catalyst. After reacting for 2 h, higher conversion over **IWW/Ti_{post}** (49 %) was observed when compared to the hydrothermally synthesized commercial TS-1 zeolites (39 %).

In BVO of cyclohexanone, both **IWW/Sn_{post}** and **IWW-5** samples catalyzed the selective formation of targeted ϵ -caprolactone. This finding is consistent with the published results that framework Ge atoms can act as the active centers in BVO reaction. The TOF values were

calculated based on the total amount of Ge atoms determined by chemical analysis (for **IWW-5**) and a sum of Ge atoms and Sn-associated LAS (for **IWW/Sn_{post}**). The TOF value achieved over **IWW-5** (TOF = 3 h⁻¹) was almost four times lower than that of **IWW/Sn_{post}** (TOF = 13 h⁻¹) zeolite, hence indicating the higher catalytic activity of framework Sn than that of Ge atoms (**Table 4-9**). Higher catalytic activity of post-synthesized **IWW** zeolite in comparison with the hydrothermally synthesized zeolite samples (**IWW/Ti_{post}** (TOF = 123 h⁻¹) vs. TS-1 (81 h⁻¹), **IWW/Sn_{post}** (13 h⁻¹) vs. Sn-**IWW_{hydro}** (2 h⁻¹), **Table 4-9**) could be related to the higher accessibility of acid centers in post-synthesized zeolite catalysts due to 1) their relative smaller crystal sizes (**Figure 4-27**); 2) preferential metalation of the outer regions of zeolite crystals²⁰⁰.

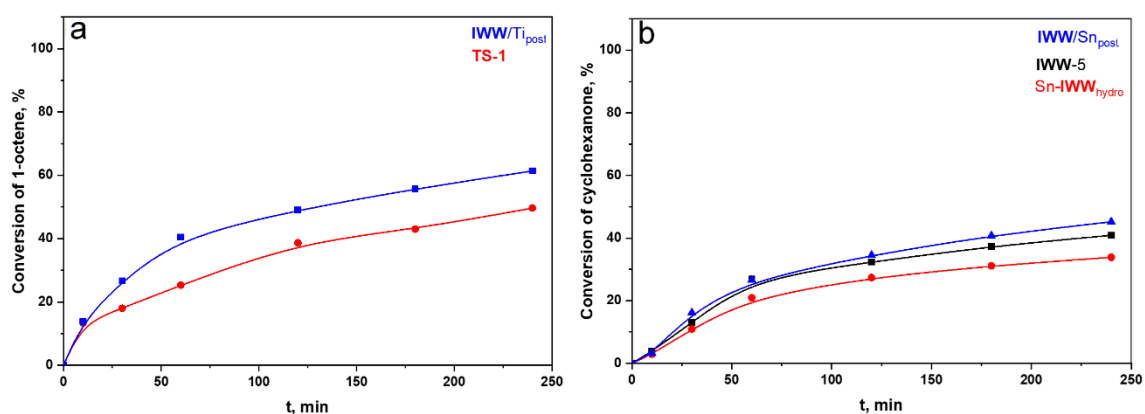


Figure 4-26. Conversion of 1-octene versus time in epoxidation reaction (a) and cyclohexanone versus time in Baeyer-Villiger oxidation (b) over catalysts under study.

Table 4-9. Catalytic activities of Ti and Sn-substituted zeolite catalysts in different model reactions.

Catalyst	Process	Targeted product	TOF, h ⁻¹
IWW-5	Epoxidation	1,2-epoxyoctane	—
TS-1			81 ^a
IWW/Ti_{post}			123 ^a
IWW-5	BVO	ε-caprolactone	3 ^b
Sn- IWW_{hydro}			2 ^c
IWW/Sn_{post}			13 ^c

^a- referred to per Ti site; ^b- referred to per Ge site; ^c- referred to per (Ge + Sn) site

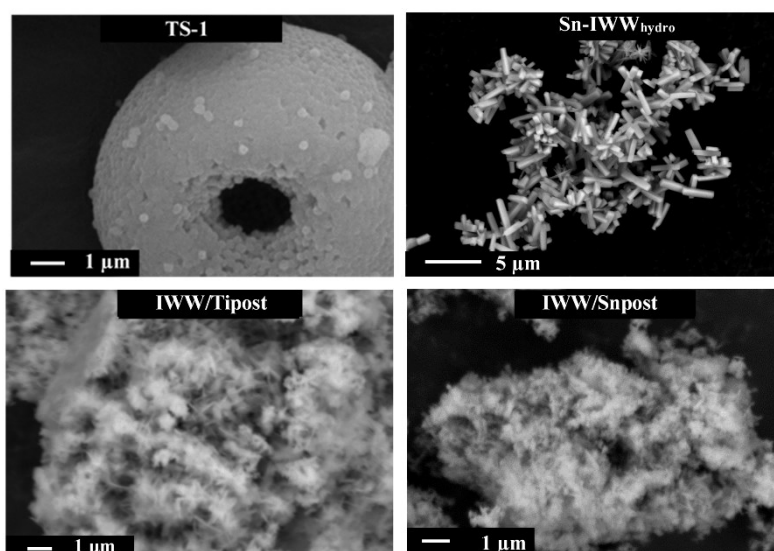


Figure 4-27. SEM images of Ti, Sn-containing IWW zeolites.

In MPV reduction of furfural, besides furfural-to-furfuryl alcohol transformation over Lewis acid sites, subsequent reactions, such as furfuryl alcohol etherification, lactonization of formed ether, transesterification of β -lactone and others, occurred to different extent over studied Sn- and Zr-substituted IWW, UTL, *CTH and *BEA zeolites, as previously reported for *BEA zeolite in Ref.¹⁵². Thus, not only furfuryl alcohol, but also isopropyl furfuryl ether, isopropyl levulinate, β -lactones and γ -valerolactone were found among the products. **Figure 4-28** shows the profiles of furfural conversion versus time for different Sn- and Zr-containing zeolite catalysts. After reacting for 2 hours, $\sim 95\%$ conversion of furfural is achieved over both Sn- and Zr-containing UTL zeolites, which is much higher than those of respective IWW (Sn: 28 %, Zr: 7 %) and *CTH (Sn: 21 %, Zr: 31 %) zeolites. Taken comparable amount of Lewis acid sites in the catalysts (**Figure 4-25**), this difference can be related to the features of UTL vs. IWW & *CTH frameworks which can affect the formation of reaction intermediates/transition state²⁰¹. UTL contains the intersected 14- ($9.5 \times 7.1 \text{ \AA}$) and 12-ring pores ($8.5 \times 5.5 \text{ \AA}$), which are large enough to accommodate the 6-membered cyclic transition state for MPV reduction with a molecular size estimated to be 6.6 \AA ²⁰¹. At the same time, only 14-ring pores ($7.8 \times 7.7 \text{ \AA}$) in *CTH and 12-ring channels ($6.7 \times 6.0 \text{ \AA}$) in IWW propagated in one dimension are appropriate for such large intermediate.

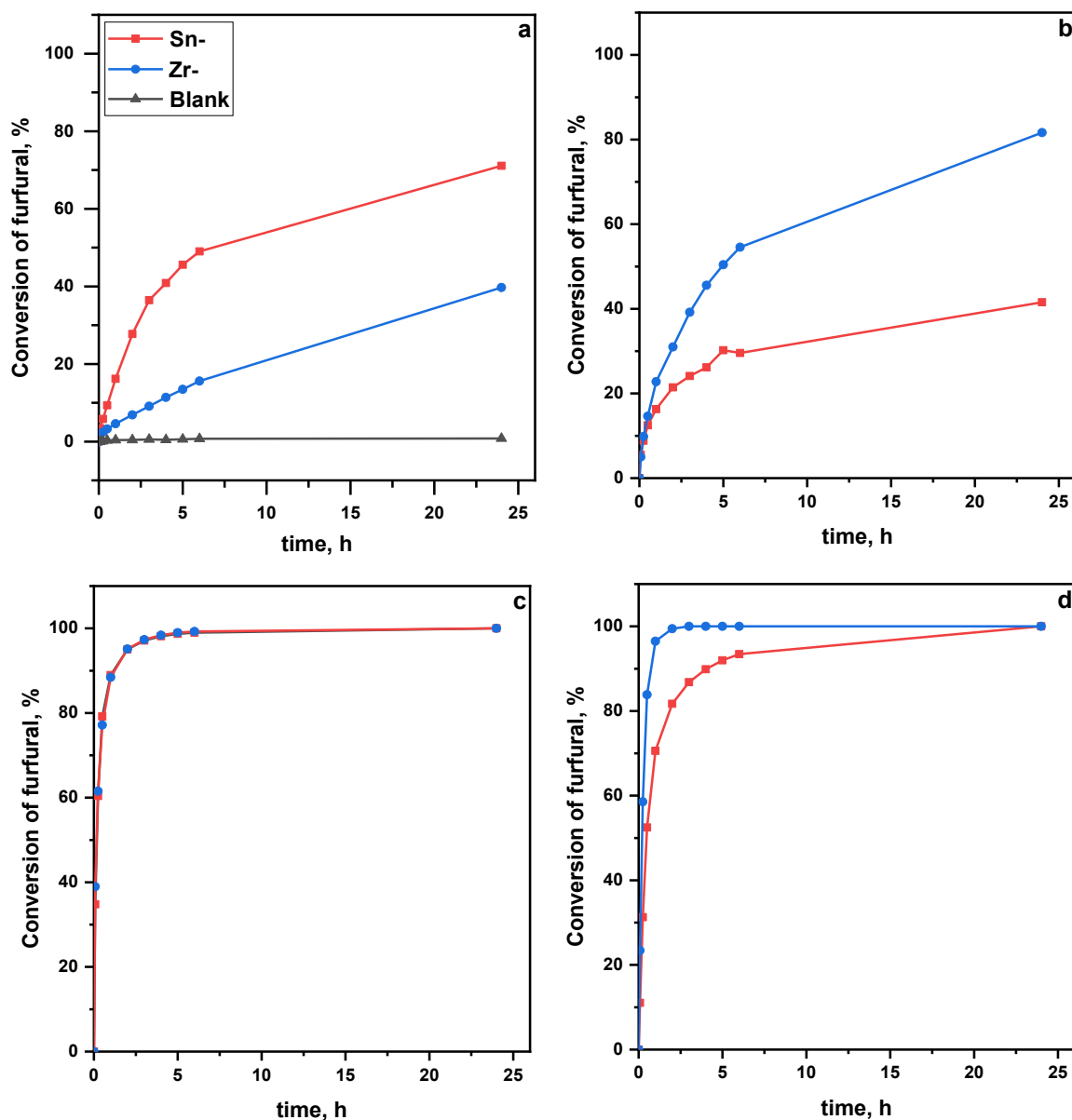


Figure 4-28. Conversion of furfural versus time in MPV reduction over Sn- and Zr-substituted **IWW** (a), ***CTH** (b), **UTL** (c) and ***BEA** (d) zeolites.

Noticeably, a comparably high conversions (81 – 99 %) were observed for T^{IV} -substituted extra-large pore **UTL** and the reference large-pore ***BEA** zeolites with 3-dimensional system of intersecting 12-ring channels (6.6×6.7 and 5.6×5.6 Å). Propagation of large 12-ring pores in all three dimensions in ***BEA** zeolite is the reason for higher furfural conversion in ***BEA** compared with the **IWW** and ***CTH** catalysts.

Moreover, the effect of the acid sites identity on the catalytic performance of T^{IV} -

substituted was evident. **UTL/Sn_{post}** showed higher catalytic activity than **UTL/Zr_{post}** zeolite (TOF: 57 h⁻¹ vs. 21 h⁻¹, **Table 4-10**), while a reverse result was reported in the literature^{152, 202}. The unusual catalytic results in **UTL/Zr_{post}** vs. **UTL/Sn_{post}** sample can be related to the lower micropore volume (0.16 vs. 0.19 cm³·g⁻¹) and BET surface area (384 vs. 478 m²·g⁻¹) than **UTL/Sn_{post}** due to the partial blockage with ZrOCl₂ species (Section 4.2.3.1).

Table 4-10. Catalytic performance of Sn and Zr-substituted zeolite catalysts in the MPV reduction of furfural.

	T ^{IV} Metal	Conversion of furfural, %	Yield of product, %					TOF, h ⁻¹
			furfuryl alcohol	Isopropyl furfuryl ether	Isopropyl levulinate	β- lactones	γ- valero- lactone	
IWW	Sn	71	19	37	4	4	5 ^a	
	Zr	40	32	4	4		2 ^b	
*CTH	Sn	42	24	11	2	1	10 ^a	
	Zr	82	76	2	1		4 ^b	
UTL	Sn	100	16	51	19	3	2	57 ^a
	Zr	100	52	31	7	2	2	21 ^b
*BEA	Sn	100		24	12	35	3	24 ^a
	Zr	100		63	5	16	2	25 ^b
Blank	no	1	n.d.	n.d.	n.d.	n.d.	n.d.	n.d.

^a- referred to per Sn site; ^b- referred to per Zr site. Reaction conditions: 80 °C, 24 h

The different acid strength is responsible for the different main products obtained over **UTL/Sn_{post}** (furfuryl ether, selectivity 51 %) ²⁰³ and **UTL/Zr_{post}** (furfuryl alcohol, selectivity 52 %). This result is consistent with previously reported higher activity of stronger Sn LAS vs. Zr LAS in etherification of 2,5-bis(hydroxymethyl)furan formed upon MPV reduction of 5-(hydroxymethyl)furfural²⁰⁴. On the other hand, furfuryl ether was found to be the main product achieved over Zr-containing ***BEA** even with a lower Lewis acid strength that is in line with

the presence of Al-associated Brønsted acid sites (**Table 4-8**), being active sites for the conversion of alcohol to ether^{203, 205}.

4.3. Controlling disassembly step within the ADOR process for the synthesis of zeolites

This section is devoted to designing post-synthesis approach aimed at controllable alternation of both structural and acidic properties of germanosilicate zeolites. Until now, a successful preparation of a set of isorecticular UTL-derived ADORable zeolites was achieved by controlling the speed of rearrangement process under the conditions of fast de-intercalation (Section 2.2.2)^{99, 206}. In particular, unavoidable fast de-intercalation of Ge-enriched D4R units off UTL zeolite in aqueous medium leading to IPC-1P layered precursor was followed by rearrangement of leached species to build-up new interlayer linkages of variable length, such as a combination of D4R/S4R in IPC-7, S4R in **OKO**, a combination of S4R/-O- in ***PCS** zeolites. However, such fast deintercalation/variable rearrangement approach was not fruitful to produce other families of isorecticular zeolites, such as **UOV**-^{44, 100}, **IWW**-¹⁰², ***CTH**-derived²⁰⁷ ones. Therefore, this section aimed at optimization hydrolysis conditions enabling to regulate both de-intercalation and rearrangement processes for the preparation of new materials. Specifically, the role of water-to-zeolite ratio and additive of framework-building element (i.e., Al) in the Assembly-Disassembly-Organization-Reassembly process determining structural and chemical properties of UTL-derived zeolites was assessed.

4.3.1. “Slow deintercalation/slow rearrangement” of UTL in water-methanol systems

Firstly, the effect of water-to-zeolite ratio on the kinetic of UTL disassembly was studied in water-methanol systems of different concentrations (**Figure 4-29**). Consistent with the previous results³⁵, full hydrolysis of UTL germanosilicate in pure water (0 % MeOH) resulted in the formation of **PCR** zeolite upon calcination even after treatment for 1 h, revealing the fast hydrolysis and de-intercalation of D4R units off UTL framework (**Figure 4-29**). In turn, using water-methanol medium allowed decelerating the disassembly process. Thus, a progressive

decrease in d -spacing (200), corresponding to sequential UTL \rightarrow IPC-7 \rightarrow IPC-2 \rightarrow IPC-6 zeolite transformation was observed. Noticeably, while decrease in the water-to-methanol ratio only slowed down the disassembly process (**Figure 4-29b**), UTL framework was stable in water-free methanol.

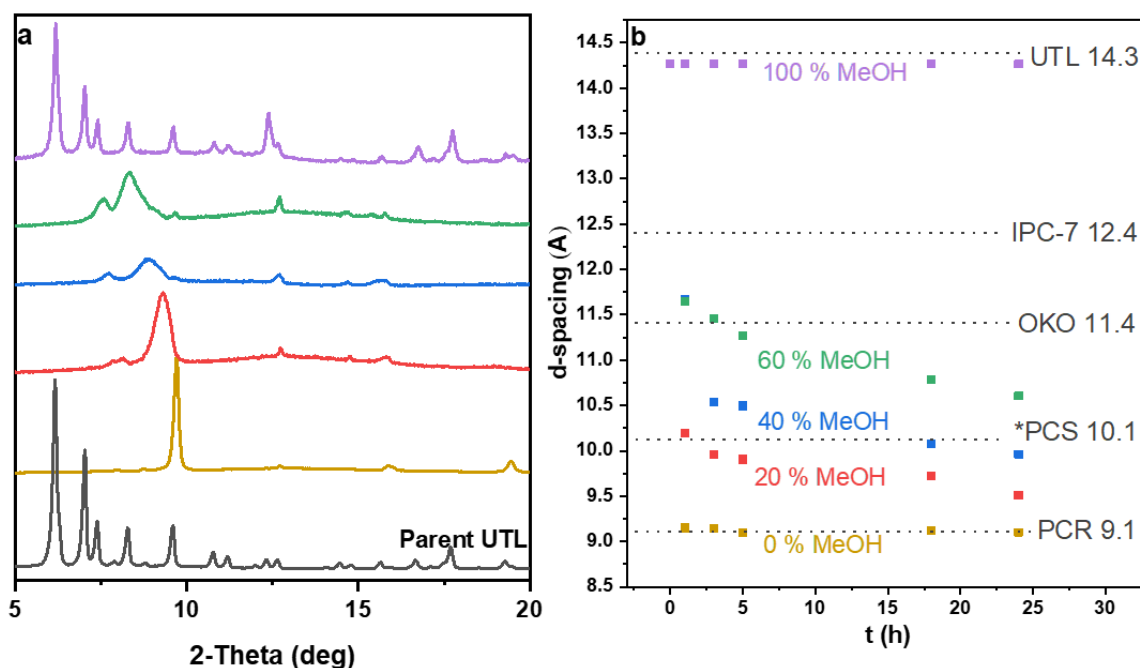


Figure 4-29. Evolution of (200) d -spacing in zeolites recovered from UTL-H₂O/MeOH systems ($T = 60\text{ }^{\circ}\text{C}$) and subsequently calcined *vs.* MeOH concentration and duration of the treatment (a) and XRD patterns of the calcined products recover after 24 h from H₂O/MeOH solutions of different concentrations (b).

These results support the mechanism involving gradual reduction of the size of interlayer units (i.e., D4R \rightarrow D4R/S4R \rightarrow S4R \rightarrow S4R/-O- transformation) promoting the generation of IPC- n zeolites under slow de-intercalation conditions. This mechanism is different from the published mechanism of IPC- n formation through the rearrangement of -O- units in IPC-1P (i.e., -O- \rightarrow S4R/-O- \rightarrow S4R)⁹⁴⁻⁹⁶. However, the products obtained *via* slow de-intercalation of UTL in water-methanol solution possess poorer textual properties (i.e., BET surface area and micropore volume, **Table 4-11**) compared to their analogues prepared in aqueous medium^{44, 97, 98, 208-210}. The result is probably caused by a partial blockage of the zeolite pores by the leached

germanium oxide species due to their lower solubility in methanol-water solution than in water.

Table 4-11. Textural characteristics of IPC-n zeolites prepared in water-methanol vs. reference zeolites prepared *via* “fast disassembly/rearrangement” approach.

Zeolite	Synthesis conditions	S _{BET} , m ² ·g ⁻¹	V _{micro} , cm ³ ·g ⁻¹	Si/Ge
IPC-7	60 % EtOH, 60 °C, 1 h	324	0.11	5
	Ref. ⁹⁷	590	0.22	80
IPC-2 (OKO)	60 % MeOH, 60 °C, 1 h	262	0.09	8
	Ref. ^{97, 98, 209-211}	334 – 406	0.15 – 0.19	> 100
IPC-6 (*PCS)	40 % MeOH, 60 °C, 18 h	170	0.07	16
	Ref. ^{97, 209, 210}	310	0.11 – 0.14	80

4.3.2. “Slow deintercalation/fast rearrangement” of UTL in Al-containing water-methanol systems

To accelerate the rearrangement process and/or generate acid centers in the formed IPC-n zeolites, structure building Al element was added into water-methanol medium. The parent UTL zeolite and samples isolated from Al-H₂O-MeOH medium after 1 min – 1 h showed similar XRD patterns, although the intensities of the diffraction lines for treated samples were significantly reduced (**Figure 4-30a**). These results revealed the change in the structural ordering of the UTL framework. Moreover, no Ge was leached from zeolite pores since a negligible change in Si/Ge ratio in respective recovered samples was found when compared to the parent UTL zeolite (**Figure 4-30b**).

Two interlayer peaks at 6.2 ° and 7.8 ° were observed in the XRD pattern of the sample recovered after 4 hours, corresponding to the (200) diffraction lines of UTL and OKO²¹¹, respectively. Extending the duration of the treatment led to simultaneous removal of the interlayer peak (200) of UTL (after 1 day) and enhancement of the (200) diffraction intensity

of **OKO**, reaching the maximum after 7 days. In turn, a significant decrease in the (200) reflection of **OKO** along with the restoration of (200) diffraction line of **UTL** was observed after the treatment for 12 days. The growing intensity and narrowing interlayer peak with prolongation of the treatment (12 – 60 days) suggest improvement of structural order of renovating zeolite.

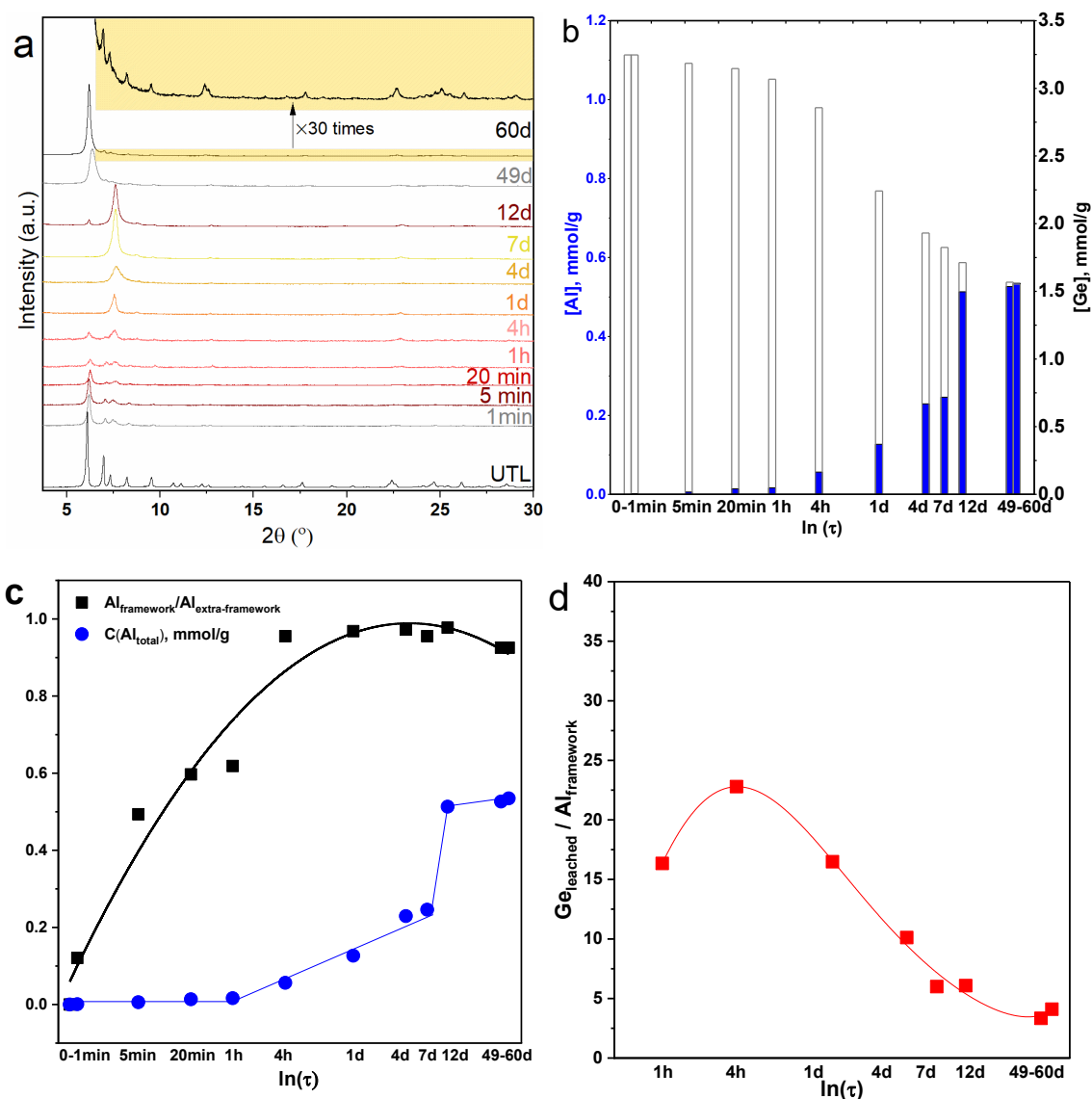


Figure 4-30. Evolution of XRD patterns (a), Ge and Al contents (b), total concentration of Al and fraction of framework Al (c), ratio between Ge leached and Al incorporated (d) for the samples recovered from Al-containing H₂O-MeOH solution (T = 60 °C) and subsequently calcined.

Unprecedentedly, “slow disassembly”/“fast rearrangement” conditions applied to UTL zeolite allowed the reconstruction of the UTL framework after 60 days. This result is supported by the XRD patterns of parent and restored samples showing the characteristic diffraction lines of UTL, although of a lower intensity and of larger width in the restored sample (**Figure 4-30a**). The change in the shape of XRD reflections may be related to a smaller size of the crystals renovated after 60 days of treatment (**Figure 4-31**). A similar result was reported in Ref.²⁰⁸, showing the fragmentation of UTL crystals upon the hydrolysis process. In addition to XRD, TEM images for parent and restored samples also showed the characteristics of UTL zeolite, that is, 1.4 nm repeated stacked layers (**Figure 4-32**).

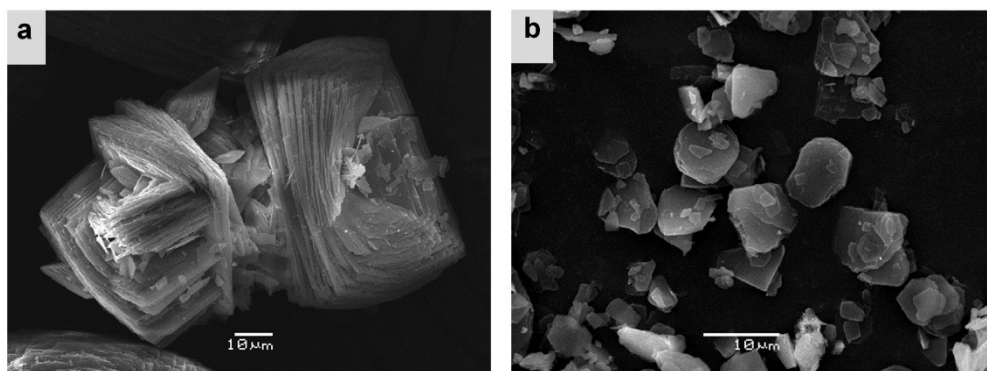


Figure 4-31. SEM images of parent UTL zeolite (a) and the sample recovered from Al-containing H₂O-MeOH solution after 60 days (b).

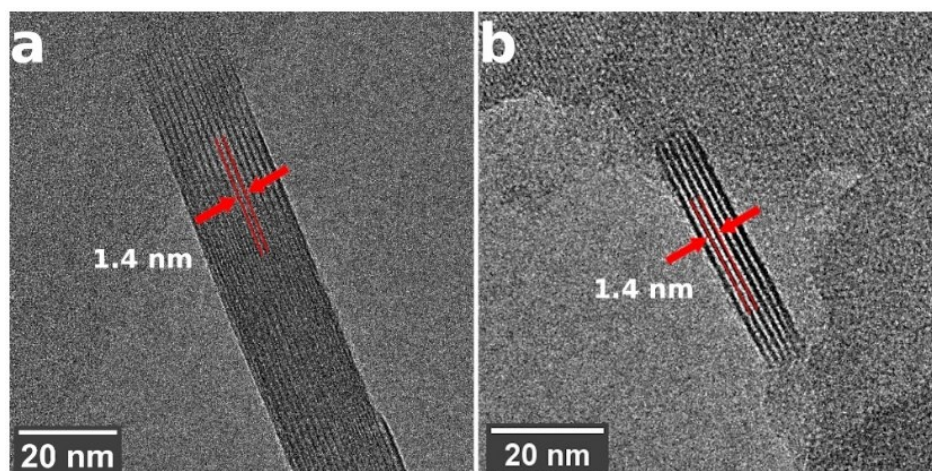


Figure 4-32. TEM images of parent UTL zeolite (a) and the sample recovered from Al-containing H₂O-MeOH solution after 60 days (b).

Chemical analysis revealed a stepwise reduction in the fraction of Ge in zeolite, which was accompanied with enhancing of Al content (4 h – 12 days, **Figure 4-30b**). At the same time, a gradual introduction of Al into framework positions of zeolite was confirmed by gradual increase in the intensity of the framework Al peak (~ 54 ppm) in the ^{27}Al MAS NMR spectra (**Figure 4-33**) and a low intensity of the peak at 0 ppm corresponding to the extra-framework Al. A delayed character of the rearrangement process was suggested considering the relationship between the amount of extracted Ge from the UTL framework and incorporated Al ($\text{Ge}_{\text{leached}}/\text{Al}_{\text{framework}}$, **Figure 4-30d**), which reached around 23 after 4 h with further drop to 4 after treatment for 49 – 60 days. Thus, the Si/Al and Si/Ge of the resulting UTL-like material (60 days) was 24 and 9, respectively, and STEM-EDS maps showed a uniform distribution of Al in the zeolite crystals (**Figure 4-34**).

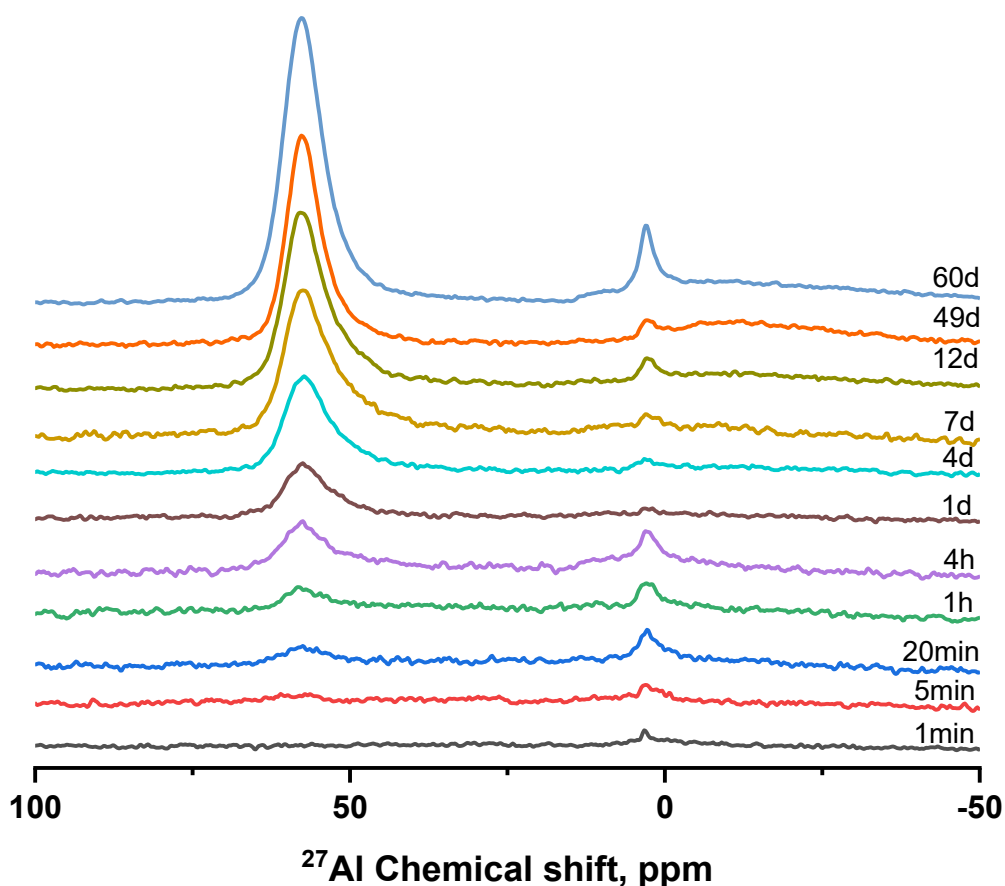


Figure 4-33. Evolution of ^{27}Al MAS NMR for the samples recovered Al-containing H_2O -MeOH solution ($T = 60\text{ }^\circ\text{C}$) and subsequently calcined.

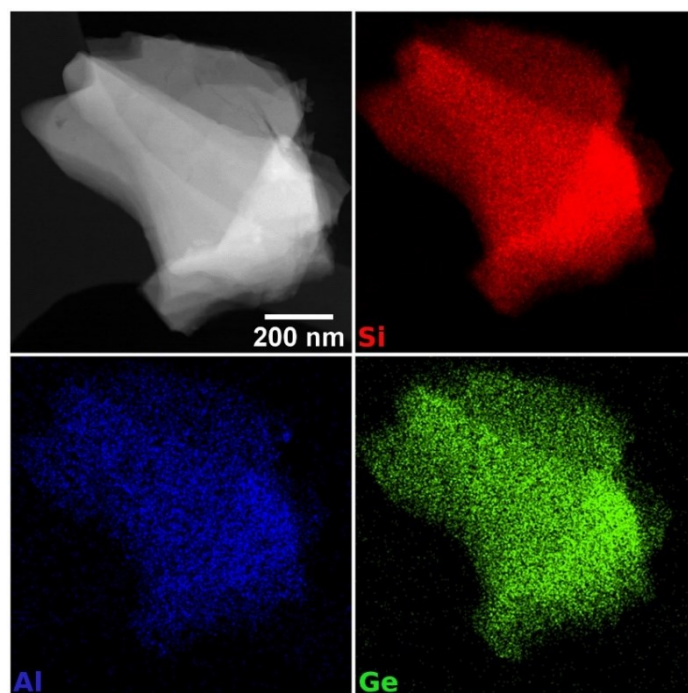


Figure 4-34. STEM image of UTL sample recovered from Al-containing H₂O-MeOH solution after 60 days with EDS maps showing distribution of Si (red), Al (blue) and Ge (green).

Further characterizations, i.e., pore size distribution (**Figure 4-35a**) and micropore volume (**Figures 4-35b** and **4-36**), also proved the reconstruction of UTL framework in Al-containing H₂O-MeOH system. The conversion of bimodal to monomodal PSD was in line with the transformation of UTL to OKO (from 20 min to 12 days)²⁰⁸. Conversely, the restoration of the peak associated with the extra-large pores (14-rings) indicated the transformation of OKO to UTL. The interaction between probe and zeolite framework is dependent on the zeolite chemical composition, thus determining the estimated pore size distribution²⁰⁹. The deviated PSD in parent germanosilicate and restored aluminosilicate UTL samples may originate from the difference in chemical composition of respective samples. A significantly lower micropore volumes of the samples recovered after 1 – 20 min (0.08 – 0.09 cm³·g⁻¹) in comparison with the parent UTL zeolite (0.21 cm³·g⁻¹, **Figure 4-35b**) is consistent with their poor crystallinity of respective samples (**Figure 4-30a**) and blockage of zeolite pores with leached Ge species (**Figure 4-30b**). With the prolongation of the treatment from 1 to 7 days, an increase in V_{micro} (~ 0.11 cm³·g⁻¹) is associated with the improvement of the structural ordering of OKO. Finally, the Al-induced UTL → Al-UTL transformation was accompanied with increase in micropore

volume V_{micro} up to $0.18 \text{ cm}^3 \cdot \text{g}^{-1}$, closely resembling the values previously reported for hydrothermally synthesized **UTL**. Moreover, the restored Al-UTL showed higher concentration of Brønsted ($0.30 \text{ mmol} \cdot \text{g}^{-1}$) and Lewis ($0.20 \text{ mmol} \cdot \text{g}^{-1}$) acid centers (**Figure 4-37**) than the hydrothermally synthesized Al-UTL zeolite (V_{micro} : $0.19 - 0.23 \text{ cm}^3 \cdot \text{g}^{-1}$,^{110, 45, 107, 110, 138}, C_{B} : $0.07 \text{ mmol} \cdot \text{g}^{-1}$, C_{L} : $0.06 \text{ mmol} \cdot \text{g}^{-1}$,^{110, 109, 110, 138}). The generated acid centers can act as active sites in a variety of reactions^{83, 212}.

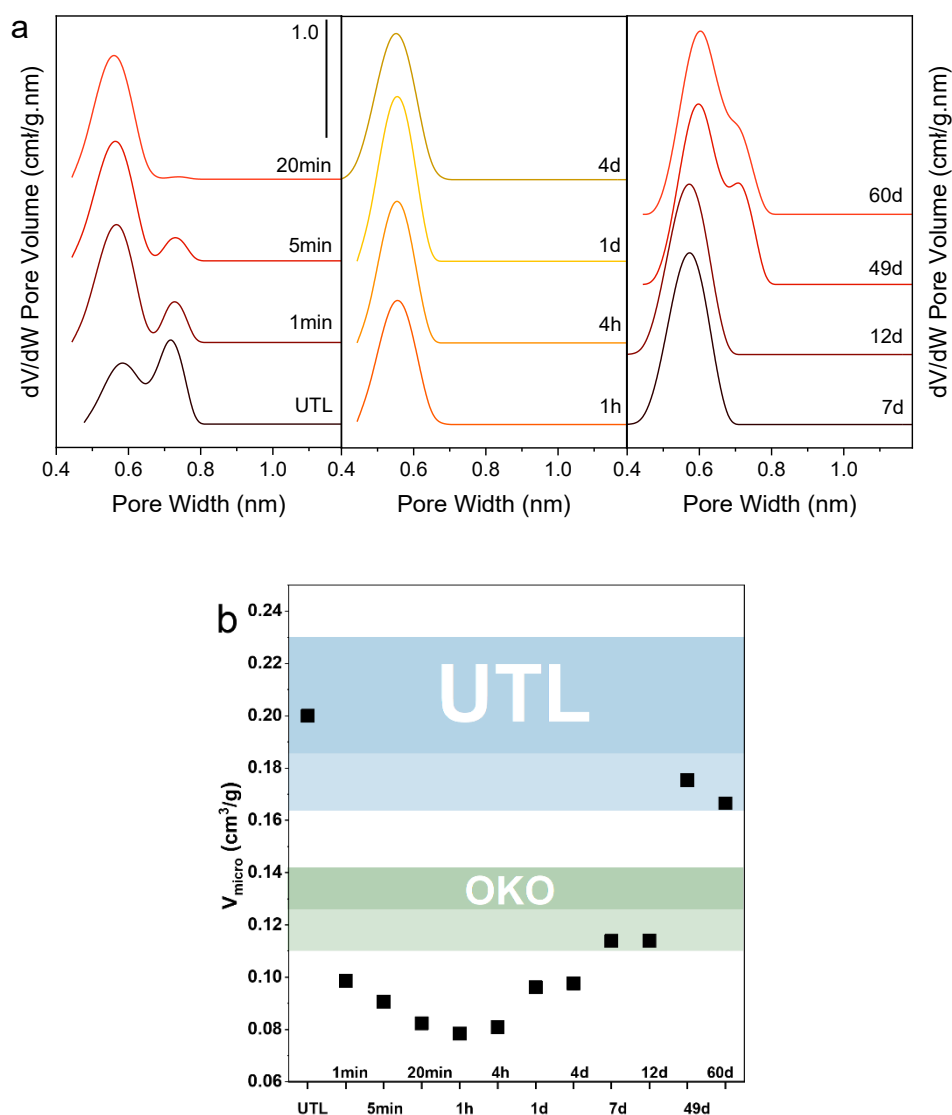


Figure 4-35. Evolution of the PSD (a) and V_{micro} (b) for the samples recovered from Al-containing H_2O -MeOH solutions ($T = 60 \text{ }^\circ\text{C}$) and subsequently calcined. Blue and green rectangles represent the ranges of V_{micro} for **UTL** and **OKO** zeolites reported in Refs.^{10, 45, 107, 139}, respectively.

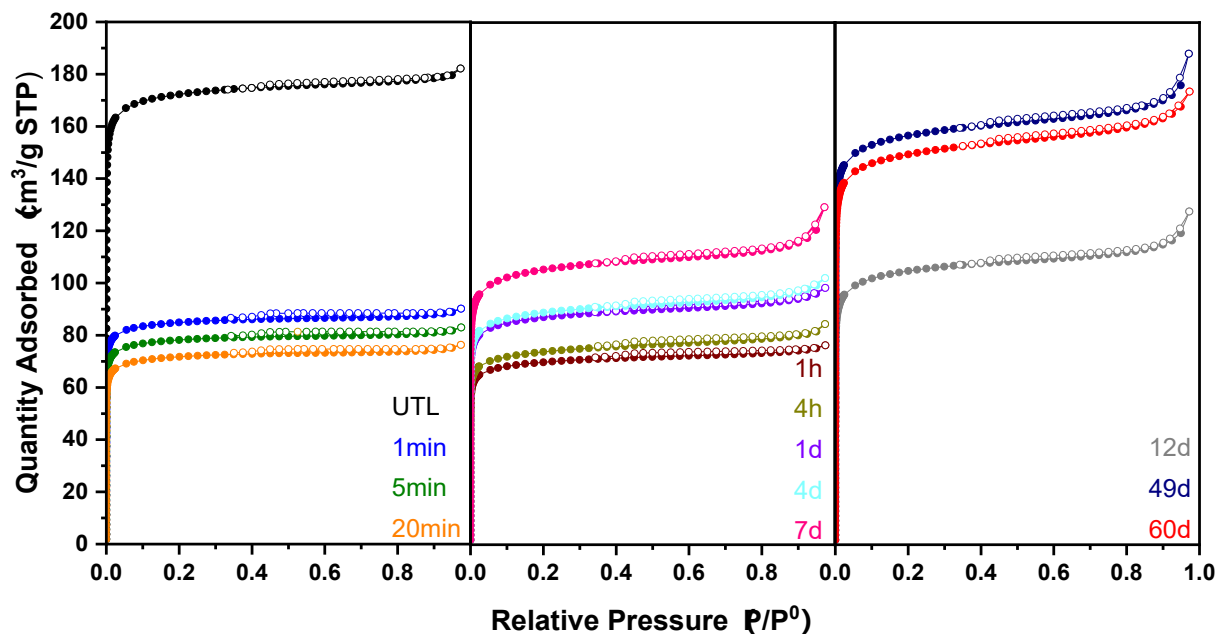


Figure 4-36. Ar adsorption (●) and desorption (○) isotherms of samples recovered from Al-containing H₂O-MeOH solution (T = 60 °C) and subsequently calcined.

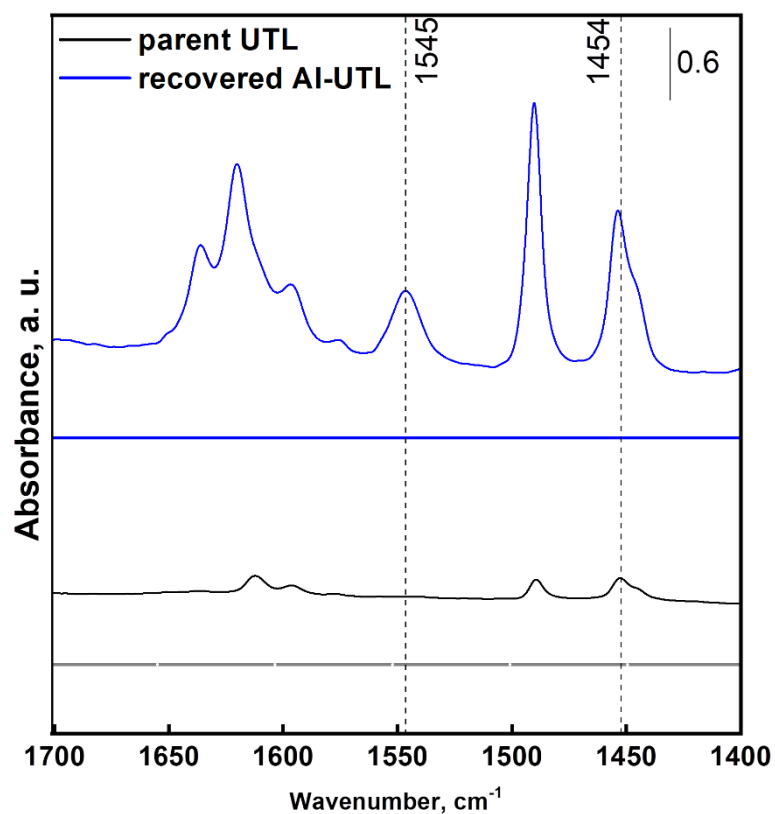
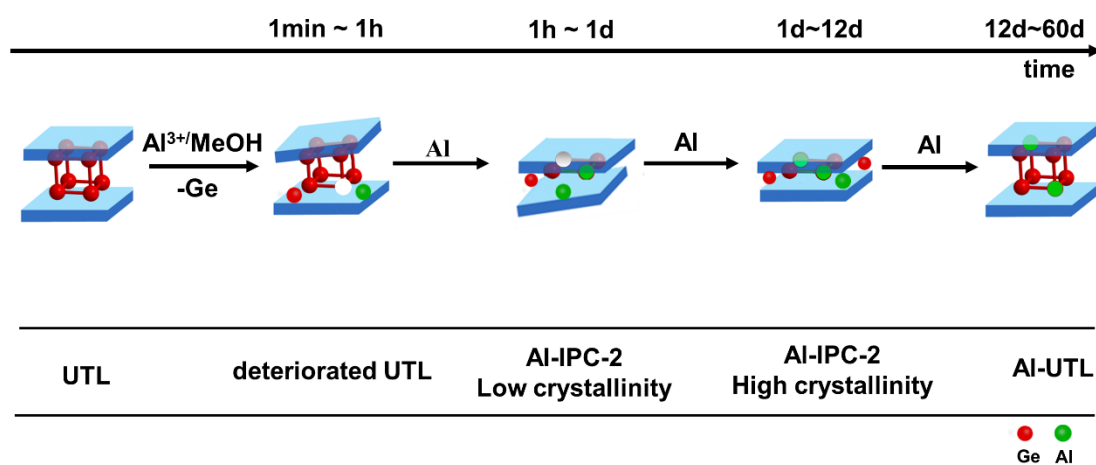


Figure 4-37. FTIR spectra of parent UTL zeolite and the sample recovered from Al-containing H₂O-MeOH solution after 60 days after activation (thick) and adsorption of pyridine (thin). The region of Py-ring vibrations is shown.

Overall, considering the results of different characterization techniques, the plausible mechanism of **UTL** → **Al-OKO** → **Al-UTL** transformation was proposed as follows (**Scheme 4-5**):

1. 1 min – 1 h: slow breakage of Ge-O(Si) bonds leading to deformation of **UTL** framework and the pore system is temporarily blocked by the extracted germanium species;
2. 1 h – 1 d: removal of leached germania from zeolite pores along with the intercalation of Al resulting in the low crystalline Al-poor **OKO** zeolite with mainly extra-framework Al;
3. 1 – 12 d: incorporation of Al into framework position and self-reorganization of zeolite layers. The resulting Al-enriched **OKO** zeolite was characterized by higher crystallinity and high fraction of tetrahedral Al;
4. 12 – 60 d: reconstruction of D4R units *via* Al-assisted rearrangement process. The resulting material was shown to be **UTL** zeolite.



Scheme 4-5. “Slow disassembly”/“fast rearrangement” of **UTL** zeolite in Al-containing H_2O - MeOH solution.

5. Conclusions

This thesis was focused on the design of zeolites with large and extra-large pores and tailored chemical composition as potential catalysts for Lewis-acid catalyzed processes used for valorization of biomass-derived renewable compounds. Since the available germanosilicates represent an endless store of structural diversity and, in addition, have a high potential for controlled transformation into new structures, post-synthesis modification of germanosilicate zeolites was selected as synthetic strategy to be developed in this thesis.

The interrelation of acidic and catalytic properties of germanosilicate zeolites was assessed. Thus, large pore **IWW** and extra-large pore **UTL** germanosilicate zeolites were shown as active and selective catalysts in ketalization of bio-renewable glycerol to cyclic ethers considered promising fuel additives. The catalytic performance of germanosilicate zeolites was related to their acid sites nature, strength and concentration. In particular, more active **IWW** zeolite catalyst was shown featuring both Lewis and Brønsted acidity, while **UTL** zeolite was found to possess exclusively Lewis acid centers, associated with Ge framework atoms.

The water-induced character of Brønsted acid centers in **IWW** germanosilicate was verified using FTIR spectroscopy of adsorbed pyridine, which revealed increasing the Brønsted-to-Lewis acid sites ratio with 1) reducing the activation temperature (450 °C → 300 °C → 200 °C) or with 2) enhanced amount of adsorbed water. The comparable conversion values of glycerol achieved over **IWW** germanosilicate and commercial aluminosilicate zeolite ***BEA** catalysts revealed that weak acid centers characteristic of germanosilicate zeolites are capable to catalyze ketalization reaction.

To further extend the catalytic application of zeolites with unusual topologies, i.e., large pore **IWW** and extra-large pore **UTL** and ***CTH** germanosilicates, we conceived and developed post-synthesis degermanation/metalation approach coupled with Ge recovery and recycling allowing to tailor Lewis acid heterogeneous catalysts with targeted chemical composition in a cost efficient way. By optimizing the degermanation conditions (pH, T, duration of the treatment), up to 94 % of Ge was recovered from zeolites with different pore-

systems (**ITH**, **IWW** and **UTL**). The recovered GeO₂ was further recycled in hydrothermal synthesis of different germanosilicates. Importantly, the separation method of Ge-containing leached solution from degermanated zeolite was found to determine the phase selectivity of zeolite formation upon Ge recycling after evaporation of leached solution. In particular, GeO₂ recovered by *filtration* and containing trace amounts of initial zeolite favored seed-assisted crystallization of parent zeolite, albeit possessing larger crystals, independently on the re-synthesis conditions applied. In turn, *microfiltration* was shown as an effective way to recover a versatile Ge source for the synthesis of different zeolites (exemplified for **ITH**, **IWW** and **UTL**). Subsequent metalation of degermanated large pore (**IWW**) and post-stabilized extra-large pore (**UTL**, ***CTH**) zeolites resulted in a set of Ti-, Sn- and Zr-substituted Lewis acid zeolites outperforming hydrothermally synthesized zeolite catalysts in model reactions, such as epoxidation of 1-octene chosen to test Ti-substituted zeolites, BVO of cyclohexanone chosen to test Sn-containing materials and Meerwein-Ponndorf-Verley reduction of furfural chosen to test Sn- and Zr-substituted zeolites.

Water-induced disassembly of **UTL** germanosilicate in combination with Ge-for-Al isomorphous substitution was optimized to regulate the competing deintercalation and rearrangement processes governing structural and acidic properties of formed ADORable zeolites. In contrast to the aqueous medium, in which de-intercalation was fast and resulted in complete leaching of Ge from the interlayer space of **UTL**, de-intercalation step was efficiently decelerated when decreasing water-to-zeolite ratio in water-methanol systems. Thus, zeolites IPC-7 (containing D4R/S4R interlayer units), **OKO** (S4R), ***PCS** (S4R/-O-) and **PCR** (-O-) with gradually decreasing *d*-spacings and micropore sizes were shown sequentially formed in the water-methanol medium according to the mechanism of gradual reduction of the size of Ge-enriched interlayer units. Unprecedentedly, a combination of Al-assisted rearrangement and slow deintercalation in the Al-containing water-methanol medium allowed to achieve the cycled structural transformation of **UTL** (D4R)-to-Al-**UTL** (D4R) through Al-**OKO** (S4R) intermediate.

The synthetic methods and materials designed in this thesis are envisaged to broaden the scope of highly active and selective heterogeneous catalysts engineered for specific applications. The follow-up research in this field should focus on: 1) addressing the role of zeolite structure and chemical composition, local arrangement of Ge atoms in the framework on the nature and strength of Ge-associated acid sites, the mechanism of Lewis-to-Bronsted acid sites transformation and its role in activity, selectivity and stability of germanosilicate zeolite catalysts; 2) developing degermanation/metalation synthetic approach towards controlling the local structure of framework metal atoms (i.e., selective incorporation of acid sites into certain crystallographic positions of the framework, selective engineering of either ‘open’ or ‘closed’ acid sites, etc.); 3) detailed characterization of synthesis-structure-activity relationships in germanosilicate zeolite-based catalysts by applying *operando* characterization techniques; and 4) studying application potential of designed zeolites in industrially relevant transformations of platform molecules into value-added chemicals.

6. References

- [1] J. V. Smith. Definition of a Zeolite. *Zeolites* 1984, 4, 309-310.
- [2] R. R. Xu, W. Pang, J. H. Yu, Q. Huo and J. Chen. *Chemistry of Zeolites and Related Porous Materials: Synthesis and Structure*. John Wiley & Sons: 2009.
- [3] Database of Ionic Radii, <http://abulafia.mt.ic.ac.uk/shannon/ptable.php>.
- [4] J. B. Jones. Al-O and Si-O Tetrahedral Distances in Aluminosilicate Framework Structures. *Acta Crystallogr. Sect. B: Struct. Crystallogr. Cryst. Chem.* 1968, B 24, 355-358.
- [5] D. Müller, W. Gessner, A. Samoson, E. Lippmaa and G. Scheler. Solid-State ^{27}Al NMR Studies on Polycrystalline Aluminates of the System $\text{CaO-Al}_2\text{O}_3$. *Polyhedron* 1986, 5, 779-785.
- [6] S. T. Wilson, B. M. Lok, C. A. Messina, T. R. Cannan and E. M. Flanigen. Aluminophosphate Molecular Sieves: A New Class of Microporous Crystalline Inorganic Solids. *J. Am. Chem. Soc.* 1982, 104, 1146-1147.
- [7] M. Taramasso, G. Perego and B. Notari. Preparation of Porous Crystalline Synthetic Material Comprised of Silicon and Titanium Oxides. US Patent, 4410501: 1983.
- [8] A. Corma, M. J. Diaz-Cabanas, J. L. Jorda, C. Martinez and M. Moliner. High-Throughput Synthesis and Catalytic Properties of a Molecular Sieve with 18- and 10-Member Rings. *Nature* 2006, 443, 842-845.
- [9] Database of Zeolite Structures, <https://europe.iza-structure.org>.
- [10] J. L. Paillaud, B. Harbuzaru, J. Patarin and N. Bats. Extra-Large-Pore Zeolites with Two-Dimensional Channels Formed by 14 and 12 Rings. *Science* 2004, 304, 990-992.
- [11] C. Q. Zhang, E. Kapaca, J. Y. Li, Y. L. Liu, X. F. Yi, A. M. Zheng, X. D. Zou, J. X. Jiang and J. H. Yu. An Extra-Large-Pore Zeolite with $24\times 8\times 8$ -Ring Channels Using a Structure-Directing Agent Derived from Traditional Chinese Medicine. *Angew. Chem. Int. Ed.* 2018, 57, 6486-6490.

- [12] C. h. Baerlocher, L. B. McCusker and D. H. Olson. Atlas of Zeolite Framework Types. Elsevier: 2007.
- [13] J. Čejka, R. E. Morris and P. Nachtigall. Zeolites in Catalysis: Properties and Applications. Royal Society of Chemistry: 2017.
- [14] S. De, S. Duttab and B. Saha. Critical Design of Heterogeneous Catalysts for Biomass Valorization: Current Thrust and Emerging Prospects. Catal. Sci. Technol. 2016, 6, 7364-7385.
- [15] V. L. Sushkevich, D. Palagin and I. I. Ivanova. With Open Arms: Open Sites of ZrBEA Zeolite Facilitate Selective Synthesis of Butadiene from Ethanol. ACS Catal. 2015, 5, 4833-4836.
- [16] J. To, A. A. Sokol, S. A. French and C. R. A. Catlow. Formation of Active Sites in TS-1 by Hydrolysis and Inversion. J. Phys. Chem. C 2007, 111, 14720-14731.
- [17] M. Moliner. State of the Art of Lewis Acid-Containing Zeolites: Lessons from Fine Chemistry to New Biomass Transformation Processes. Dalton Trans. 2014, 43, 4197-4208.
- [18] J. Čejka and B. Wichterlová. Acid-Catalyzed Synthesis of Mono- and Dialkyl Benzenes over Zeolites: Active Sites, Zeolite Topology, and Reaction Mechanisms. Catal. Rev. Sci. Eng. 2002, 44, 375-421.
- [19] I. Fecheté, Y. Wang and J. C. Vedrine. The Past, Present and Future of Heterogeneous Catalysis. Catal. Today 2012, 189, 2-27.
- [20] J. Přeč. Catalytic Performance of Advanced Titanosilicate Selective Oxidation Catalysts—A Review. Catal. Rev. Sci. Eng. 2018, 60, 71-131.
- [21] J. G. Goodwin Jr, S. Natesakhawat, A. A. Nikolopoulos and S. Y. Kim. Etherification on Zeolites: MTBE Synthesis. Catal. Rev. Sci. Eng. 2002, 44, 287-320.
- [22] K. Li, J. Valla and J. Garcia-Martinez. Realizing the Commercial Potential of Hierarchical Zeolites: New Opportunities in Catalytic Cracking. ChemCatChem 2014, 6, 46-66.

- [23] M. F. Alotibi, B. A. Alshammari, M. H. Alotaibi, F. M. Alotaibi, S. Alshihri, R. M. Navarro and J. L. G. Fierro. ZSM-5 Zeolite Based Additive in FCC Process: A Review on Modifications for Improving Propylene Production. *Catal. Surv. Asia* 2020, 24, 1-10.
- [24] M. S. Beheshti, M. Behzad, J. Ahmadpour and H. Arabi. Modification of H-[B]-ZSM-5 Zeolite for Methanol to Propylene (MTP) Conversion: Investigation of Extrusion and Steaming Treatments on Physicochemical Characteristics and Catalytic Performance. *Microporous Mesoporous Mater.* 2020, 291, 109699.
- [25] X. B. Zhao, J. Z. Li, P. Tian, L. Y. Wang, X. F. Li, S. F. Lin, X. W. Guo and Z. M. Liu. Achieving a Superlong Lifetime in the Zeolite-Catalyzed MTO Reaction under High Pressure: Synergistic Effect of Hydrogen and Water. *ACS Catal.* 2019, 9, 3017-3025.
- [26] A. I. Lupulescu and J. D. Rimer. In Situ Imaging of Silicalite-1 Surface Growth Reveals the Mechanism of Crystallization. *Science* 2014, 344, 729-732.
- [27] Y. N. Zhou, H. Y. Liu, X. R. Rao, Y. Y. Yue, H. B. Zhu and X. J. Bao. Controlled Synthesis of ZSM-5 Zeolite with an Unusual Al Distribution in Framework from Natural Aluminosilicate Mineral. *Microporous Mesoporous Mater.* 2020, 305, 110357.
- [28] J. Grand, H. Awala and S. Mintova. Mechanism of Zeolites Crystal Growth: New Findings and Open Questions. *CrystEngComm* 2016, 18, 650-664.
- [29] J. Y. Li, A. Corma and J. H. Yu. Synthesis of New Zeolite Structures. *Chem. Soc. Rev.* 2015, 44, 7112-7127.
- [30] W. J. Roth, P. Nachtigall, R. E. Morris and J. Čejka. Two-Dimensional Zeolites: Current Status and Perspectives. *Chem. Rev.* 2014, 114, 4807-4837.
- [31] W. J. Roth and J. Čejka. Two-Dimensional Zeolites: Dream or Reality? *Catal. Sci. Technol.* 2011, 1, 43-53.
- [32] M. Choi, K. Na, J. Kim, Y. Sakamoto, O. Terasaki and R. Ryoo. Stable Single-Unit-Cell Nanosheets of Zeolite MFI as Active and Long-Lived Catalysts. *Nature* 2009, 461, 246-249.

- [33] J. Jung, C. Jo, K. Cho and R. Ryoo. Zeolite Nanosheet of a Single-Pore Thickness Generated by a Zeolite-Structure-Directing Surfactant. *J. Mater. Chem.* 2012, 22, 4637-4640.
- [34] W. Park, D. Yu, K. Na, K. E. Jelfs, B. Slater, Y. Sakamoto and R. Ryoo. Hierarchically Structure-Directing Effect of Multi-Ammonium Surfactants for the Generation of MFI Zeolite Nanosheets. *Chem. Mater.* 2011, 23, 5131-5137.
- [35] W. J. Roth, O. V. Shvets, M. Shamzhy, P. Chlubná, M. Kubů, P. Nachtigall and J. Čejka. Post-synthesis Transformation of Three-Dimensional Framework into a Lamellar Zeolite with Modifiable Architecture. *J. Am. Chem. Soc.* 2011, 133, 6130-6133.
- [36] B. B. Schaack, W. Schrader and F. Schüth. How are Heteroelements (Ga and Ge) Incorporated in Silicate Oligomers? *Chem. Eur. J.* 2009, 15, 5920-5925.
- [37] J. D. Epping and B. F. Chmelka. Nucleation and growth of zeolites and inorganic mesoporous solids: Molecular insights from magnetic resonance spectroscopy. *Curr. Opin. Colloid Interface Sci.* 2006, 11, 81-117.
- [38] B. B. Schaack, W. Schrader and F. Schuth. Structural Insight into Germanium-Containing Silicate Species by Electrospray Ionization Mass Spectrometry (ESI-MS) and ESI-MS/MS. *J. Phys. Chem. B* 2009, 113, 11240-11246.
- [39] O. V. Shvets, N. Kasian, A. Zúkal, J. Pinkas and J. Čejka. The Role of Template Structure and Synergism between Inorganic and Organic Structure Directing Agents in the Synthesis of UTL Zeolite. *Chem. Mater.* 2010, 22, 3482-3495.
- [40] J. X. Jiang, Y. F. Yun, X. D. Zou, J. L. Jorda and A. Corma. ITQ-54: A Multi-Dimensional Extra-Large Pore Zeolite with 20×14×12-Ring Channels. *Chem. Sci.* 2015, 6, 480-485.
- [41] X. L. Liu, U. Ravon and A. Tuel. Fluoride Removal from Double Four-Membered Ring (D4R) Units in As-Synthesized Ge-Containing Zeolites. *Chem. Mater.* 2011, 23, 5052-5057.
- [42] B. B. Schaack, W. Schrader, A. Corma and F. Schuth. Nucleation of ITQ-21 Studied by ESI-MS. *Chem. Mater.* 2009, 21, 4448-4453.

- [43] Y. Lorgouilloux, M. Dodin, E. Mugnaioli, C. Marichal, P. Caullet, N. Bats, U. Kolb and J. L. Paillaud. IM-17: A New Zeolitic Material, Synthesis and Structure Elucidation from Electron Diffraction ADT Data and Rietveld Analysis. *RSC Adv.* 2014, 4, 19440-19449.
- [44] V. Kasneryk, M. Shamzhy, M. Opanasenko, P. S. Wheatley, S. A. Morris, S. E. Russell, A. Mayoral, M. Trachta, J. Čejka and R. E. Morris. Expansion of the ADOR Strategy for the Synthesis of Zeolites: The Synthesis of IPC-12 from Zeolite UOV. *Angew. Chem. Int. Ed.* 2017, 56, 4324-4327.
- [45] A. Corma, M. J. Diaz-Cabanas, F. Rey, S. Nicolopoulos and K. Boulahya. ITQ-15: The First Ultralarge Pore Zeolite with a Bi-Directional Pore System Formed by Intersecting 14- and 12-Ring Channels, and its Catalytic Implications. *Chem. Commun.* 2004, 1356-1357.
- [46] A. Corma, F. Rey, S. Valencia, J. L. Jorda and J. Rius. A Zeolite with Interconnected 8-, 10- and 12-Ring Pores and its Unique Catalytic Selectivity. *Nat. Mater.* 2003, 2, 493-497.
- [47] R. Castaneda, A. Corma, V. Fornés, J. Martínez-Triguero and S. Valencia. Direct Synthesis of a 9×10 Member Ring Zeolite (Al-ITQ-13): A Highly Shape-Selective Catalyst for Catalytic Cracking. *J. Catal.* 2006, 238, 79-87.
- [48] X. Y. Ren, J. C. Liu, Y. Li, J. H. Yu and R. R. Xu. Hydrothermal Synthesis of an ITH-Type Germanosilicate Zeolite in a Non-Concentrated Gel System. *J. Porous Mater.* 2013, 20, 975-981.
- [49] M. Shamzhy, M. Opanasenko, Y. Y. Tian, K. Konysheya, O. Shyets, R. E. Morris and J. Čejka. Germanosilicate Precursors of ADORable Zeolites Obtained by Disassembly of ITH, ITR, and IWR Zeolites. *Chem. Mater.* 2014, 26, 5789-5798.
- [50] G. Sastre, A. Pulido, R. Castaneda and A. Corma. Effect of the Germanium Incorporation in the Synthesis of EU-1, ITQ-13, ITQ-22, and ITQ-24 Zeolites. *J. Phys. Chem. B* 2004, 108, 8830-8835.
- [51] A. Corma, M. J. Diaz-Cabanas, J. L. Jorda, F. Rey, G. Sastre and K. G. Strohmaier. A Zeolitic Structure (ITQ-34) with Connected 9- and 10-Ring Channels Obtained with

- Phosphonium Cations as Structure Directing Agents. *J. Am. Chem. Soc.* 2008, 130, 16482-16483.
- [52] J. X. Jiang, J. L. Jorda, M. J. Diaz-Cabanas, J. H. Yu and A. Corma. The Synthesis of an Extra-Large-Pore Zeolite with Double Three-Ring Building Units and a Low Framework Density. *Angew. Chem. Int. Ed.* 2010, 49, 4986-4988.
- [53] A. Corma, M. T. Navarro, F. Rey, J. Rius and S. Valencia. Pure Polymorph C of Zeolite Beta Synthesized by Using Framework Isomorphous Substitution as a Structure-Directing Mechanism. *Angew. Chem. Int. Ed.* 2001, 40, 2337-2340.
- [54] S. Smeets, L. Koch, N. Mascello, J. Sesseg, L. B. McCusker, M. Hernandez-Rodriguez, S. Mitchell and J. Perez-Ramirez. Structure Analysis of a BEC-Type Germanosilicate Zeolite including the Location of the Flexible Organic Cations in the Channels. *CrystEngComm* 2015, 17, 4865-4870.
- [55] H. L. Li and O. M. Yaghi. Transformation of Germanium Dioxide to Microporous Germanate 4-Connected Nets. *J. Am. Chem. Soc.* 1998, 120, 10569-10570.
- [56] D. L. Dorset, K. G. Strohmaier, C. E. Kliewer, A. Corma, M. J. Diaz-Cabanas, F. Rey and C. J. Gilmore. Crystal Structure of ITQ-26, a 3D Framework with Extra-Large Pores. *Chem. Mater.* 2008, 20, 5325-5331.
- [57] M. Dodin, J. L. Paillaud, Y. Lorgouilloux, P. Caultett, E. Elkaim and N. Bats. A Zeolitic Material with a Three-Dimensional Pore System Formed by Straight 12- and 10-Ring Channels Synthesized with an Imidazolium Derivative as Structure-Directing Agent. *J. Am. Chem. Soc.* 2010, 132, 10221-10223.
- [58] M. Moliner, F. Rey and A. Corma. Towards the Rational Design of Efficient Organic Structure-Directing Agents for Zeolite Synthesis. *Angew. Chem. Int. Ed.* 2013, 52, 13880-13889.
- [59] C. S. Blackwell, R. W. Broach, M. G. Gatter, J. S. Holmgren, D. Y. Jan, G. J. Lewis, B. J. Mezza, T. M. Mezza, M. A. Miller, J. G. Moscoso, R. L. Patton, L. M. Rohde, M. W. Schoonover, W. Sinkler, B. A. Wilson and S. T. Wilson. Open-Framework Materials

- Synthesized in the TMA⁺/TEA⁺ Mixed-Template System: The New Low Si/Al Ratio Zeolites UZM-4 and UZM-5. *Angew. Chem. Int. Ed.* 2003, 42, 1737-1740.
- [60] T. B. Reed and D. W. Breck. Crystalline Zeolites. II. Crystal Structure of Synthetic Zeolite, Type A. *J. Am. Chem. Soc.* 1956, 78, 5972-5977.
- [61] S. Seo, T. Yang, J. Shin, D. Jo, X. Zou and S. B. Hong. Two Aluminophosphate Molecular Sieves Built from Pairs of Enantiomeric Structural Building Units. *J. Am. Chem. Soc.* 2018, 57, 3727-3732.
- [62] G. Robert and J. MeurigáThomas. Synthesis and Structure of a Novel Large-Pore Microporous Magnesium-Containing Aluminophosphate (DAF-1). *J. Chem. Soc., Chem. Commun.* 1993, 633-635.
- [63] P. Y. Feng, X. H. Bu and G. D. Stucky. Hydrothermal Syntheses and Structural Characterization of Zeolite Analogue Compounds based on Cobalt Phosphate. *Nature* 1997, 388, 735-741.
- [64] M. Estermann, L. B. Mccusker, C. Baerlocher, A. Merrouche and H. Kessler. A Synthetic Gallophosphate Molecular-Sieve with a 20-Tetrahedral-Atom Pore Opening. *Nature* 1991, 352, 320-323.
- [65] J. M. Bennett and B. K. Marcus. *The Crystal Structures of Several Metal Aluminophosphate Molecular Sieves.* Elsevier: 1988.
- [66] J. M. Bennett and R. M. Kirchner. The Structure of As-Synthesized AIPO4-16 Determined by A New Framework Modeling Method and Rietveld Refinement of Synchrotron Powder Diffraction Data. *Zeolites* 1991, 11, 502-506.
- [67] J. L. Jordá, F. Rey, G. Sastre, S. Valencia, M. Palomino, A. Corma, A. Segura, D. Errandonea, R. Lacomba and F. J. Manjón. Synthesis of a Novel Zeolite through a Pressure-Induced Reconstructive Phase Transition Process. *Angew. Chem. Int. Ed.* 2013, 125, 10652-10656.
- [68] L. A. Villaescusa, P. A. Barrett and M. A. Camblor. ITQ-7: A New Pure Silica Polymorph with a Three-Dimensional System of Large Pore Channels. *Angew. Chem. Int. Ed.* 1999, 38, 1997-2000.

- [69] A. Corma, M. Puche, F. Rey, G. Sankar and S. J. Teat. A Zeolite Structure (ITQ-13) with Three Sets of Medium-Pore Crossing Channels Formed by 9- and 10-Rings. *Angew. Chem. Int. Ed.* 2003, 115, 1188-1191.
- [70] P. A. Barrett, T. Boix, M. Puche, D. H. Olson, E. Jordan, H. Koller and M. A. Cambor. ITQ-12: A New Microporous Silica Polymorph Potentially Useful for Light Hydrocarbon Separations. *Chem. Commun.* 2003, 2114-2115.
- [71] D. L. Dorset, G. J. Kennedy, K. G. Strohmaier, M. J. Diaz-Cabanas, F. Rey and A. Corma. P-Derived Organic Cations as Structure-Directing Agents: Synthesis of a High-Silica Zeolite (ITQ-27) with a Two-Dimensional 12-Ring Channel System. *J. Am. Chem. Soc.* 2006, 128, 8862-8867.
- [72] L. Tang, L. Shi, C. Bonneau, J. Sun, H. Yue, A. Ojuva, B. L. Lee, M. Kritikos, R. G. Bell, Z. Bacsik, J. Mink and X. Zou. A Zeolite Family with Chiral and Achiral Structures Built from the Same Building Layer. *Nat. Mater.* 2008, 7, 381-385.
- [73] M. Opanasenko, M. Shamzhy, Y. Z. Wang, W. F. Yan, P. Nachtigall and J. Čejka. Synthesis and Post-Synthesis Transformation of Germanosilicate Zeolites. *Angew. Chem. Int. Ed.* 2020, 59, 19380-19389.
- [74] J. G. Jiang, J. H. Yu and A. Corma. Extra-Large-Pore Zeolites: Bridging the Gap between Micro and Mesoporous Structures. *Angew. Chem. Int. Ed.* 2010, 49, 3120-3145.
- [75] S. Lopez-Orozco, A. Inayat, A. Schwab, T. Selvam and W. Schwieger. Zeolitic Materials with Hierarchical Porous Structures. *Adv. Mater.* 2011, 23, 2602-2615.
- [76] J. C. Groen, L. A. A. Peffer, J. A. Moulijn and J. Perez-Ramirez. On the Introduction of Intracrystalline Mesoporosity in Zeolites upon Desilication in Alkaline Medium. *Microporous Mesoporous Mater.* 2004, 69, 29-34.
- [77] Q. Guo, F. Fan, E. A. Pidko, W. N. van der Graaff, Z. Feng, C. Li and E. J. Hensen. Highly Active and Recyclable Sn-MWW Zeolite Catalyst for Sugar Conversion to Methyl Lactate and Lactic Acid. *ChemSusChem* 2013, 6, 1352-1356.

- [78] Y. Goa, H. Yoshitake, P. Wu and T. Tatsumi. Controlled Detitanation of ETS-10 Materials through the Post-Synthetic Treatment and Their Applications to the Liquid-Phase Epoxidation of Alkenes. *Microporous Mesoporous Mater.* 2004, 70, 93-101.
- [79] V. Kasneryk, M. Shamzhy, M. Opanasenko and J. Čejka. Tuning of Textural Properties of Germanosilicate Zeolites ITH and IWW by Acidic Leaching. *J. Energy Chem.* 2016, 25, 318-326.
- [80] C. Marcilly. *Acido-Basic Catalysis: Application to Refining and Petrochemistry.* Technip Ophrys Editions: 2006.
- [81] J. Heda, P. Niphadkar, S. Mudliar and V. Bokade. Highly Efficient Micro-Meso Acidic H-USY Catalyst for One Step Conversion of Wheat Straw to Ethyl Levulinate (Biofuel Additive). *Microporous Mesoporous Mater.* 2020, 306, 110474.
- [82] V. Valtchev, G. Majano, S. Mintova and J. Perez-Ramirez. Tailored Crystalline Microporous Materials by Post-Synthesis Modification. *Chem. Soc. Rev.* 2013, 42, 263-290.
- [83] M. Shamzhy, M. Opanasenko, P. Concepcion and A. Martinez. New Trends in Tailoring Active Sites in Zeolite-based Catalysts. *Chem. Soc. Rev.* 2019, 48, 1095-1149.
- [84] J. C. Groen, L. A. A. Peffer, J. A. Moulijn and J. Perez-Ramirez. Mechanism of Hierarchical Porosity Development in MFI Zeolites by Desilication: The Role of Aluminium as a Pore-Directing Agent. *Chem. Eur. J.* 2005, 11, 4983-4994.
- [85] D. Zhang, C. Jin, M. Zou and S. Huang. Mesopore Engineering for Well-Defined Mesoporosity in Al-Rich Aluminosilicate Zeolites. *Chem. Eur. J.* 2019, 25, 2675-2683.
- [86] J. C. Groen, J. C. Jansen, J. A. Moulijn and J. Perez-Ramirez. Optimal Aluminum-Assisted Mesoporosity Development in MFI Zeolites by Desilication. *J. Phys. Chem. B* 2004, 108, 13062-13065.
- [87] J. C. Groen, J. A. Moulijn and J. Perez-Ramirez. Desilication: On the Controlled Generation of Mesoporosity in MFI Zeolites. *J. Mater. Chem.* 2006, 16, 2121-2131.
- [88] D. Verboekend and J. Perez-Ramirez. Design of Hierarchical Zeolite Catalysts by Desilication. *Catal. Sci. Technol.* 2011, 1, 879-890.

- [89] J. C. Groen, S. Abello, L. A. Villaescusa and J. Perez-Ramirez. Mesoporous Beta Zeolite Obtained by Desilication. *Microporous Mesoporous Mater.* 2008, 114, 93-102.
- [90] Y. P. Khitev, I. I. Ivanova, Y. G. Kolyagin and O. A. Ponomareva. Skeletal Isomerization of 1-Butene over Micro/Mesoporous Materials based on FER Zeolite. *Appl. Catal. A: Gen.* 2012, 441, 124-135.
- [91] C. J. Heard, L. Grajciar, F. Uhlik, M. Shamzhy, M. Opanasenko, J. Čejka and P. Nachtigall. Zeolite (In)Stability under Aqueous or Steaming Conditions. *Adv. Mater.* 2020, 32, 2003264.
- [92] R. Bandyopadhyay, Y. Kubota, N. Sugimoto, Y. Fukushima and Y. Sugi. Synthesis of Borosilicate Zeolites by the Dry Gel Conversion Method and their Characterization. *Microporous Mesoporous Mater.* 1999, 32, 81-91.
- [93] L. Burel, N. Kasian and A. Tuel. Quasi All-Silica Zeolite Obtained by Isomorphous Degermanation of an As-Made Germanium-Containing Precursor. *Angew. Chem. Int. Ed.* 2014, 53, 1360-1363.
- [94] S. E. Henkelis, M. Mazur, C. M. Rice, P. S. Wheatley, S. E. Ashbrook and R. E. Morris. Kinetics and Mechanism of the Hydrolysis and Rearrangement Processes within the Assembly-Disassembly-Organization-Reassembly Synthesis of Zeolites. *J. Am. Chem. Soc.* 2019, 141, 4453-4459.
- [95] S. E. Henkelis, S. A. Morris, M. Mazur, P. S. Wheatley, L. N. McHugh and R. E. Morris. Monitoring the Assembly-Disassembly-Organisation-Reassembly Process of Germanosilicate UTL through in Situ Pair Distribution Function Analysis. *J. Mater. Chem. A* 2018, 6, 17011-17018.
- [96] S. A. Morris, G. P. M. Bignami, Y. Tian, M. Navarro, D. S. Firth, J. Čejka, P. S. Wheatley, D. M. Dawson, W. A. Slawinski, D. S. Wragg, R. E. Morris and S. E. Ashbrook. In Situ Solid-State NMR and XRD Studies of the ADOR Process and the Unusual Structure of Zeolite IPC-6. *Nat. Chem.* 2017, 9, 1012-1018.
- [97] P. S. Wheatley, P. Chlubná, H. Greer, W. Zhou, V. R. Seymour, D. M. Dawson, S. E. Ashbrook, A. B. Pinar, L. B. McCusker, M. Opanasenko, J. Čejka and R. E. Morris.

- Zeolites with Continuously Tuneable Porosity. *Angew. Chem. Int. Ed.* 2014, 53, 13210-13214.
- [98] E. Verheyen, L. Joos, K. Van Havenbergh, E. Breynaert, N. Kasian, E. Gobechiya, K. Houthoofd, C. Martineau, M. Hinterstein, F. Taulelle, V. Van Speybroeck, M. Waroquier, S. Bals, G. Van Tendeloo, C. E. Kirschhock and J. A. Martens. Design of Zeolite by Inverse Sigma Transformation. *Nat. Mater.* 2012, 11, 1059-1064.
- [99] S. E. Henkelis, M. Mazur, C. M. Rice, G. P. M. Bignami, P. S. Wheatley, S. E. Ashbrook, J. Čejka and R. E. Morris. A Procedure for Identifying Possible Products in the Assembly-Disassembly-Organization-Reassembly (ADOR) Synthesis of Zeolites. *Nat. Protoc.* 2019, 14, 781-794.
- [100] V. Kasneryk, M. Shamzhy, M. Opanasenko, P. S. Wheatley, R. E. Morris and J. Čejka. Insight into the ADOR Zeolite-to-Zeolite Transformation: The UOV Case. *Dalton Trans.* 2018, 47, 3084-3092.
- [101] N. Kasian, A. Tuel, E. Verheyen, C. E. A. Kirschhock, F. Taulelle and J. A. Martens. NMR Evidence for Specific Germanium Siting in IM-12 Zeolite. *Chem. Mater.* 2014, 26, 5556-5565.
- [102] V. Kasneryk, M. Shamzhy, J. Zhou, Q. Yue, M. Mazur, A. Mayoral, Z. Luo, R. E. Morris, J. Čejka and M. Opanasenko. Vapour-Phase-Transport Rearrangement Technique for the Synthesis of New Zeolites. *Nat. Commun.* 2019, 10, 5129.
- [103] X. Liu, W. Mao, J. Jiang, X. Lu, M. Peng, H. Xu, L. Han, S. A. Che and P. Wu. Topotactic Conversion of Alkali-Treated Intergrown Germanosilicate CIT-13 into Single-Crystalline ECNU-21 Zeolite as Shape-Selective Catalyst for Ethylene Oxide Hydration. *Chem. Eur. J.* 2019, 25, 4520-4529.
- [104] H. Koller, C. Y. Chen and S. I. Zones. Selectivities in Post-Synthetic Modification of Borosilicate Zeolites. *Top. Catal.* 2015, 58, 451-479.
- [105] S. I. Zones, A. Benin, S. J. Hwang, D. Xie, S. Elomari and M. F. Hsieh. Studies of Aluminum Reinsertion into Borosilicate Zeolites with Intersecting Channels of 10- and 12-Ring Channel Systems. *J. Am. Chem. Soc.* 2014, 136, 1462-1471.

- [106] M. Shamzhy and F. S. D. Ramos. Tuning of Acidic and Catalytic Properties of IWR Zeolite by Post-Synthesis Incorporation of Three-Valent Elements. *Catal. Today* 2015, 243, 76-84.
- [107] M. Shamzhy, O. V. Shvets, M. Opanasenko, P. S. Yaremov, L. G. Sarkisyan, P. Chlubná, A. Zukal, V. R. Marthala, M. Hartmann and J. Čejka. Synthesis of Isomorphously Substituted Extra-Large Pore UTL Zeolites. *J. Mater. Chem.* 2012, 22, 15793-15803.
- [108] M. Shamzhy, M. Opanasenko, F. S. D. Ramos, L. Brabec, M. Horacek, M. Navarro-Rojas, R. E. Morris, H. D. Pastore and J. Čejka. Post-Synthesis Incorporation of Al into Germanosilicate ITH Zeolites: The Influence of Treatment Conditions on the Acidic Properties and Catalytic Behavior in Tetrahydropyranylation. *Catal. Sci. Technol.* 2015, 5, 2973-2984.
- [109] M. Shamzhy, P. Eliasova, D. Vitvarova, M. Opanasenko, D. S. Firth and R. E. Morris. Post-Synthesis Stabilization of Germanosilicate Zeolites ITH, IWW, and UTL by Substitution of Ge for Al. *Chem. Eur. J.* 2016, 22, 17377-17386.
- [110] M. Shamzhy, O. V. Shvets, M. Opanasenko, L. Kurfirtova, D. Kubicka and J. Čejka. Extra-Large-Pore Zeolites with UTL Topology: Control of the Catalytic Activity by Variation in the Nature of the Active Sites. *Chemcatchem* 2013, 5, 1891-1898.
- [111] F. Gao, M. Jaber, K. Bozhilov, A. Vicente, C. Fernandez and V. Valtchev. Framework Stabilization of Ge-Rich Zeolites via Postsynthesis Alumination. *J. Am. Chem. Soc.* 2009, 131, 16580-16586.
- [112] S. I. Zones, C. Y. Chen, A. Benin and S. J. Hwang. Opportunities for Selective Catalysis within Discrete Portions of Zeolites: The Case for SSZ-57LP. *J. Catal.* 2013, 308, 213-225.
- [113] R. Caicedo-Realpe and J. Perez-Ramirez. Mesoporous ZSM-5 Zeolites Prepared by a Two-Step Route Comprising Sodium Aluminate and Acid Treatments. *Microporous Mesoporous Mater.* 2010, 128, 91-100.

- [114] H. P. Winoto, Z. A. Fikri, J. M. Ha, Y. Park, H. Lee, D. J. Suh and J. Jae. Heteropolyacid Supported on Zr-Beta Zeolite as an Active Catalyst for One-Pot Transformation of Furfural to γ -Valerolactone. *Appl. Catal. B: Environ.* 2019, 241, 588-597.
- [115] B. Tang, W. C. Song, S. Y. Li, E. C. Yang and X. J. Zhao. Post-Synthesis of Zr-MOR as a Robust Solid Acid Catalyst for the Ring-Opening Aminolysis of Epoxides. *New J. Chem.* 2018, 42, 13503-13511.
- [116] V. L. Sushkevich and I. I. Ivanova. Ag-Promoted ZrBEA Zeolites Obtained by Post-Synthetic Modification for Conversion of Ethanol to Butadiene. *ChemSusChem* 2016, 9, 2216-2225.
- [117] J. Wang, K. Okumura, S. Jaenicke and G. K. Chuah. Post-Synthesized Zirconium-Containing Beta Zeolite in Meerwein-Ponndorf-Verley Reduction: Pros and Cons. *Appl. Catal. A: Gen.* 2015, 493, 112-120.
- [118] M. Liu, S. Jia, C. Li, A. Zhang, C. Song and X. Guo. Facile Preparation of Sn- β Zeolites by Post-Synthesis (Isomorphous Substitution) Method for Isomerization of Glucose to Fructose. *Chin. J. Catal.* 2014, 35, 723-732.
- [119] J. Dijkmans, J. Demol, K. Houthoofd, S. Huang, Y. Pontikes and B. Sels. Post-Synthesis Sn β : An Exploration of Synthesis Parameters and Catalysis. *J. Catal.* 2015, 330, 545-557.
- [120] F. F. Guan, T. T. Ma, X. Yuan, H. Y. Zeng and J. Wu. Sn-Modified NaY Zeolite Catalysts Prepared by Post-Synthesis Methods for Baeyer-Villiger Oxidation. *Catal. Lett.* 2018, 148, 443-453.
- [121] M. M. Antunes, S. Lima, P. Neves, A. L. Magalhaes, E. Fazio, A. Fernandes, F. Neri, C. M. Silva, S. M. Rocha, M. F. R. Eiro, M. Pillinger, A. Urakawa and A. A. Valente. One-Pot Conversion of Furfural to Useful Bio-Products in the Presence of a Sn,Al-Containing Zeolite Beta Catalyst Prepared via Post-Synthesis Routes. *J. Catal.* 2015, 329, 522-537.
- [122] B. Yang and P. Wu. Post-Synthesis and Catalytic Performance of FER Type Sub-Zeolite Ti-ECNU-8. *Chin. Chem. Lett.* 2014, 25, 1511-1514.

- [123] Y. Oumi, T. Manabe, H. Sasaki, T. Inuzuka and T. Sano. Preparation of Ti Incorporated Y Zeolites by a Post-Synthesis Method under Acidic Conditions and Their Catalytic Properties. *Appl. Catal. A: Gen.* 2010, 388, 256-261.
- [124] P. Li, G. Q. Liu, H. H. Wu, Y. M. Liu, J. G. Jiang and P. Wu. Postsynthesis and Selective Oxidation Properties of Nanosized Sn-Beta Zeolite. *J. Phys. Chem. C* 2011, 115, 3663-3670.
- [125] P. Wolf, C. Hammond, S. Conrad and I. Hermans. Post-Synthetic Preparation of Sn-, Ti- and Zr-Beta: A Facile Route to Water Tolerant, Highly Active Lewis Acidic Zeolites. *Dalton Trans.* 2014, 43, 4514-4519.
- [126] P. A. Kots, V. L. Sushkevich, O. A. Tyablikov and I. I. Ivanova. Synthesis of Zr-Containing BEC-Type Germanosilicate with High Lewis Acidity. *Microporous Mesoporous Mater.* 2017, 243, 186-192.
- [127] X. Liu, H. Xu, L. Zhang, L. Han, J. Jiang, P. Oleynikov, L. Chen and P. Wu. Isomorphous Incorporation of Tin Ions into Germanosilicate Framework Assisted by Local Structural Rearrangement. *ACS Catal.* 2016, 6, 8420-8431.
- [128] X. Liu, L. Zhang, H. Xu, J. G. Jiang, M. M. Peng and P. Wu. Pore Size-Tunable Titanosilicates Post-Synthesized from Germanosilicate by Structural Reorganization and H_2TiF_6 -Assisted Isomorphous Substitution. *Appl. Catal. A: Gen.* 2018, 550, 11-19.
- [129] A. Corma. From Microporous to Mesoporous Molecular Sieve Materials and their Use in Catalysis. *Chem. Rev.* 1997, 97, 2373-2419.
- [130] J. Abbot and F. N. Guerzoni. Roles of Brønsted and Lewis sites during Cracking of n-Octane on H-Mordenite. *Appl. Catal. A: Gen.* 1992, 85, 173-188.
- [131] J. W. Ward. The Nature of Active Sites on Zeolites: V. In Situ Spectroscopic Observations of Hydrogen Y Zeolite during Cumene Cracking. *J. Catal.* 1968, 11, 259-260.
- [132] E. T. Vogt and B. M. Weckhuysen. Fluid Catalytic Cracking: Recent Developments on the Grand Old Lady of Zeolite Catalysis. *Chem. Soc. Rev.* 2015, 44, 7342-7370.

- [133] J. W. Teng, G. L. Zhao, Z. K. Xie and Q. L. Chen. Effect of ZSM-5 Zeolite Crystal Size on Propylene Production from Catalytic Cracking of C~4 Olefins. *Chin. J. Catal.* 2004, 25, 602-606.
- [134] U. Freese, F. Heinrich and F. Roessner. Acylation of Aromatic Compounds on H-Beta Zeolites. *Catal. Today* 1999, 49, 237-244.
- [135] A. Corma and H. Garcia. Lewis Acids as Catalysts in Oxidation Reactions: From Homogeneous to Heterogeneous Systems. *Chem. Rev.* 2002, 102, 3837-3892.
- [136] I. W. C. E. Arends, R. A. Sheldon, M. Wallau and U. Schuchardt. Oxidative Transformations of Organic Compounds Mediated by Redox Molecular Sieves. *Angew. Chem. Int. Ed.* 1997, 36, 1144-1163.
- [137] M. Shamzhy, C. Ochoa-Hernandez, V. Kasneryk, M. Opanasenko and M. Mazur. Direct Incorporation of B, Al, and Ga into Medium-Pore ITH Zeolite: Synthesis, Acidic, and Catalytic Properties. *Catal. Today* 2016, 277, 37-47.
- [138] N. Žilková, M. Shamzhy, O. Shvets and J. Čejka. Transformation of Aromatic Hydrocarbons over Isomorphously Substituted UTL: Comparison with Large and Medium Pore Zeolites. *Catal. Today* 2013, 204, 22-29.
- [139] Y. Zhou, S. A. Kadam, M. Shamzhy, J. Čejka and M. Opanasenko. Isorecticular UTL-Derived Zeolites as Model Materials for Probing Pore Size-Activity Relationship. *ACS Catal.* 2019, 9, 5136-5146.
- [140] N. Kasian, G. Vanbutsele, K. Houthoofd, T. I. Koranyi, J. A. Martens and C. E. A. Kirschhock. Catalytic Activity and Extra-Large Pores of Germanosilicate UTL Zeolite Demonstrated with Decane Test Reaction. *Catal. Sci. Technol.* 2011, 1, 246-254.
- [141] M. Shamzhy, O. V. Shvets, M. Opanasenko, D. Procházková, P. Nachtigall and J. Čejka. The Effect of Synthesis Conditions and Nature of Heteroelement on Acidic Properties of Isomorphously Substituted UTL Zeolites. *Adv. Porous Mater.* 2013, 1, 103-113.
- [142] M. Boronat, A. Corma, M. Renz and P. M. Viruela. Predicting the Activity of Single Isolated Lewis Acid Sites in Solid Catalysts. *Chem. Eur. J.* 2006, 12, 7067-7077.

- [143] J. Přeč and J. Čejka. UTL Titanosilicate: An Extra-Large Pore Epoxidation Catalyst with Tunable Textural Properties. *Catal. Today* 2016, 277, 2-8.
- [144] J. Dijkmans, D. Gabriëls, M. Dusselier, F. de Clippel, P. Vanelderen, K. Houthoofd, A. Malfliet, Y. Pontikes and B. F. Sels. Productive Sugar Isomerization with Highly Active Sn in Dealuminated β Zeolites. *Green Chem.* 2013, 15, 2777-2785.
- [145] Y. Román-Leshkov, M. Moliner, J. A. Labinger and M. E. Davis. Mechanism of Glucose Isomerization using a Solid Lewis Acid Catalyst in Water. *Angew. Chem. Int. Ed.* 2010, 49, 8954-8957.
- [146] M. Boronat, A. Corma and M. Renz. Mechanism of the Meerwein-Ponndorf-Verley-Oppenauer (MPVO) Redox Equilibrium on Sn- and Zr-Beta Zeolite Catalysts. *J. Phys. Chem. B* 2006, 110, 21168-21174.
- [147] H. Y. Luo, D. F. Consoli, W. R. Gunther and Y. Román-Leshkov. Investigation of the Reaction Kinetics of Isolated Lewis Acid Sites in Beta Zeolites for the Meerwein-Ponndorf-Verley Reduction of Methyl Levulinate to γ -Valerolactone. *J. Catal.* 2014, 320, 198-207.
- [148] A. Corma, M. E. Domine and S. Valencia. Water-Resistant Solid Lewis Acid Catalysts: Meerwein-Ponndorf-Verley and Oppenauer Reactions Catalyzed by Tin-Beta Zeolite. *J. Catal.* 2003, 215, 294-304.
- [149] J. D. Lewis, S. Van de Vyver and Y. Roman-Leshkov. Acid-Base Pairs in Lewis Acidic Zeolites Promote Direct Aldol Reactions by Soft Enolization. *Angew. Chem. Int. Ed.* 2015, 54, 9835-8.
- [150] S. Van de Vyver, C. Odermatt, K. Romero, T. Prasomsri and Y. Román-Leshkov. Solid Lewis Acids Catalyze the Carbon-Carbon Coupling between Carbohydrates and Formaldehyde. *ACS Catal.* 2015, 5, 972-977.
- [151] Y. Z. Zhu, G. K. Chuah and S. Jaenicke. Selective Meerwein-Ponndorf-Verley Reduction of α , β -Unsaturated Aldehydes over Zr-Zeolite Beta. *J. Catal.* 2006, 241, 25-33.

- [152] M. Koehle and R. F. Lobo. Lewis Acidic Zeolite Beta Catalyst for the Meerwein-Ponndorf-Verley Reduction of Furfural. *Catal. Sci. Technol.* 2016, 6, 3018-3026.
- [153] L. Botti, S. A. Kondrat, R. Navar, D. Padovan, J. S. Martinez-Espin, S. Meier and C. Hammond. Solvent-Activated Hafnium-Containing Zeolites Enable Selective and Continuous Glucose-Fructose Isomerisation. *Angew. Chem. Int. Ed.* 2020, 59, 20017-20023.
- [154] J. H. Kang, D. Xie, S. I. Zones, S. Smeets, L. B. McCusker and M. E. Davis. Synthesis and Characterization of CIT-13, a Germanosilicate Molecular Sieve with Extra-Large Pore Openings. *Chem. Mater.* 2016, 28, 6250-6259.
- [155] A. Corma, G. Rey, V. Valencia and T. Martinez. Microporous Crystalline Zeolite Material (Zeolite ITQ-22), Synthesis Method Thereof and Use of Same as a Catalyst. US Patent, 7449169B2: 2008.
- [156] H. Xu, J. G. Jiang, B. T. Yang, L. Zhang, M. Y. He and P. Wu. Post-Synthesis Treatment gives Highly Stable Siliceous Zeolites through the Isomorphous Substitution of Silicon for Germanium in Germanosilicates. *Angew. Chem. Int. Ed.* 2014, 53, 1355-1359.
- [157] W. P. Ding, G. D. Meitzner, D. O. Marler and E. Iglesia. Synthesis, Structural Characterization, and Catalytic Properties of Tungsten-Exchanged H-ZSM5. *J. Phys. Chem. B* 2001, 105, 3928-3936.
- [158] H. S. Lacheen and E. Iglesia. Structure of Zirconium-Exchanged H-ZSM5 Prepared by Vapor Exchange of $ZrCl_4$. *Chem. Mater.* 2007, 19, 1877-1882.
- [159] S. Dzwigaj, M. J. Peltre, P. Massiani, A. Davidson, M. Che, T. Sen and S. Sivasanker. Incorporation of Vanadium Species in a Dealuminated β Zeolite. *Chem. Commun.* 1998, 87-88.
- [160] F. T. Muniz, M. A. Miranda, C. Morilla Dos Santos and J. M. Sasaki. The Scherrer Equation and the Dynamical Theory of X-Ray Diffraction. *Acta Crystallogr. Sect. A: Found. Adv.* 2016, 72, 385-390.
- [161] S. Brunauer, P. H. Emmett and E. Teller. Adsorption of Gases in Multimolecular Layers. *J. Am. Chem. Soc.* 1938, 60, 309-319.

- [162] K. A. Cychosz, R. Guillet-Nicolas, J. Garcia-Martinez and M. Thommes. Recent Advances in the Textural Characterization of Hierarchically Structured Nanoporous Materials. *Chem. Soc. Rev.* 2017, 46, 389-414.
- [163] J. Jagiello and M. Thommes. Comparison of DFT Characterization Methods based on N₂, Ar, CO₂, and H₂ Adsorption Applied to Carbons with Various Pore Size Distributions. *Carbon* 2004, 42, 1227-1232.
- [164] J. W. Harris, M. J. Cordon, J. R. Di Iorio, J. C. Vega-Vila, F. H. Ribeiro and R. Gounder. Titration and Quantification of Open and Closed Lewis Acid Sites in Sn-Beta Zeolites that Catalyze Glucose Isomerization. *J. Catal.* 2016, 335, 141-154.
- [165] C. A. Emeis. Determination of Integrated Molar Extinction Coefficients for Infrared-Absorption Bands of Pyridine Adsorbed on Solid Acid Catalysts. *J. Catal.* 1993, 141, 347-354.
- [166] J. Zhang, Q. D. Yue, M. Mazur, M. Opanasenko, M. Shamzhy and J. Cejka. Selective Recovery and Recycling of Germanium for the Design of Sustainable Zeolite Catalysts. *ACS Sustain. Chem. Eng.* 2020, 8, 8235-8246.
- [167] B. Gil, K. Kalahurska and A. Kowalczyk. A Study of the External and Internal Sites of 2D and 3D Zeolites through the FTIR Investigation of the Adsorption of Ammonia and Pivalonitrile. *Appl. Catal. A: Gen.* 2019, 578, 63-69.
- [168] H. Kosslick, V. A. Tuan, R. Fricke, C. Peuker, W. Pilz and W. Storek. Synthesis and Characterization of Ge-ZSM-5 Zeolites. *J. Phys. Chem.* 1993, 97, 5678-5684.
- [169] M. Moliner, M. J. Díaz-Cabañas, V. Fornés, C. Martínez and A. Corma. Synthesis Methodology, Stability, Acidity, and Catalytic Behavior of the 18×10 Member Ring Pores ITQ-33 Zeolite. *J. Catal.* 2008, 254, 101-109.
- [170] M. I. Zaki, M. A. Hasan, F. A. Al-Sagheer and L. Pasupulety. In Situ FTIR Spectra of Pyridine Adsorbed on SiO₂-Al₂O₃, TiO₂, ZrO₂ and CeO₂: General Considerations for the Identification of Acid Sites on Surfaces of Finely Divided Metal Oxides. *Colloids Surf. A* 2001, 190, 261-274.

- [171] S. Bordiga, C. Lamberti, F. Bonino, A. Travert and F. Thibault-Starzyk. Probing Zeolites by Vibrational Spectroscopies. *Chem. Soc. Rev.* 2015, 44, 7262-7341.
- [172] V. L. Sushkevich, P. A. Kots, Y. G. Kolyagin, A. V. Yakimov, A. V. Marikutsa and I. I. Ivanova. Origin of Water-Induced Brønsted Acid Sites in Sn-BEA Zeolites. *J. Phys. Chem. C* 2019, 123, 5540-5548.
- [173] P. Chlubná, Y. Tian, A. B. Pinar, M. Kubů, J. Čejka and R. E. Morris. The Assembly-Disassembly-Organization-Reassembly Mechanism for 3D-2D-3D Transformation of Germanosilicate IWW Zeolite. *Angew. Chem. Int. Ed.* 2014, 126, 7168-7172.
- [174] M. R. Nanda, Y. S. Zhang, Z. S. Yuan, W. S. Qin, H. S. Ghaziaskar and C. B. Xu. Catalytic Conversion of Glycerol for Sustainable Production of Solketal as a Fuel Additive: A Review. *Renewable Sustainable Energy Rev.* 2016, 56, 1022-1031.
- [175] I. Podolean, J. Zhang, M. Shamzhy, V. I. Parvulescu and J. Čejka. Solvent-Free Ketalization of Polyols over Germanosilicate Zeolites: The Role of the Nature and Strength of Acid Sites. *Catal. Sci. Technol.* 2020, 10, 8254-8264.
- [176] G. N. Li, B. Wang and D. E. Resasco. Water Promotion (or Inhibition) of Condensation Reactions Depends on Exposed Cerium Oxide Catalyst Facets. *ACS Catal.* 2020, 10, 5373-5382.
- [177] M. S. Rahaman, T. K. Phung, M. A. Hossain, E. Chowdhury, S. Tulaphol, S. B. Lalvani, M. O'Toole, G. A. Willing, J. B. Jasinski, M. Crocker and N. Sathitsuksanoh. Hydrophobic Functionalization of HY Zeolites for Efficient Conversion of Glycerol to Solketal. *Appl. Catal. A: Gen.* 2020, 592, 117369.
- [178] G. L. Catuzo, C. V. Santilli and L. Martins. Hydrophobic-Hydrophilic Balance of ZSM-5 Zeolites on the Two-Phase Ketalization of Glycerol with Acetone. *Catal. Today* 2020. DOI: 10.1016/j.cattod.2020.07.008.
- [179] C. H. Nicolas and M. Pera-Titus. Synthesis and Characterisation of Nanocomposite Ge-MFI-Alumina Membranes for CO₂/N₂ Separation from Wet Flue Gases. *Microporous Mesoporous Mater.* 2012, 153, 254-262.

- [180] S. G. Li, V. A. Tuan, R. D. Noble and J. L. Falconer. A Ge-Substituted ZSM-5 Zeolite Membrane for the Separation of Acetic Acid from Water. *Ind. Eng. Chem. Res.* 2001, 40, 6165-6171.
- [181] K. Stawicka, A. E. Diaz-Alvarez, V. Calvino-Casilda, M. Trejda, M. A. Bañares and M. Ziolk. The Role of Brønsted and Lewis Acid Sites in Acetalization of Glycerol over Modified Mesoporous Cellular Foams. *J. Phys. Chem. C* 2016, 120, 16699-16711.
- [182] J. Kowalska-Kuś, A. Held and K. Nowińska. Solketal Formation in a Continuous Flow Process over Hierarchical Zeolites. *ChemCatChem* 2020, 12, 510-519.
- [183] N. J. Venkatesha, Y. S. Bhat and B. S. J. Prakash. Dealuminated BEA Zeolite for Selective Synthesis of Five-Membered Cyclic Acetal from Glycerol under Ambient Conditions. *RSC Adv.* 2016, 6, 18824-18833.
- [184] P. S. Reddy, P. Sudarsanam, B. Mallesham, G. Raju and B. M. Reddy. Acetalisation of Glycerol with Acetone over Zirconia and Promoted Zirconia Catalysts under mild Reaction Conditions. *J. Ind. Eng. Chem.* 2011, 17, 377-381.
- [185] S. Gadamsetti, N. P. Rajan, G. S. Rao and K. V. Chary. Acetalization of Glycerol with Acetone to Bio Fuel Additives over Supported Molybdenum Phosphate Catalysts. *J. Mol. Catal. A: Chem.* 2015, 410, 49-57.
- [186] M. Kapkowski, W. Ambrozkiwicz, T. Siudyga, R. Sitko, J. Szade, J. Klimontko, K. Balin, J. Leltko and J. Polanski. Nano Silica and Molybdenum Supported Re, Rh, Ru or Ir Nanoparticles for Selective Solvent-Free Glycerol Conversion to Cyclic Acetals with Propanone and Butanone under Mild Conditions. *Appl. Catal. B: Environ.* 2017, 202, 335-345.
- [187] J. Kowalska-Kus, A. Held, M. Frankowski and K. Nowinska. Solketal Formation from Glycerol and Acetone over Hierarchical Zeolites of different Structure as Catalysts. *J. Mol. Catal. A: Chem.* 2017, 426, 205-212.
- [188] P. Manjunathan, S. P. Maradur, A. B. Halgeri and G. V. Shanbhag. Room Temperature Synthesis of Solketal from Acetalization of Glycerol with Acetone: Effect of Crystallite Size and the Role of Acidity of Beta Zeolite. *J. Mol. Catal. A: Chem.* 2015, 396, 47-54.

- [189] C. X. A. da Silva, V. L. C. Gonçalves and C. J. A. Mota. Water-Tolerant Zeolite Catalyst for the Acetalisation of Glycerol. *Green Chem.* 2009, 11, 38-41.
- [190] P. N. Bartlett, C. Y. Cummings, W. Levason, D. Pugh and G. Reid. Halometallate Complexes of Germanium(II) and (IV): Probing the Role of Cation, Oxidation State and Halide on the Structural and Electrochemical Properties. *Chem. Eur. J.* 2014, 20, 5019-5027.
- [191] I. H. Lim, W. Schrader and F. Schuth. The Formation of Zeolites from Solution-Analysis by Mass Spectrometry. *Microporous Mesoporous Mater.* 2013, 166, 20-36.
- [192] M. Shamzhy, J. Prech, J. Zhang, V. Ruaux, H. El-Siblani and S. Mintova. Quantification of Lewis Acid Sites in 3D and 2D TS-1 Zeolites: FTIR Spectroscopic Study. *Catal. Today* 2020, 345, 80-87.
- [193] A. Ramanathan, M. C. Castro Villalobos, C. Kwakernaak, S. Telalovic and U. Hanefeld. Zr-TUD-1: A Lewis Acidic, Three-Dimensional, Mesoporous, Zirconium-Containing Catalyst. *Chem. Eur. J.* 2008, 14, 961-972.
- [194] J. P. Nogier, Y. Millot, P. P. Man, T. Shishido, M. Che and S. Dzwigaj. Probing the Incorporation of Ti(IV) into the BEA Zeolite Framework by XRD, FTIR, NMR, and DR UV-jp810722bis. *J. Phys. Chem. C* 2009, 113, 4885-4889.
- [195] K. Barbera, P. Lanzafame, A. Pistone, S. Millesi, G. Malandrino, A. Gulino, S. Perathoner and G. Centi. The Role of Oxide Location in HMF Etherification with Ethanol over Sulfated ZrO₂ Supported on SBA-15. *J. Catal.* 2015, 323, 19-32.
- [196] T. Horiuchi, Y. Teshima, T. Osaki, T. Sugiyama, K. Suzuki and T. Mori. Improvement of Thermal Stability of Alumina by Addition of Zirconia. *Catal. Lett.* 1999, 62, 107-111.
- [197] H. C. Li, J. Wang, D. H. Zhou, D. X. Tian, C. Shi, U. Mueller, M. Feyen, H. Gies, F. S. Xiao, D. De Vos, T. Yokoi, X. H. Bao and W. P. Zhang. Structural Stability and Lewis Acidity of Tetravalent Ti, Sn, or Zr-Linked Interlayer-Expanded Zeolite COE-4: A DFT Study. *Microporous Mesoporous Mater.* 2015, 218, 160-166.

- [198] Z. G. Zhu, Y. J. Guan, H. K. Ma, H. Xu, J. G. Jiang, H. Y. Lu and P. Wu. Hydrothermal Synthesis of Boron-Free Zr-MWW and Sn-MWW Zeolites as Robust Lewis Acid Catalysts. *Chem. Commun.* 2020, 56, 4696-4699.
- [199] M. S. Holm, S. Saravanamurugan and E. Taarning. Conversion of Sugars to Lactic Acid Derivatives Using Heterogeneous Zeotype Catalysts. *Science* 2010, 328, 602-605.
- [200] P. Y. Dapsens, C. Mondelli, J. Jagielski, R. Hauert and J. Pérez-Ramírez. Hierarchical Sn-MFI Zeolites Prepared by Facile Top-Down Methods for Sugar Isomerisation. *Catal. Sci. Technol.* 2014, 4, 2302-2311.
- [201] H. Zhang, W. Yang, I. I. Roslan, S. Jaenicke and G. K. Chuah. A Combo Zr-HY and Al-HY Zeolite Catalysts for the One-Pot Cascade Transformation of Biomass-Derived Furfural to γ -Valerolactone. *J. Catal.* 2019, 375, 56-67.
- [202] Y. Injongkol, T. Maihom, P. Treesukul, J. Sirijaraensre, B. Boekfa and J. Limtrakul. Theoretical Study on the Reaction Mechanism of Hydrogenation of Furfural to Furfuryl Alcohol on Lewis Acidic BEA Zeolites: Effects of Defect Structure and Tetravalent Metals Substitution. *Phys. Chem. Chem. Phys.* 2017, 19, 24042-24048.
- [203] H. P. Winoto, B. S. Ahn and J. Jae. Production of γ -Valerolactone from Furfural by a Single-Step Process using Sn-Al-Beta Zeolites: Optimizing the Catalyst Acid Properties and Process Conditions. *J. Ind. Eng. Chem.* 2016, 40, 62-71.
- [204] J. D. Lewis, S. Van de Vyver, A. J. Crisci, W. R. Gunther, V. K. Michaelis, R. G. Griffin and Y. Roman-Leshkov. A Continuous Flow Strategy for the Coupled Transfer Hydrogenation and Etherification of 5-(Hydroxymethyl)furfural using Lewis Acid Zeolites. *ChemSusChem* 2014, 7, 2255-2265.
- [205] J. A. Melero, G. Morales, J. Iglesias, M. Paniagua and C. López-Aguado. Rational Optimization of Reaction Conditions for the One-Pot Transformation of Furfural to γ -Valerolactone over Zr-Al-Beta Zeolite: Toward the Efficient Utilization of Biomass. *Ind. Eng. Chem. Res.* 2018, 57, 11592-11599.
- [206] G. P. M. Bignami, D. M. Dawson, V. R. Seymour, P. S. Wheatley, R. E. Morris and S. E. Ashbrook. Synthesis, Isotopic Enrichment, and Solid-State NMR Characterization of

- Zeolites Derived from the Assembly, Disassembly, Organization, Reassembly Process. *J. Am. Chem. Soc.* 2017, 139, 5140-5148.
- [207] D. S. Firth, S. A. Morris, P. S. Wheatley, S. E. Russell, A. M. Z. Slawin, D. M. Dawson, A. Mayoral, M. Opanasenko, M. Polozij, J. Čejka, P. Nachtigall and R. E. Morris. Assembly-Disassembly-Organization-Reassembly Synthesis of Zeolites Based on cfi-Type Layers. *Chem. Mater.* 2017, 29, 5605-5611.
- [208] D. N. Rainer, C. M. Rice, S. J. Warrender, S. E. Ashbrook and R. E. Morris. Mechanochemically Assisted Hydrolysis in the ADOR Process. *Chem. Sci.* 2020, 11, 7060-7069.
- [209] J. Jagiello, M. Sterling, P. Eliasova, M. Opanasenko, A. Zukal, R. E. Morris, M. Navaro, A. Mayoral, P. Crivelli, R. Warringham, S. Mitchell, J. Perez-Ramirez and J. Čejka. Structural Analysis of IPC Zeolites and Related Materials using Positron Annihilation Spectroscopy and High-Resolution Argon Adsorption. *Phys. Chem. Chem. Phys.* 2016, 18, 15269-15277.
- [210] A. Zukal, M. Shamzhy, M. Kubů and J. Čejka. The Effect of Pore Size Dimensions in Isorecticular Zeolites on Carbon Dioxide Adsorption Heats. *J. CO₂ Util.* 2018, 24, 157-163.
- [211] W. J. Roth, P. Nachtigall, R. E. Morris, P. S. Wheatley, V. R. Seymour, S. E. Ashbrook, P. Chlubná, L. Grajciar, M. Položij, A. Zukal, O. Shvets and J. Čejka. A Family of Zeolites with Controlled Pore Size Prepared using a Top-Down Method. *Nat. Chem.* 2013, 5, 628-633.
- [212] J. Přeč, P. Pizarro, D. P. Serrano and J. Čejka. From 3D to 2D Zeolite Catalytic Materials. *Chem. Soc. Rev.* 2018, 47, 8263-8306.

7. Enclosures

1. **Zhang J.**, Yue Q., Mazur M., Opanasenko M., Shamzhy M., Čejka J. Selective Recovery and Recycling of Germanium for the Design of Sustainable Zeolite Catalysts. *ACS Sustainable Chemistry & Engineering*, 2020, 8, 8235-8246.
2. **Zhang J.**, Veselý O., Tošner Z., Mazur M., Opanasenko M., Čejka J., Shamzhy M. Towards Controlling Disassembly Step within the ADOR Process for the Synthesis of Zeolites. *Chemistry of Materials*, 2021, 33, 1228-1237.
3. Podolean I., **Zhang J.**, Shamzhy M., Pârvulescu V. I., Čejka J. Solvent-Free Ketalization of Polyols over Germanosilicate Zeolites: The Role of the Nature and Strength of Acid Sites. *Catalysis Science & Technology*, 2020, 10, 8254-8264.
4. Shamzhy M., Přeč J., **Zhang J.**, Ruaux V., El-Siblani H., Mintova S. Quantification of Lewis Acid Sites in 3D and 2D TS-1 Zeolites: FTIR Spectroscopic Study. *Catalysis Today*, 2020, 345, 80-87.